Evaluating the Effect of Wind-induced Exfiltration on the Hygrothermal Performance of Walls of Low-rise Buildings

Felipe Merino Gordo

A Thesis

in

The Department

of

Building, Civil and Environmental Engineering

Presented in Partial Fulfillment of the Requirements

for the Degree of Master of Applied Science (Building Engineering) at

Concordia University

Montreal, Quebec, Canada

November 2019

CONCORDIA UNIVERSITY

School of Graduate Studies

This is to certify that the thesis prepared

By: Felipe Merino Gordo

Entitled: Evaluating the Effect of Wind-induced Exfiltration on the Hygrothermal
                Performance of Walls of Low-rise Buildings

and submitted in partial fulfillment of the requirements for the degree of

Master of Applied Science (Building Engineering)

complies with the regulations of the University and meets the accepted standards with respect to
originality and quality.

Signed by the final Examining Committee:

                    _____ Chair
                        Dr. Ted Stathopoulos

                    _____ Examiner
                        Dr. Hua Ge

                    _____ Examiner
                        Dr. Hoi Dick Ng

                    _____ Supervisor
                        Dr. Bruno Lee

Approved by   _____
                        Chair of Department or Graduate Program Director

_____ 2011   _____
                            Dean of Faculty

ii

Abstract

Evaluating the Effect of Wind-induced Exfiltration on the Hygrothermal
Performance of Walls of Low-rise Buildings

Felipe Merino Gordo

With the increasing levels of insulation employed for energy saving purposes, building envelopes require a reliable hygrothermal analysis to avoid mould and other moisture-related problems. Air leakage has long been identified as one of the primary drivers of moisture transport through building envelopes. Wind is always mentioned as one of the three driving forces of air leakage, but seldom is wind explicitly considered for hygrothermal analysis. In other words, under current practice, hygrothermal analysis will yield exactly the same result regardless of whether the building is in a windy or a windless area.

This study focused on identifying the wind speed and wall orientation that would increase the risk of developing mould in the wall assemblies for a low-rise building. Wind pressure coefficients were used to calculate wind-induced pressure differentials acting across the walls which were then integrated into the Air Infiltration Model. Design variables were structured into a parametric study. The wall performance was evaluated in a heat, air, and moisture (HAM) simulation program.

Through a parametric study this thesis has qualitatively illustrated that wind-induced exfiltration can have a significant effect on the hygrothermal performance of walls of low-rise buildings, and that under some conditions, if wind is ignored mould risk can be underestimated. Based on the limited work of this study, wind speeds under which mould is more likely to be underestimated were quantified, the corresponding wind speed values are not meant to be definitive but rather a demonstration that a similar guideline is worthwhile to be developed.

Acknowledgements

Table of Contents

List of Figures

List of Tables

Nomenclature

ACH	Air changes per hour
ACH_{cav}	Air changes per hour in the ventilation cavity
C_{in}	Water vapour concentration of indoor air
$C_{sat.p}$	Water vapour saturation concentration at condensation plane
C_p	Wind pressure coefficient
C_{pi}	Wind-induced internal pressure coefficient
k_{cl}	Moisture leakage factor
MC	Moisture content
RH	Relative humidity
RSI-value	Thermal resistance
S_w	Moisture source strength
T_{cat}	Terrain category
q_{cl}	Airflow through the "moisture leaks" of the envelope component
θ_w	Wall orientation

1 Introduction

The following sections provide the background for the research, define the gap encountered in the literature review, describe the problem and outline the thesis structure and the objectives of this research project.

1.1 Problem statement

Water, in any of its three physical phases, is arguably the main factor of building deterioration. In its liquid phase, water damage to a building can occur due to leaking pipes, rain infiltration, capillary suction from foundations, and even tsunamis. The cold weather brings other forms of damage such as brick and concrete wall deterioration from ice formation and problems relating to frost heaving in specific soil types. Finally, imperfections in the construction allow moisture-laden air from the interior to flow through the building envelope. If the surface of a material is cold enough, water vapour will condensate, and if the wetting of the assembly is sustained, moisture problems such as mould would develop.

The engineering and construction industries have found practical and effective solutions for many of these water-borne problems. In particular, water vapour permeability in buildings has been effectively handled by the use of water vapour resistant barriers. Furthermore, wind barriers and better construction techniques have improved the general airtightness of buildings. Despite these solutions, however, moisture leakage due to exfiltration has remained a problem.

Airtightness in buildings is mainly focused on delivering a better energy performance of the building. In addition, the inclusion of airtightness requirements in building standards such as Passive-House ("Passive House Institute" n.d.), ASHRAE 90.2 (2002) and National Energy Codes for Building (NECB)(NRCC 2017) has helped to keep highly insulated envelopes safe from moisture problems. However, even after meeting the energy standards, local imperfections can cause damage by moisture convection. For example, in a case study by Borsch-Laaks, Zirkelbach, Künzel, & Schafaczek (2009), newly constructed homes that managed to achieve high levels of airtightness, presented severe moisture damage after the first winter.

Moreover, modern construction systems, with several layers of materials and increasing levels of insulation, are deeply associated with moisture problems. Several investigators have studied the complications encountered on high R-Value walls regarding moisture (Desmarais 2000; J. Lstiburek 2001; Straube & Smegal 2010; Kosny, Asiz, Smith, Shrestha, & Fallahi 2014; Said 2006). These investigators identified key factors influencing the durability of the wall systems: interior insulation, vapour permeance of the different material layers, the assembly of the materials, and more importantly, the air leakage.

Wind-induced infiltration is seldom included in hygrothermal performance analysis. The unpredictability and stochastic nature of wind contribute to the difficulties in including wind-induced infiltration in the hygrothermal analysis. Although several authors have done stochastic studies on hygrothermal performance (Wang 2018; Wang & Ge 2018; Pallin 2013; Pallin, Hun, Jackson, & Desjarlais 2015), only one study by Pallin, et al. (2015), considered the effect of wind over the infiltration. Pallin, et al., included the air infiltration rate as a constant in the stochastic model, but no conclusions were made regarding the impact of wind.

Although there are some methods to estimate wind-induced infiltration, those are energy-assessment-related, and do not differentiate infiltration from exfiltration, which might produce errors if those estimations are used for hygrothermal analysis.

Another reason which explains why wind-induced air leakage has been disregarded in the hygrothermal analysis is the difficulty in determining the leakage path. The amount of moisture transported could easily be determined if the airflows were known (TenWolde 1989). Investigators have evaluated different air leakage paths and airflows (Wolf & Tyler 2013a, 2013b; Hun, Atchley, & Childs 2016); however, it is challenging to extrapolate the results because they are very case-specific.

Finally, considering the effect of wind can be argued by stating that hygrothermal analysis is mainly intended for buildings located in urban or suburban areas. In these areas, surrounding structures or trees significantly shelter the building being studied, making wind-induced air leakage less relevant than stack effect.

Despite continually being disregarded in the analysis, wind is constantly mentioned as one of the driving forces of air leakage in almost all hygrothermal performance-related study. In addition, air

leakage is the most important parameter in terms of hygrothermal performance, demonstrated by several studies (Bomberg, Kisilewicz, & Nowak 2016; Desmarais, Derome, & Fazio 2000;Ilomets, Kalamees, & Vinha 2018; CMHC 2007; Domhagen & Wahlgren 2017; Fox 2014; Hun et al. 2016; Künzel 2012, 2014; Langmans, Klein, & Roels 2012; J. Lstiburek 2002, 2009; Pallin 2013; Rode, Hens, & Janssen 2008; Wang & Ge 2017). Hence, there is a need to study the impact of wind-induced air leakage, and specifically exfiltration, on the hygrothermal performance of walls to provide a more rigorous and reliable assessment.

1.2   Objectives and scope

The objective of this study was to qualify if the inclusion of wind induced exfiltration in a hygrothermal model had a significant effect over the hygrothermal performance of low-rise building[1] walls. To that end, a parametric study was executed to evaluate the wind-induced air exfiltration across a wall, and its implications on the hygrothermal performance of the wall assembly.

Based on the parametric study this research quantify certain wind conditions under which the hygrothermal performance of the wall assembly might be negatively affected if wind is not considered in the hygrothermal analysis A comparison was realized between hygrothermal simulation models using stack pressure differentials as the driving force for air exfiltration and models that use the combined effect of the stack and wind-induced pressures.

Five cities were used for the simulations to assess different climates, average wind speeds, and the importance that wind direction holds over the process. The study included the following parameters to weigh their relevance: Terrain category (T_{cat}), moisture leakage factor (k_{cl}), Air changes per hour in the ventilation cavity (ACH_{cav}), internal pressure (C_{pi}), thermal resistance of the wall insulation (RSI-$value$), and wall orientation (θ_w).

The conclusions of the study are only valid for the five selected cities and mineral wool insulation with board siding. The limited work of this study provides some selected performance indicators and numerical values that are not meant to be definitive but rather a demonstration that a similar workflow and recommendations are worthwhile to be developed.

---

[1] Defined as structures of three storeys or fewer above grade (ASHRAE 90.2 2007)

1.3   Thesis organization

The literature review in Chapter 2 provides the underlying knowledge for the assumptions adopted in this study and identifies the knowledge gap of previous studies. The air leakage driving forces, with an emphasis on the wind effect, are reviewed. Air leakage standards and air leakage modelling methods for hygrothermal analysis are discussed. Finally, performance indicators are determined for the study.

Chapter 3 describes the workflow used in this study. Chapter 4 describes the modelling setup and the values for the parameters investigated. Chapter 5 presents the results and discusses them using performance indicators of HAM in building such as moisture content, relative humidity, and Mould index to compare the different cases. A summary of the results is presented in Chapter 6. Finally, Chapter 7 presents the general conclusions, the contribution of this work and proposed future research.

2 Literature Review

The following sections review the existing literature related to the subject of this thesis. The objective of this literature review is to identify the research gap and to provide support to the assumptions taken.

2.1 Hygrothermal Analysis

Hygrothermal signifies relative to moisture and temperature (Oxford English Dictionary 2019). In the building engineering field, hygrothermal analysis refers specifically to the study of heat, air and moisture (HAM) transport through the building enclosure or structure. As part of the design process of a building envelope, hygrothermal models are generally used to compare relative performance between different alternatives, and in that case the accuracy of the model is not critical (Straube & Schumacher 2001). On the other hand, hygrothermal analysis can be used to perform forensic analysis (Lawton 1999), then the accuracy and reliability of the model are critical.

Several are the factors influencing the hygrothermal performance of an envelope assembly: material properties, weather, indoor climate, boundary conditions, initial condition and air leakage are some of them (Defraeye, Blocken, & Carmeliet 2011; Djebbar, Reenen, & Kumaran 2001; Hens 2015; Janssen, Blocken, & Carmeliet 2007; Künzel 2005; Antretter, Karagiozis, TenWolde, & Holm 2007; Hens 2002; McClung, Ge, Straube, & Wang 2010; Pankratz, & Holm, 2004). Research has been done to study each of the influencing factors and the combination of them. Practice, field measurements, and experimental studies have provided extensive knowledge over the influencing factors (Fox, Straube, Ge, & Trainor 2014; Ge, Deb Nath, & Chiu 2017; Ge, Wang, & Baril 2018; Langmans, Desta, Alderweireldt, & Roels 2016; Simpson 2010; Straube & Lstiburek 2013). More recently, the development of HAM simulation software has provided the possibility of predicting performance being a valuable tool for decision making. Finally, research that combines field measurements or experimental studies and HAM simulation, has provided guidelines for more reliable assumptions for hygrothermal modelling (Fox 2014; Kalamees et al. 2010; McClung et al. 2010; R. Wang 2018; Zirkelbach, Künzel, & Bludau 2008).

Air leakage has been identified as the main driver of moisture transport through the envelope. Kalamees, Alev, & Pärnalaas (2017) studied the air leakage levels in timber frame buildings, but the effect of wind was not measured. Most of the research done to investigate the effect of wind

on the air leakage refers to energy conservation and performance (Ng, Ojeda Quiles, Dols, & Emmerich 2018; Sherman, Modera, & Grimsrud 1980; Younes, Shdid, & Bitsuamlak 2012).

Another parameter relevant for hygrothermal performance of walls is the ventilation rate of the cavity behind the rain-screen. Stovall & Karagiozis (2004) developed a parametric model to estimate cavity ventilation rates depending on temperature and wind speeds for brick walls. The research focused on the ventilation rates product of winds normal to the wall, the angle of incidence of wind was not studied.

High R-value wall assemblies and their association with moisture problems have been widely investigated. Several researchers compare the hygrothermal performance of different high R-value wall assemblies (Straube & Smegal 2010; Kosny, Asiz, Smith, Shrestha, & Fallahi 2014; Said 2006). The comparison focuses on the different materials and how they are assembled, R-values, thermal performance and durability. The aim of this type of study is to understand which wall performs better under certain boundary conditions. Hence, the boundary conditions are generally simplified, and air leakage may, or may not be considered at all. Pihelo, Kikkas, & Kalamees (2016) studied the hygrothermal effect of varying the R-value of the wind barrier. They considered air leakage but nothing is said about the wind.

The thermal performance of duo-pitched roofs under the effect of wind was measured in a study by Janssens & Hens (2007), but the research did not considered or measured the hygrothermal performance.

Most of the time when wind is mentioned in hygrothermal studies, it is to investigate the effect of wind-driven rain. Wind-driven rain is the main way of bulk water ingress in the building envelope and it has been extensively researched (Baskaran & Brown 1995; Blocken & Carmeliet 2004; Cornick et al. 2009; Derome, Kubilay, Defraeye, Blocken, & Carmeliet 2017; Ge et al. 2017; Künzel 2006)

Stochastic studies are constantly used for risk assessment or to understand the uncertainty of certain assumptions. Vereecken et al. (2015) proposed a methodology based on a Monte Carlo analysis to select interior insulation measures that balance energy savings and hygrothermal risks. But, air leakage was not considered at all. Wang & Ge (2018) investigate the relevance of material properties and air leakage rate through a stochastic analysis. They conclude that material properties

are less important than air and rain leakage, but nothing is said about how wind contributes to air leakage. Pallin (2013) proposed a risk assessment methodology for retrofitting measures that consider the variability of hygrothermal influencing parameters. Although the study mentions wind as a relevant parameter, it is finally disregarded because of the difficulties to assess it. Pallin, Hun, Jackson, & Desjarlais (2015) did a durability assessment in which air infiltration is treated as a stochastic variable. In their research, wind is considered to calculate air leakage rates, but no conclusion is done regarding the wind influence on the hygrothermal performance of the wall assemblies.

2.2 Air Leakage

Air leakage has become increasingly critical as Building Codes and Standards emphasize energy conservation. Initially, insulation was enough to upgrade a building to save energy, but as insulation levels increase, so has the relative importance of other mechanisms of heat loss, such as thermal bridges or air leakage. Moreover, the combination of higher levels of insulation with high levels of air leakage has increased moisture and durability problems (Hens 1995).

Air leakage in buildings is understood as the uncontrolled or accidental introduction of air from outside into the building and is usually used instead of the more formal term infiltration. More precisely, ASHRAE Fundamentals (ASHRAE Fundamentals 2017) defines Infiltration as "the flow of outdoor air into a building through cracks and other unintentional openings and the normal use of exterior doors for entrance or egress." On the other hand, it defines exfiltration as "the leakage of indoor air out of a building through similar types of openings."

Air leakage is driven by pressure differences across the envelope caused by wind, stack effect or buoyancy, and operating mechanical air-moving systems. Both infiltration and exfiltration play an essential role in energy conservation in buildings and, as such, has been included in most Building Energy Simulation (BES) tools or software. One of the models to take account of the effect of infiltration on energy calculation can be seen in EnergyPlus (EnergyPlus 2018) and is based on a preliminary study by Grimsrud, Sherman, Blomsterberg, & Rosenfeld (1979). In this study, they mention that the inclusion of surface pressures calculated from wind tunnel measurements, considering the effects of shielding, and separating wind dominated from temperature dominated pressure effects are some necessary modifications to their model in order to better predict

infiltration. Later, in another study supporting the development of a parametric model to estimate infiltration in residential houses considering the wind effect, the authors presented wind and stack measurements shown in Table 1, in which it can be seen that, in most cities, the infiltration due to Wind-effect is higher than the infiltration due to Stack-effect. This observation demonstrates that wind plays an essential role in building infiltration and that disregarding its influence might lead to underestimating the total infiltration and, consequently, the total energy consumption and moisture-related problems.

Infiltration for reference Case in 59 TRY Cities					Infiltration for reference Case in 59 TRY Cities				
City		Stack-effect infiltration	Wind-effect infiltration	Total infiltration	City		Stack-effect infiltration	Wind-effect infiltration	Total infiltration
		$m^3/h \cdot cm^2$					$m^3/h \cdot cm^2$		
Albany	NY	0.21	0.23	0.31	Lubbock	TX	0.15	0.28	0.31
Albuquerque	NM	0.17	0.15	0.23	Madison	WI	0.20	0.19	0.28
Amarillo	TX	0.17	0.30	0.35	Medford	OR	0.18	0.10	0.21
Atlanta	GA	0.14	0.21	0.25	Memphis	TN	0.14	0.20	0.24
Bismark	ND	0.23	0.21	0.31	Miami	FL	0.03	0.19	0.19
Boise	ID	0.18	0.18	0.25	Minneapolis	MN	0.22	0.21	0.31
Boston	MA	0.19	0.30	0.36	Nashville	TN	0.15	0.21	0.26
Brownsville	TX	0.06	0.24	0.25	New Orleans	LA	0.11	0.20	0.23
Buffalo	NY	0.19	0.27	0.33	New York	NY	0.17	0.26	0.31
Burlington	VT	0.21	0.21	0.29	Norfolk	VA	0.15	0.26	0.31
Charleston	SC	0.12	0.20	0.23	Oklahoma	OK	0.16	0.30	0.34
Cheyenne	W	0.19	0.27	0.34	Omaha	NE	0.19	0.21	0.29
Chicago	IL	0.19	0.21	0.28	Philadelphia	PA	0.18	0.25	0.31
Cincinnati	OH	0.17	0.19	0.26	Phoenix	AZ	0.11	0.09	0.14
Cleveland	OH	0.19	0.24	0.31	Pittsburg	PA	0.18	0.23	0.29
Columbia	SC	0.18	0.22	0.29	Portland	ME	0.20	0.18	0.27
Detroit	MI	0.19	0.24	0.31	Portland	OR	0.16	0.21	0.27
Dodge City	KS	0.18	0.28	0.33	Raleigh	NC	0.15	0.19	0.24
El Paso	TX	0.13	0.17	0.22	Richmond	VA	0.17	0.18	0.24
Port Worth	TX	0.12	0.23	0.26	Sacramento	CA	0.14	0.12	0.19
Fresno	CA	0.12	0.12	0.18	Salt Lake City	UT	0.19	0.17	0.25
Great Falls	MT	0.20	0.40	0.45	San Antonio	TX	0.11	0.20	0.23
Houston	TX	0.10	0.23	0.25	San Diego	CA	0.10	0.13	0.16
Indianapolis	IN	0.19	0.23	0.30	San Francisco	CA	0.13	0.18	0.22
Jackson	MS	0.12	0.20	0.24	Seattle	WA	0.17	0.21	0.27
Jacksonville	FL	0.09	0.19	0.21	St. Louis	MO	0.18	0.22	0.29
Kansas City	MO	0.18	0.21	0.28	Tampa	FL	0.06	0.19	0.20
Lake Charles	LA	0.11	0.19	0.22	Tulsa	OK	0.15	0.22	0.27
Los Angeles	CA	0.10	0.16	0.19	Washington	D.C.	0.16	0.16	0.23
Louisville	KY	0.18	0.23	0.29					

Table 1: From Grimsrud, Sherman, & Sonderegger, (1983) – Stack and wind effect infiltration rates for US cities. It can be seen that wind-effect infiltration is comparable and sometimes higher than stack-effect infiltration. Values are coloured in red where wind infiltration is higher than stack infiltration.

Air leakage also plays an essential role in hygrothermal performance as shown by the "IEA ANNEX 24 - Heat, Air and Moisture Transfer In Highly Insulated Building Envelopes

(HAMTIE)" (Hens 2002) where moisture sources that define the hygrothermal loads are ranked according to their relevance as follows:

1. air exfiltration,
2. initial moisture,
3. latent heat,
4. wind-driven rain

While the effect of wind-induced infiltration has been adequately addressed for energy conservation, its effect has not been evaluated for hygrothermal performance. The explicit evaluation of wind effect over the infiltration and its impact on hygrothermal loads is frequently disregarded mainly because of the difficulties and uncertainties that impose the wind study. By understanding the air leakage mechanisms and applying them to a hygrothermal model it is possible to evaluate the wind effect.

2.2.1 Air Leakage Mechanisms

As previously mentioned, air leakage is driven by three forces: stack effect, wind pressure and the operation of air-moving mechanical equipment. The three forces and the combination of them will be reviewed in the following sections. This knowledge will provide the basis to integrate wind-induced leakage to the hygrothermal model.

2.2.1.1 Stack effect

The stack effect is produced by the difference in density of the air because of temperature between the indoor and outdoor air. According to ASHRAE Fundamentals (ASHRAE Fundamentals 2017), if vertical density gradients are neglected, any single zone is defined by an effective stack height, or the height of the connected air volume, and the neutral pressure level (NPL).

The stack pressure differential usually produces air infiltration at the bottom of the walls and air exfiltration at the top part, as shown in a study by Kalamees et al. (2010). Stack pressure differentials are especially relevant in colder regions where the temperature differences between indoor and outdoor air are higher. The stack pressure differentials may be determined using a

9

simplified calculation for engineering practice purposes in order to assess the hygrothermal performance of walls and roofs as shown by Zirkelbach et al. (2009).

Contrary to the more predictable stack-effect, wind-induced infiltration and exfiltration are more difficult to predict due to the variability of wind speeds and directions. The next section describes the equations that are commonly used to evaluate wind pressures over building surfaces.

2.2.1.2 Wind effect

Wind pressure over a building depends on the wind speed, wind direction, air density, surface orientation, and surrounding conditions. When wind hits a surface, it creates a distribution of static pressures, these static pressures are generally positive on the windward side and negative on the leeward side but can be negative or positive depending on the wind angle and surface shape.

2.2.1.2.1 Local Wind Pressure Coefficients

Pressures on surfaces are typically expressed in terms of a non-dimensional pressure coefficient (C_p), representing a ratio between the difference of the pressure at the location and time of interest and the static reference pressure (ambient pressure) and the dynamic pressure of the wind at the same place and time.

For low-rise buildings, the reference height where the wind speed is measured usually is typically at eaves height. Since the wind speed fluctuates with time, the C_p also varies with time, and since the pressure over a building varies depending on the position where it is being measured, the C_p also varies within the surface. Figure 1 shows a graphical distribution of local C_p in a low-rise building.
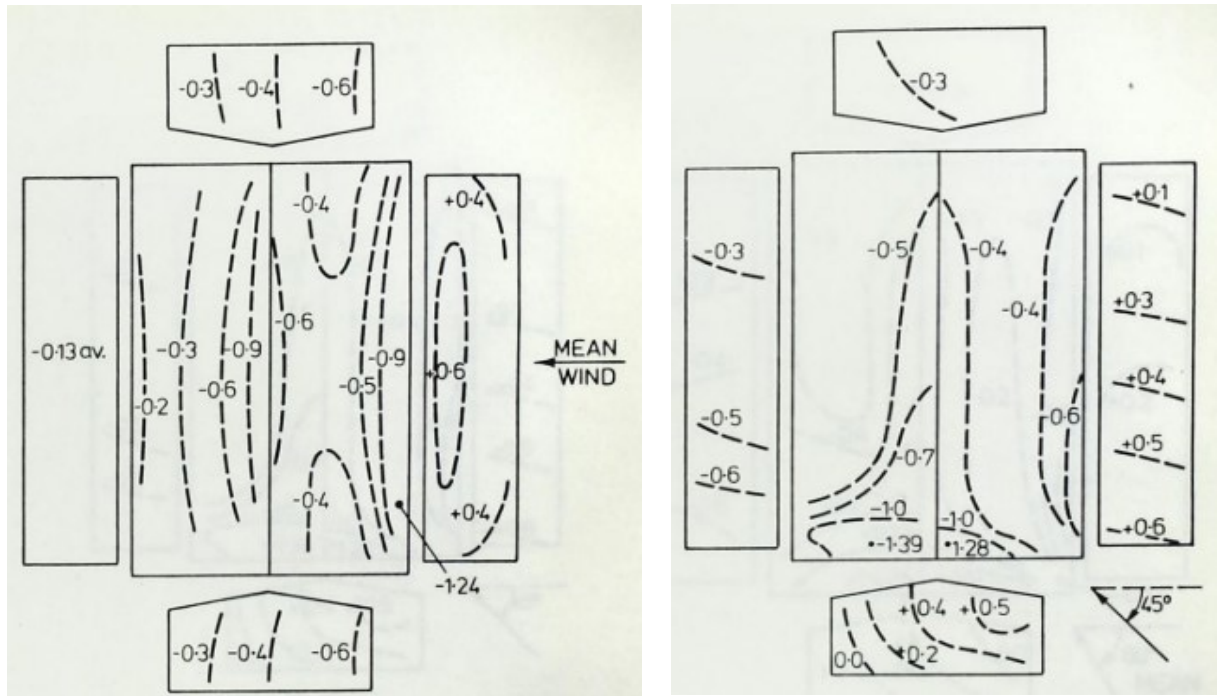
Figure 1: Local C_p examples from Holmes (1983)

A study by Gavanski & Uematsu (2014) shows that higher suction peak pressures occur on the lateral edge of the walls rather than in the center of the wall, contrary to winds generating positive pressures where the center of the element is affected by the highest pressure. Local C_p values are relevant in terms of structural loading, but their application to estimate infiltration is too complex, averaging them over the surface makes the calculation easier. Moreover, according to ASHRAE Fundamentals (ASHRAE Fundamentals 2017) surface averaged wall C_p can be used to estimate air infiltration.

A review of pressure coefficients by Cóstola, Blocken, & Hensen (2009) used in building energy simulation and airflow network programs establishes that C_p coefficients can be determined by field measurements (Jensen & Franck 1965; Levitan, Holmes, Mehta, & Vann 1991), Wind tunnel experiments (Holscher & Niemann 1998; Reinhold 1982), Computational Fluid Dynamics (CFD) analysis (Stathopoulos 1997; B. Blocken, Stathopoulos, & Carmeliet 2007), databases (Liddament 1986;Tamura 2012), parametric models (Swami & Chandra 1987; Grosso 1992; Muehleisen & Patrizi 2013; Allen 1984; Eldin 2007) and more recently, Artificial Intelligence (Bre, Gimenez, & Fachinotti 2018) can be considered to obtain C_p coefficients.

Field measurements are case-specific, wind tunnel experiments might be more general, but the data is not always available to the public, CFD analysis requires extensive knowledge and practice to achieve a reliable model. On the other hand, parametric models are based both on field measurements and wind tunnel experiments grouped in databases, which makes them applicable in more general cases. Moreover, they are easily integrated into calculation sheets or in any programming language, making them suitable for engineering practice.

2.2.1.2.2 Surface-Averaged Wall Pressure Coefficients

Several parametric models to calculate surface-averaged pressure coefficients exist, the most well-known being the Swami-Chandra model (Swami & Chandra 1987) developed to estimate C_p over walls to use for hourly calculation of natural ventilation. One limitation of the S&C model is that it can only be applied to buildings with rectangular floor plans (Bre et al. 2018). Another shortcoming is that it does not take into account the sheltering effects of nearby obstacles. To overcome this weak point, Grosso (1992) proposed a set of complex parametric models. However, due to the complexity and the lack of reliable experimental data, Grosso acknowledges that the real contribution of his work may be the proposed methodology rather than the specific parametric equations that resulted from his research.

Muehleisen & Patrizi (2013) developed another parametric model, resulting in a simple rational equation that was calibrated with the large and detailed database of the Wind Engineering Information Center at the Tokyo Polytechnic University (TPU) (Y. Quan, Y. Tamura, M. Matsui, S. Cao 2007; Tamura 2012). The equation fits the database with a coefficient of determination R^2 = 0.993. Due to the ease of applying the S&C and M&P models in calculation sheets or programing language, these two methods will be selected. Further details will be given in the following sections.

2.2.1.2.3 Wind-Induced Internal Pressure in Buildings

Internal pressure in buildings due to the effect of the wind is of great interest for structural reasons. Most of the studies on this topic research the impact of sudden openings in the presence of strong winds, i.e., the opening of doors and windows, or windows that were broken by flying debris in

case of strong winds or hurricanes. Studies of internal pressure on buildings focus predominantly on the instantaneous loads on the structure and the response time of the internal pressure. Different considerations in regards to the openings areas and their location in the building, or nominally sealed buildings are assessed in different studies (J. D. Ginger, Mehta, & Yeatts 1997; Stathopoulos, Surry, & Davenport 1979; John D Ginger 2000; Kopp, Oh, & Inculet 2012).

The internal pressure of the building is strictly dependent on the location and distribution of the leakage zones. However according to ASHRAE Fundamentals (ASHRAE Fundamentals 2017), if uniformly distributed leakage is assumed for all the walls, C_{pi} can be calculated by integration resulting in a value of -0.2. Similar values were measured on a nominally sealed building by Ginger et al. (1997) obtaining a mean pressure coefficient of -0.14.

2.2.1.3   Mechanical effect

Mechanical ventilation affects internal pressures in buildings, and mechanical equipment can suffer extreme reductions in its capacity by the wind effect. The airflow generated by this equipment can be reduced or even reversed depending on the direction and speed of the wind.

Mechanical equipment and its operation are designed and intentionally included as part of the building design. If done correctly, pressure differences across the envelope will be controlled by the mechanical equipment, and the airflows and direction of them will be well known and should not create problems (Ricketts 2014).

Nowadays, most of the construction assemblies are hollow or multilayered (i.e., wall assemblies with gypsum and OSB boards and metallic studs) and contain several services that connect one element or zone with another. If the mechanical equipment is not well implemented and is accidentally connected with the interior cavity of the building components, it can generate interstitial pressure fields and cause serious hygrothermal issues as discussed by Lstiburek (1998 and 2006).

Pressure differences produced by the operation of mechanical equipment are not considered in this research because mechanical ventilation systems are seldom present in low-rise buildings, and if they are, they will probably control the pressure differential across the building envelope.

2.3 Air Leakage Modelling Methods for Hygrothermal Analysis

Even though Building Codes and Standards are continually increasing the requirements for airtightness in buildings, and new materials and construction systems are facilitating to achieve those more stringent requirements, it is impossible to absolutely avoid moisture problems. Seals and tape fail with time, and some mistakes during the construction or omissions (lack of detailing) in design can always occur. Hence, it is essential to assess the hygrothermal performance of the buildings and their components to ensure a reliable and robust response of the system.

Although it can be argued that with the development of more complete and user-friendly 2D and 3D HAM simulation software, or CFD tools, it should be easier to assess different components, the reality is that the complexity is still too much. Moreover, the quantity and uncertainty of assumptions that need to be made, (i.e., the airflow path) make it non-desirable for engineering practice.

Two air modelling methods are discussed in this literature review, the Air Convection method and the Air Infiltration method. Both methods were validated using a simulation approach (Künzel, Zirkelbach, & Schafaczek 2012), and a study by Wang & Ge (2017) discusses and validates both methods by means of an experimental setup and comparing measurements with simulations.

2.3.1 Air Convection Method

This method was developed as an adaptation to the multi-physics model for assessing the effect of air cavity convection on the wetting and drying behaviour of wood-frame walls, developed by Karagiozis & Künzel (2010). The original method evaluates the airflow in the ventilation air cavity influenced by wind pressure, thermal buoyancy, and moisture concentration buoyancy. The calculated airflow rate is included in the hygrothermal model using outdoor air as the source.

The same principles are followed for the insulation cavity to assess possible moisture issues due to air convection. In this case, a fictional 1 mm air layer is created in the frame cavity; then an airflow rate is assigned to the air layer. The airflow rate depends on the airtightness of the component. Finally, indoor air is selected as the source.

Because of the uncertainty of the airflow path, both the position of the fictional air layer and the airflow rate have to be determined either by experience or by comparison to an experimental setup, Wang & Ge (2017) and Fox (2014) discuss this matter. Generally speaking it could be said that if the insulation has a close-fitting to the wall frame and is less air-permeable, i.e., cellulose, the location of the air layer would be closer to the interior side and that the airflow rate would be a smaller fraction of that represented by the airtightness of the building, 25% or 50%. On the contrary, if the insulation has a loose-fitting and is more air-permeable, i.e., low-density mineral fibre, then the location of the air layer would be closer to the exterior wall sheathing, and the airflow rate would be similar to the airtightness of the building.

Among the disadvantages of this method, it could be mentioned:

- High variability on the *ACH* used in some researches ranging from 16 to 850 (Künzel et al., 2012; Fox, 2014).

- The trial-and-error approach is used to locate the 1 mm air layer to best represent the effect of the injected air on the wood frame.

- In practice, the *ACH* is assumed as constant using the general air leakage of the building (i.e., 0.6 *ACH* for a passive house building).

2.3.2 Air Infiltration Method

The air infiltration method is proposed by Zirkelbach et al. (2009). The main characteristic of this method is that it allows calculating an unsteady source of vapour convection for lightweight constructions. In the model, the airflow itself is not essential as it is the precipitating condensation on the surface that is being analyzed.

The amount of vapour condensation is calculated from the difference between the water vapour concentration present in the indoor air and the water-saturated vapour concentration in the condensation surface. Then, the amount of vapour condensation is multiplied by the moisture leaks (k_{cl}) and the pressure differential that induce moisture flow. Künzel et al. (2012), and Pallin et al. (2015) determined that about 5% to 10% of the total air leakage in a building corresponds to moisture leaks, and only such leakages should be considered in the vapour convective model.

In order to determine the amount of vapour condensation, it would be necessary to know the proportion of humidification-relevant leaks (in the component itself) in the total leakage of the building envelope. Unfortunately, there are currently hardly any definite statements about this. Most studies are primarily concerned with the energetic aspects of leaks and tend to marginalize the humidification risk. Zirkelbach et al. (2009) estimate that component air leakage is about 1/15 of the whole building air leakage. Künzel et al. (2012) and Künzel (2014) calculate the corresponding k_{cl} by dividing those component leakages values by 50 Pa.

Wang & Ge (2017) compared the air infiltration modelling method with the results obtained in a field experiment that used a component leakage (q_{cl}) of 0.24 L/m²s at 5 Pa for the insulation cavity of the wall or 0.11 L/m²s at 5 Pa for the total wall area. The results showed good agreement between the Air Infiltration Model and the measurements when the q_{cl} simulated was 75% of the total q_{cl} for the North oriented fibreglass wall and 50% of the total q_{cl} for the South oriented fibreglass wall. For the cellulose insulated wall, the best agreement between measurement and simulation was obtained when the q_{cl} simulated was between 50% and 25% of the total q_{cl} for the North and South oriented wall, respectively. If those results are converted to k_{cl} by dividing by 5 [Pa], the k_{cl}'s obtained range from 0.02 to 0.06 [m³/ (m²h·Pa)] for 25% and 75% of the total q_{cl} using the total wall area (0.11 L/m²s at 5 Pa). Those values are comparable to the ASHRAE values mentioned by Künzel et al. (2012) and ASHRAE Standard 160 (2016).

The model assumes that: the heat effects of penetrating air (sensible and latent) are neglected; only condensation at the surface is considered, i.e., no sorption at high RH; and that the convective drying is excluded. Originally this method explicitly excludes the effect of the wind due to: the temporary and unsteady nature of wind; changing wind directions leads to alternate the condensation and drying processes; and because strong winds might turn some moisture leaks into energy leak.

Karagiozis (2014) mentioned the need to simplify wind treatment to include it in the model proposed by Zirkelbach et al. (2009). Moreover, ASHRAE Standard 160 (2016), in its section 4.4.1 suggests the possibility to consider wind-induced pressures in the hygrothermal analysis, although it does not indicate how to do it.

3 Methodology

3.1 Hygrothermal Model

The following section describes the workflow that was developed to include wind in the hygrothermal model for this research.
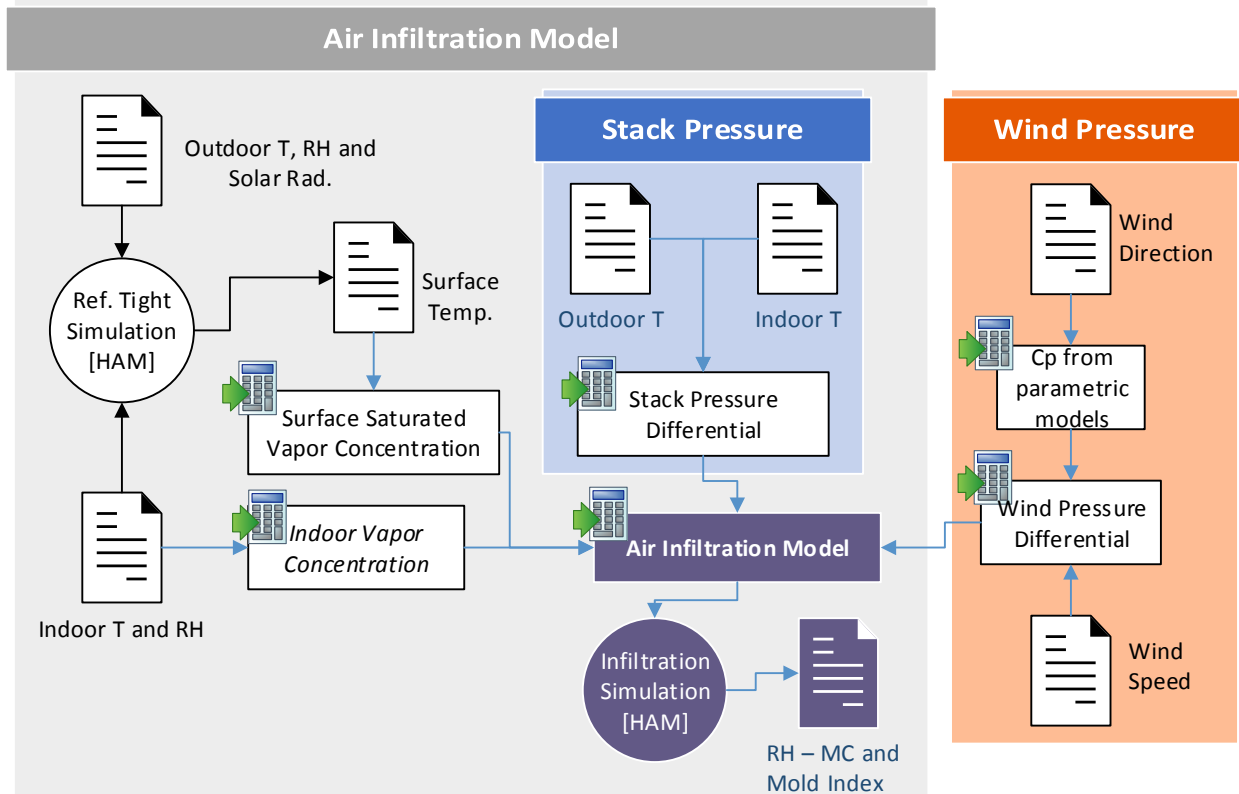
Figure 2: Workflow chart

The workflow is composed of two parts. The first one is the calculation of the original Air Infiltration Model (grey section) according to Zirkelbach et al. (2009). The first part includes the calculation of vapour concentrations and the stack effect pressure differential. The second part corresponds to the calculation of the wind pressure differential which is then integrated into the Air Infiltration Model.

Air Infiltration Model

According to Zirkelbach et al. (2009), the moisture source is calculated using the following equations:

$$S_w = q_{cl} \cdot (C_{in} - C_{sat.P}) \qquad [1]$$

$$q_{cl} = k_{cl} \cdot \Delta P \qquad [2]$$

Where,

S_w	= Moisture source strength [kg/m²·h]
q_{cl}	= Airflow through the "moisture leaks" of the envelope component [m³/m²·h]
C_{in}	= Water vapour concentration of indoor air [kg/m³]
$C_{sat.p}$	= Water vapour saturation concentration at condensation plane [kg/m³]
k_{cl}	= Air permeability of moisture leaks [m³/m²·h·Pa]
ΔP	= Stack effect pressure differential

For the calculation of $C_{sat.p}$, the temperature of the surface where condensation is expected must be known. For that purpose, the reference tight cases are simulated using a HAM software (*DELPHIN* 2018) and the temperature of the surface is obtained. The C_{in} is calculated depending on the *RH* and temperature of the indoor air which are known.

Stack Pressure Differential

According to ASHRAE Fundamentals (ASHRAE Fundamentals 2017), the stack pressure difference at any vertical position can then be calculated using equation 3:

$$\Delta P_s = (\rho_0 - \rho_i) \cdot g \cdot (H_{NPL} - H) = \rho_0 \cdot \left(\frac{T_i - T_0}{T_i}\right) \cdot g \cdot (H_{NPL} - H) \qquad [3]$$

Where,

T_0 = Outdoor temperature [K]

T_i = Indoor temperature [K]

ρ_0 = Outdoor air density [kg/m^3]

ρ_i = Indoor air density [kg/m^3]

H_{NPL} = Height of neutral pressure level above reference plane without any other driving forces [m]

g = Gravitational acceleration=9.81 [m/s^2]

If uniform leakage distribution is assumed, it can be demonstrated that H_{NPL} = H/2, then the stack pressure differential can be calculated as:

$$\Delta P_s = \rho_0 \cdot \left(\frac{T_o - T_i}{T_i}\right) \cdot g \cdot \frac{H}{2} \qquad [4]$$

Wind Pressure Differential

The wind-induced static pressure over a surface is almost proportional to the velocity pressure of the undisturbed airstream, and if no height change or pressure loss is assumed it can be calculated by the Bernoulli equation (ASHRAE Fundamentals 2017)

$$P_w = C_p \cdot P_v \qquad [5]$$

Where C_p is the local wind pressure coefficient at a location on the building surface and P_v is defined by:

$$P_v = \frac{\rho_0 \cdot U_H^2}{2} \qquad [6]$$

Where,

P_v = Wind velocity pressure at a reference height [m]

U_H = Wind speed at the reference height [m/s]

ρ_0 = Outdoor air density [kg/m^3]

The unsteady nature of wind causes surface pressure to fluctuate with time, which forces the use of time-averaged wind speeds. The shortest period that can be considered "steady-state" condition is 600 s and the longest is typically considered 3600 s, which is what can be found in most weather files used for energy or hygrothermal simulation. Instantaneous pressures can create peak pressures two or three times the mean value, and although immediate pressures are significant to calculate structural loads, mean values are more appropriate in regards to infiltration (ASHRAE Fundamentals 2017).

The effect of the ground roughness and geography affects wind speeds, where wind speeds are reduced as they approach the ground. Moreover, wind speed is usually measured in a different place from the one of interest and most probably at a different height. It is possible to transform wind speeds measured at one height and in one type of terrain to a different height and a different kind of terrain by using the Boundary Layer Theory and estimations of terrain effects. Equation [7] and Table 2 can be used for that purpose (ASHRAE Fundamentals 2017):

$$U_H = U_{met} \cdot \left(\frac{\delta_{met}}{H_{met}}\right)^{a_{met}} \cdot \left(\frac{H}{\delta}\right)^{a} \qquad [7]$$

Where,

U_{met} = Wind speed at meteorological station [m/s]

δ_{met} = Layer thickness at meteorological station [m]

a_{met} = Exponent at meteorological station

δ = Layer thickness at building location [m]

a = Exponent at building location

Wind speed is usually measured at meteorological stations, typically at a 10 m height and located in flat, open terrain (i.e., category 3 in Table 2), and the reference point to determine wind speed and Pressure coefficients for low-rise buildings are usually at eaves height.

Although equation [7] is less reliable for heights below the average height of obstacles surrounding the building such as vegetation or other structures, the effect of shielding for low-rise buildings is for the most part accounted for by reducing P_v with the corresponding coefficients presented in Table 2 (ASHRAE Fundamentals 2017).

Table 2: Terrain Category

Terrain Category	Description	Exponent a	Layer Thickness δ [m]
1	Large city centers, in which at least 50% of buildings are higher than 25 m over a distance of at least 0.8 km or 10 times the height of the structure upwind, whichever is greater.	0.33	460
2	Urban and suburban areas, wooded areas, or other terrain with numerous closely spaced obstructions having the size of single-family dwellings or larger, over a distance of at least 460 m or 10 times the height of the structure upwind, whichever is greater.	0.22	370
3	Open terrain with scattered obstructions having heights generally less than 9m, including flat open country typical of meteorological station surroundings.	0.14	270
4	Flat, unobstructed areas exposed to wind flowing over water for at least 1.6 km, over a distance of 460 m or 10 times the height of the structure inland, whichever is greater.	0.1	210

This section described the equations necessary to determine the dynamic wind pressures P_v The next step in determining the wind Pressure over the building surface is the calculation of the pressure coefficient C_p which is described in the next section.

Local Pressure Coefficient

Pressures on surfaces are typically expressed in terms of a non-dimensional pressure coefficient (C_p), representing a ratio between the difference of the pressure at the location and time of interest and the static reference pressure (ambient pressure) and the dynamic pressure of the wind at the same place and time:

$$C_p(t) = \frac{P(t) - P_0}{\frac{1}{2} \cdot \rho \cdot \overline{u}^2} \qquad [8]$$

The two C_p parametric models that were used in this study correspond to surface-averaged wall pressure coefficients. As mentioned before, surface-averaged pressure coefficients can be used to estimate infiltration rates, this makes parametric models ideal for the objectives of this study.

Surface Averaged Pressure Coefficient

Swami-Chandra Model

Swami & Chandra (1987) developed an equation to estimate C_p over walls to be used for hourly calculation of natural ventilation. The model was derived by a non-linear regression to measured data from eight different researches for low-rise buildings. The wind incidence angle and building side ratio were found to predict the data with a correlation factor of 0.8

$$\overline{C_p}(\theta, G) = \overline{C_p}(0) \cdot \ln \left[\begin{array}{c} a_0 - a_1 \cdot \sin\dfrac{\theta}{2} - a_2 \cdot \sin^2 \theta + a_3 \cdot \sin^3(2G\theta) + \\ a_4 \cdot \cos\dfrac{\theta}{2} + a_5 \cdot G^2 \cdot \sin^2\dfrac{\theta}{2} + a_6 \cdot \cos^2\dfrac{\theta}{2} \end{array} \right] \qquad [9]$$

Where θ is the angle of incidence of the wind over the wall, $G = ln(S)$, with S the building side ratio D/B, being D, the depth of the building and B, the breadth of the building, and $\overline{C_p}(0)$ is the $\overline{C_p}$ for $\theta = 0$, assumed to be 0.6 independently of G according to Swami and Chandra. And $a_0 = 1.248$, $a_1 = 0.703$, $a_2 = 1.175$, $a_3 = 0.131$, $a_4 = 0.769$ and, $a_5 = 0.07$, $a_6 = 0.171$

Muelhsein-Patrizi Model

Muehleisen & Patrizi (2013) developed a parametric equation derived from wind databases that allow calculating the C_p of a low-rise building depending on the angle of incidence of the wind (θ) and $G= ln(S)$, with S the building side ratio as defined for the Swami-Chandra model. The model was developed through curve fits to the low-rise data from the Tokyo database (Tamura 2012); the equation is:

$$\overline{C_p}(\theta, G) = \frac{a_0 + a_1 \cdot G + a_2 \cdot \theta + a_3 \cdot \theta^2 + a_4 \cdot G \cdot \theta}{1 + b_1 \cdot G + b_2 \cdot \theta + b_3 \cdot \theta^2 + b_4 \cdot G \cdot \theta} \qquad [10]$$

Where $a_0 = 6.12 \times 10^{-1}$, $a_1 = -1.78 \times 10^{-1}$, $a_2 = -1.15 \times 10^{-2}$, $a_3 = 3.28 \times 10^{-5}$, $a_4 = 1.67 \times 10^{-3}$ and, $b_1 = -3.12 \times 10^{-1}$, $b_2 = -1.59 \times 10^{-2}$, $b_3 = 9.82 \times 10^{-5}$, $b_4 = 2.15 \times 10^{-3}$

Note that in the original paper by (Muehleisen & Patrizi 2013) b_2 has a typo mistake which was later discussed and fixed in (Bre et al. 2018).

The previous sections provided the base to calculate wind pressure acting over the surfaces of the building. As a consequence of those external pressures, the internal pressure of the building is influenced. This effect is described in the following section.

Internal Pressure in Buildings

Finally, the wind-induced pressure across the building envelope can be found using the coefficient $C_{p(in-out)}$, which is defined as:

$$C_{p\,(in-out)} = C_p - C_{pi} \qquad [11]$$

Using equation [4] and equation [5] it is possible to calculate stack and wind pressure differentials acting over the building envelope, accounting for two of the three drivers for air infiltration. The last force that induces air infiltration, the mechanical effect, is discussed in the following section.

As mentioned in Section 2.2.1.2.3, if uniformly distributed leakage is assumed for all the walls, C_{pi} can be calculated by integration resulting in a value of -0.2 (ASHRAE Fundamentals 2017). For this research 0 and -0.2 are the values assumed.

Combination of Driving Forces

Airflows and pressure can be related by the commonly called power-law equation.

$$Q = c(\Delta P)^n \tag{[12]}$$

Where,

Q = Airflow through the opening [m³/s]

c = Flow coefficient [m³/(s·Pa^n)]

ΔP = Pressure differential [Pa]

n = Pressure exponent

Because of this nonlinear relationship between airflow and pressure, it is incorrect to add airflow rates due to different driving pressures. Walker & Wilson (1993) discuss empirical models to superpose the various driving forces that produce air leakage. They demonstrate that adding flows is strictly incorrect and that it is physically reasonable to add the pressures acting on the building.

Figure 3 shows a graphical representation of stack and wind driving pressures added together. Fig 3a corresponds to stack pressure with the NPL at mid-height. Fig 3b represents wind pressures of the same magnitude on the windward and leeward side. Finally, Fig 3c shows the addition of forces, in this figure, the wind pressure balance the stack effect, generating a zero pressure differential on the top windward side an on the bottom leeward side.

The relative importance of each driving force will depend on the factors affecting each of them. In the case of stack pressure, the affecting factors are: the temperature difference between indoor and outdoor, building height and internal resistance of the building to airflow. In the case of wind, the influencing factors are wind speeds and direction, local terrain, and immediate shielding of the building. Both driving forces are affected by the location of the leakage openings.
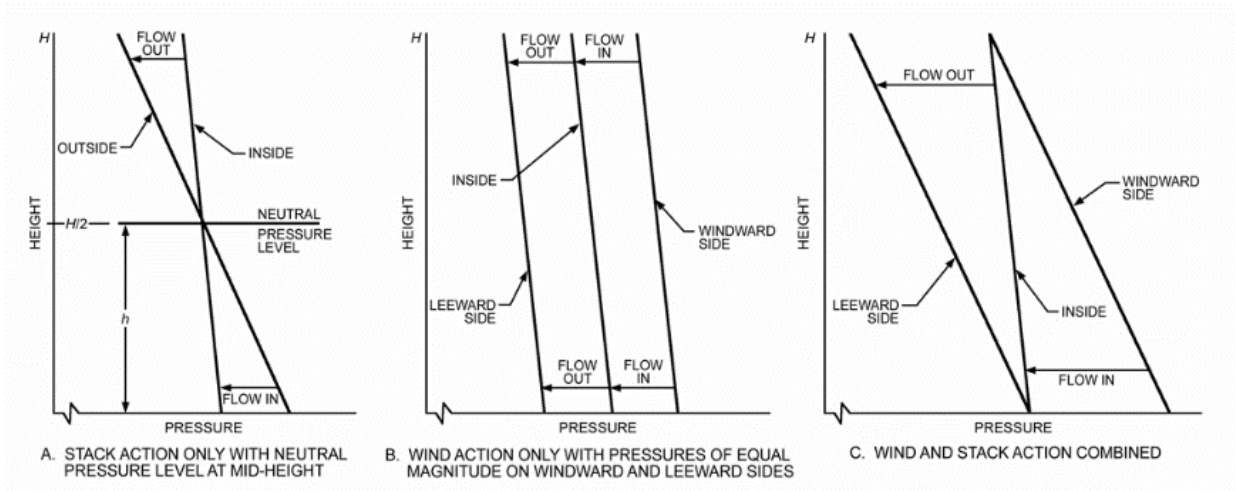
Figure 3: Distribution of Indoor and Outdoor Pressures over the height of the building. From (ASHRAE Fundamentals 2017)

Finally, equation 13 shows the total pressure differential that is considered in this study.

$$\Delta P_{Total} = \Delta P_s + \Delta P_w \qquad \text{[13]}$$

Where:

and,

ΔP_s is defined by equation [4]

$\Delta P_w = C_{p\,(in-out)} \cdot P_v$

In order to estimate total airflows, it is still necessary to determine the flow coefficient value (c in equation 12). The flow coefficient represents the efficiency of a crack or hole to allow fluid flow through it, but in terms of a whole building, the flow coefficient can be related to the level of airtightness of the building.

3.2 Performance Indicators for Hygrothermal Analysis

HAM models are usually used to compare different assemblies, but in order to make the comparison possible, some indicators need to be defined. Different hygrothermal performance indicators are found in literature, and different standards and guidelines define some thresholds for each of those parameters. The performance indicators used in this study are relative humidity, moisture content, and Mould index and are discussed in more detail in the following sections.

3.2.1 Relative Humidity

ASHRAE Standard 160 (2009) established the criteria for moisture performance evaluation using the relative humidity as the performance indicator. The following conditions are necessary to minimize mould growth:

a) 30-day running average of surface RH < 80% when the 30 day running average surface temperature is between 5°C and 40°C.

b) 7-day running average surface RH < 98% when the 7day running average surface temperature is between 5°C and 40°C

c) 24-hour running average surface RH < 100% when the 24 hour running average surface temperature is between 5°C and 40°C

Later, in the 2016 edition of the same standard the relative humidity criteria is replaced by the mould index that will be covered in Section 3.2.3.

3.2.2 Moisture Content

A safety margin of 20% Moisture content is indicated by ASHRAE Fundamentals (2017). Although wood decay requires moisture content at fibre saturation, around 30% moisture content, because wood moisture content varies widely depending on the location of the sample, moisture content of 20% indicates the possibility of fibre saturation at another point in the structure. Moreover, once established, decay fungi can generate water to allow its own growth, hence the importance of avoiding a moisture content of 20% or higher.

Finally, the presence of metallic fasteners and nails, given their high thermal conductivity are usually a cold spot where condensation can occur, and at a moisture content of 20% or more, corrosion of metallic fasteners is accelerated, therefore higher moisture content must be avoided.

3.2.3 Mould Index

According to ASHRAE Standard 160 (2016), mould criteria is usually the most restrictive in terms of hygrothermal performance. There are several models to evaluate mould potential, Vereecken & Roels (2012) and Gradeci, Labonnote, Time, & Köhler (2017) provide a complete bibliographical source. In principle, all models take into consideration the main factors that influence mould development, relative humidity higher than 70-80%, temperatures in the range of -5 °C to 50°C, and the time factor. The difference between models is mainly how the influencing factors are incorporated, and the relevance that they play in each model.

Amongst all models, two are widely known and applied, the VTT Mould Growth Index (Viitanen & Ritschkoff 1991) and the bio-hygrothermal IBP model included in the WUFI software family (Sedlbauer 2001). The VTT Mould Growth Index is an empirical model validated experimentally that describes the growth rate as a percentage of surface covered by mould with a six-value scale ranking the so-called Mould index. On the other hand, the bio-hygrothermal IBP model describes the growth of mould hyphen in mm dependent on ambient conditions.

Ojanen, Viitanen, Peuhkuri, Vinha, & Salminen (2010) improved the initial model by adding sensitivity classes for different materials usually employed in construction. Greater detail of the experiments that were carried out to improve the model can be found in a study by Viitanen et al. (2010)

H. Viitanen, Krus, Ojanen, Eitner, & Zirkelbach (2015) compared the two models and developed a conversion function between the models. They highlighted that the main difference between the models is that under unfavourable conditions the VTT model presents retrogressive growth and the IBP model presents zero growth, and more importantly, that the VTT limits the mould growth to a climate-dependent maximum value, whereas the IBP model allows continuous growth given that the climatic conditions are appropriate. Another proposition included in the study is the inclusion of a colour classification for the risk evaluation, according to the author's experience.

For surfaces that are not in direct contact with the interior air, a three-colour scheme is proposed, where green (negligible risk) is up to a mould index of 2, yellow (the user should decide if it is acceptable or no) is up to a mould index of 3, and finally, red (unacceptable) for a mould index higher than 3.

ASHRAE Standard 160 (2016) adopts the VTT model as its moisture performance evaluation criteria and implements the Mould index value of 3 as the threshold for rejection of an assembly.

Furthermore, the VTT model is easier to implement in a calculation sheet or a programming language as it is based on simple equations that must be accumulated for each time-step.

The calculation of the VTT Mould index can be done by following the steps described in ASHRAE Standard 160 (2016) and transcribed here:

i.   Select a sensitivity class from Table 3.
ii.   The initial mould index is zero (M=0 at time t=0).
iii. The mould index for the next step is accumulated with the next equation:

$$M_t = M_{t-1} + \Delta M \qquad\qquad [14]$$

Where,

M_t = Mould index for the current time-step

M_{t-1} = Mould index for the previous time-step

ΔM = Mould increment calculated according to equation [17]

iv.   If the surface temperature is greater than 0 at the current time-step, then the critical relative humidity is calculated using equations [15] or [16] depending on the material sensitivity class selected. Figure 4 show both equations.

Very Sensitive or Sensitive Class:

$$RH_{crit} = \begin{cases} -0.00267 \cdot T_s^3 + 0.16 \cdot T_s^2 - 3.13 \cdot T_s + 100 \ when \ T_s \leq 20°C \\ 80 \ when \ T_s \leq 20°C \qquad [T_s \ in \ °C] \end{cases} \qquad [15]$$

Medium Resistant or Resistant Class:

$$RH_{crit} = \begin{cases} -0.00267 \cdot T_s^3 + 0.16 \cdot T_s^2 - 3.13 \cdot T_s + 100 \ when \ T_s \leq 7°C \\ 85 \ when \ T_s \leq 7°C \qquad [T_s \ in \ °C] \end{cases} \qquad [16]$$

Figure 4 shows the critical relative humidity as a function of the surface temperature.
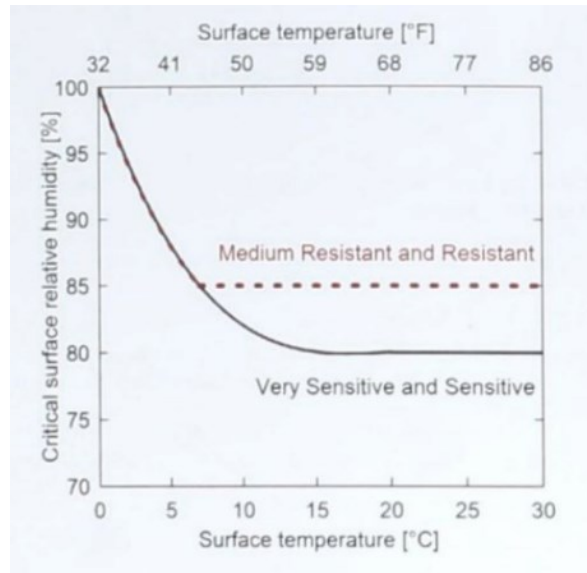
Figure 4: Critical surface relative humidity as a function of surface temperature for different material sensitivity classes. Source
ASHRAE Standard 160 (2016)

v.   If the relative humidity of the surface is higher than the critical relative humidity, then an increase in the mould index is calculated according to equation [17].

$$\Delta M = \frac{k_1 \cdot k_2}{168 \cdot \exp(-0.68 \cdot \ln(T_s) - 13.9 \cdot \ln(RH_s) + 0.14 \cdot W + 66.02)} \qquad [T_s \ in \ °C] \quad [17]$$

vi. The factor k_1 is selected from Table 4, and factor k_2 is calculated according to equation [18].

$$k_2 = max \begin{cases} 1 - \exp[2.3 \cdot (M - M_{max})] \\ 0 \end{cases} \qquad \text{[18]}$$

Where, M_{max} is the maximum mould index corresponding to the surface temperature and relative humidity at the current time-step, calculated using equation [19].

$$M_{max} = A + B \cdot \left(\frac{RH_{crit} - RH_s}{RH_{crit} - 100}\right) - C \cdot \left(\frac{RH_{crit} - RH_s}{RH_{crit} - 100}\right)^2 \qquad \text{[19]}$$

Where the coefficients *A, B,* and *C* are selected from Table 3 according to the sensitivity class.
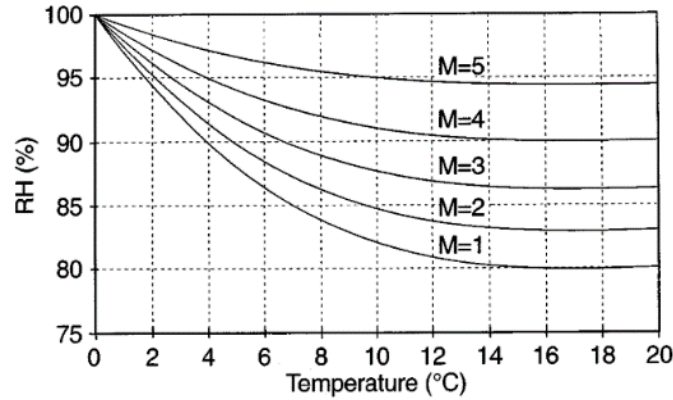
Figure 5: Temperature-dependent critical relative humidity needed for mould growth at different values of mould index. The curves are generated by solving eq. [19] for a known value of Mmax. Source (Hukka & Viitanen 1999)

vii.   If the conditions are not favourable for Mould, i.e. $T_s \leq 0$ or $RH_s \leq RH_{crit}$ then a decrease in the mould index is calculated according to equation [20]

$$\Delta M = \begin{cases} -0.00133 \cdot k_3 & when \ t_{decl} \leq 6 \\ 0 & when \ 6 < t_{decl} \leq 24 \\ -0.000667 \cdot k_3 & when \ t_{decl} > 24 \end{cases} \qquad \text{[20]}$$

Where,

k_3 = Mould index decline coefficient specific to the material.

t_{decl} = Cumulative number of hours from the moment when conditions change from favourable ($T_s > 0°C$ and $RH_s > RH_{crit}$) to unfavourable ($T_s \leq 0°C$ or $RH_s \leq RH_{crit}$)

The recommended value for k_3 is 0.1 representing materials that exhibit little mould growth, while a value k_3 of 0.25 is representative of materials that exhibit a higher growth rate and reflects the dynamic characteristic of the mould index. The mould index should always be a positive value, if after calculating the mould index value using equation [14] the value is negative, then the mould index has to be set to 0.

Table 3: Description of Sensitivity Classes

Sensitivity Class	Materials
Very sensitive	Untreated wood; includes lots of nutrients for biological growth
Sensitivity	Planed wood, paper coated products, wood-based boards
Medium resistant	Cement or plastic based materials, mineral fibers
Resistant	Glass and metal products, materials with efficient protective compound treatments

Table 4: Coefficients depending on Sensitivity Class of material

Sensitivity Class	k_1 if M < 1	if M ≥ 1	W	A	B	C
Very sensitive	1	2	0	1	7	2
Sensitive	0.578	0.386	1	0.3	6	1
Medium resistant	0.072	0.097	1	0	5	1.5
Resistant	0.033	0.014	1	0	3	1

4 Parametric Study

The following section describes the parametric study that was used for the simulation experiment. This parametric study featured the following aspects to reach the objectives of this research:

- Consider diverse levels of assembly air tightness.
- Included different levels of wind pressure, taking into account distinct types of terrains.
- Study different wind conditions (speed and direction), which is done by studying five different cities.
- Evaluate the orientation that produces the highest wind pressure and a North oriented wall, which is the standard for hygrothermal performance.
- Assume different levels of insulation.
- Integrate a range of air cavity ventilation values.
- Consider the internal pressure of the building.

Four *RSI* values, two different orientations, and four cavity *ACH* rates are combined to generate 32 reference cases per city. These cases are tight, meaning that they do not consider any air exfiltration. These reference cases then, represent the vapour diffusion effect.

Afterwards, stack pressures are used in the Air Infiltration Model to create results that would represent the actual standard of calculation (actual practice). For each of the 32 tight cases, three different air infiltration standards are applied, generating a total of 96 cases per city.

Finally, using total pressure differentials, it is possible to calculate q_{cl} and S_w according to the Air Infiltration Model to include the effect of wind over the hygrothermal performance of the wall.

Given the large number of variables (parameters) considered, a programming language will be used to create and run the simulations.

DELPHIN is a HAM simulation software that provides the possibility of accessing the model file in text format, enabling the option of using Python to automatically create and run the simulations while dynamically modifying the required parameters.

4.1 Selection of Cities

Five cities are selected to evaluate the effect of wind-induced pressure over hygrothermal performance. The cities are chosen for having different annual mean wind speeds, different wind direction distribution, and have weather cold enough to have moisture condensation on the wall sheathing, therefore only cities located in ASHRAE zone 5 or higher are considered. Table 5 shows the mean, standard deviation, and the maximum wind speed obtained from TMY weather files for the five selected cities.

Table 5: Mean Wind Speeds for each city. Data from TMY files.

	Wind Speed [m/s]				
	St. Johns	Rochester	Chicago	Montreal	Vancouver
Mean	6.1	5.7	4.6	4.1	3.2
Std.	3.3	2.7	2.3	2.5	2.2
Max.	21.6	19.1	15.4	15.5	13.6

All the selected cities are under categories 5 or 6 according to ASHRAE 90.2 (2002)

Table 6: ASHRAE 90.2 (2002) Climate Zone

City	ASHRAE Climate zone (ASHRAE 90.2)
Chicago (IL, US)	5
Montreal (QC, CA)	6
Rochester (MN, US)	6
St. Johns (NF, CA)	6
Vancouver (BC, CA)	5

To further describe and analyze the wind characteristics of each city, a wind rose plot is utilized. In each plot, the wall orientation that is subject to the highest total wind negative pressure is shown. To facilitate the visualization, and to emphasize that the wall direction maximizes wind pressures that generate suction, the wind roses are rotated, and show contrary to standard the direction where wind blows to. Additionally, the inner circles in the wind roses show the percentage of time that wind blows in a particular direction.
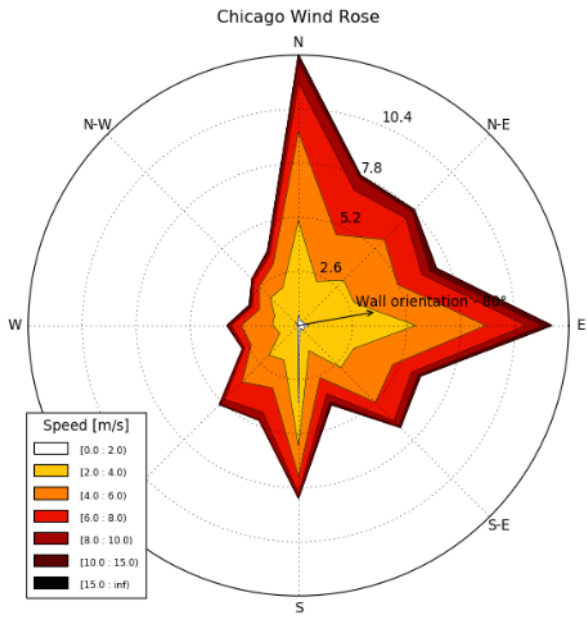
Figure 6: Chicago Wind Rose
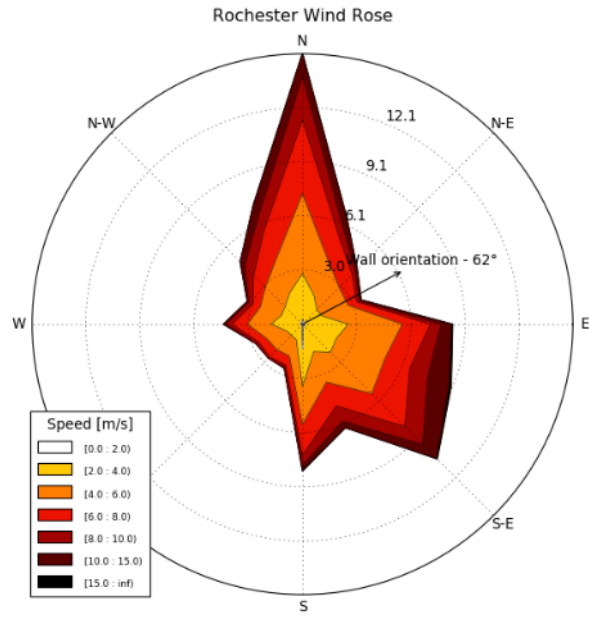
Figure 7: Rochester Wind Rose
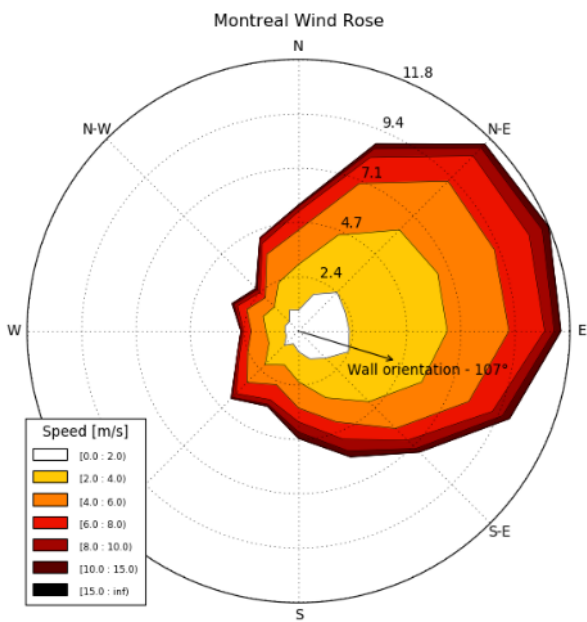
Figure 8: Montreal Wind Rose
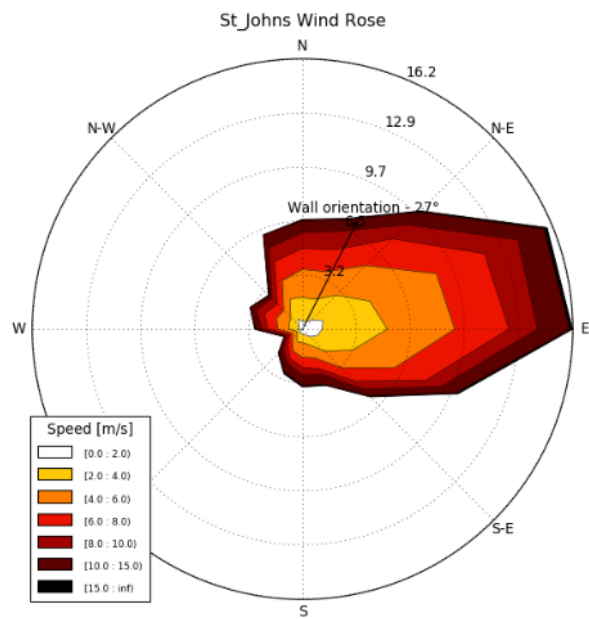
Figure 9: St. Johns Wind Rose
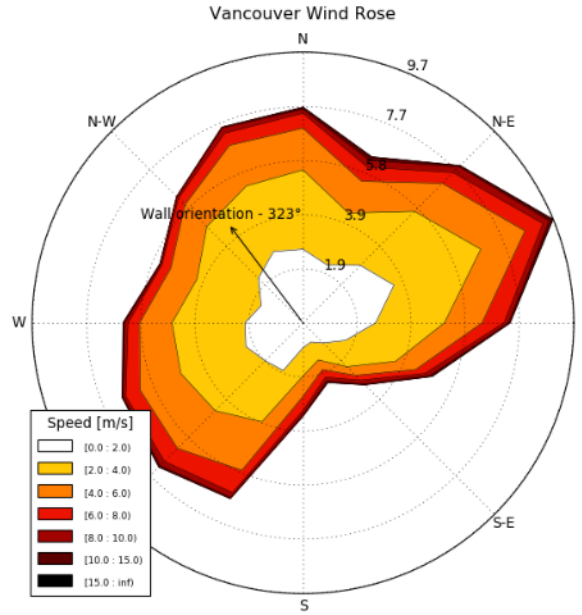
Figure 10: Vancouver Wind Rose

4.2 Moisture Leaks

The previous sections defined the pressure differentials acting over the building envelope, but the infiltration rate is also defined by the airtightness of the building. In other words, two different buildings subject to the same pressure differential can have different infiltration rates depending on their level of airtightness. Some energy and hygrothermal standards are reviewed in the following paragraphs.

As mentioned before, airtightness is critical for energy conservation and hygrothermal performance, and since insulation levels continually increase striving for better energy performance, higher is the relative importance of airtightness. Hence, several Guidelines and Standards for airtightness have been created and are being used by the construction and engineering industry. Table 7 shows some of the most common standards and Guidelines:

Reference	Whole Building Rates per m2 of Exterior Envelope	
	m³/(h·m²) @ 50 Pa	L/(s·m²) @ 75 Pa
ASHRAE Fundamentals - Chapter 16, Tight Building (2013)	1.4	0.5
U.S. Army Corps of Engineers (2012)	3.5	1.27
National Energy Code for Buildings 2011 (Sentence 3.3.4.9.(6) and 8.4.3.4.(3))	4.0	1.45
ASHRAE Fundamentals - Chapter 16, Average Building (2013)	4.1	1.5
Air Barrier Association of America's recommendation (2016)	5.5	2
ASHRAE 90.1-2013 (Sentence C.3.5.5.3)	5.6	2.03
ASHRAE Fundamentals - Chapter 16, Leaky Building (2013)	8.3	3

Above mentioned are standards for energy conservation and efficiency measures which consider the leakages through the whole building, meaning cracks, windows, doors, penetrations for services, or other paths for air to leak through. But not all the air leaking represents a potential moisture problem. Figure 11 represents two different paths for air leakage with distinct consequences:

High airflow and direct flow path.
The flow path is warmed and air do
not lose enough temperature.
Low potential for condensation.

Slow airflow and indirect flow path.
Allows air to lose temperature.
High potential for condensation
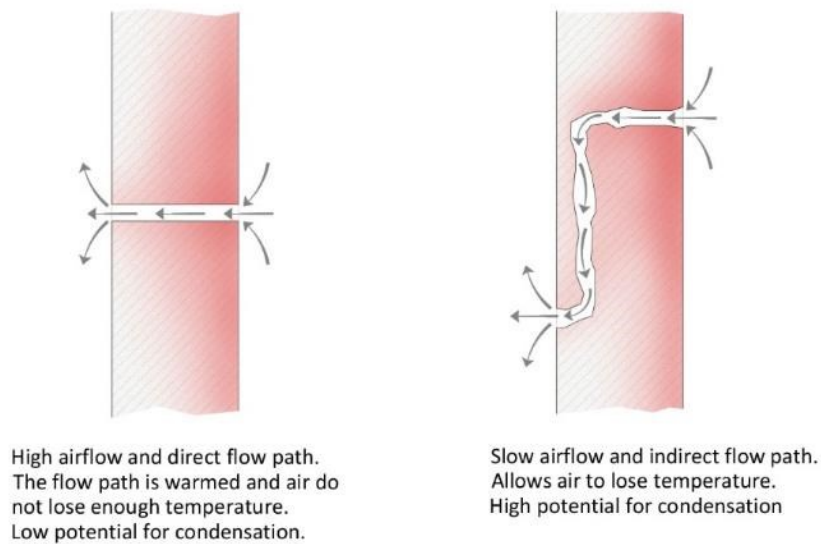
Figure 11: Graphical representation of the moisture and energy leaks. Adapted from (Künzel, Zirkelbach, & Schafaczek 2011)

On the left, a direct path for airflow represents an energy leak where the flow path is warmed by the indoor air leaking, thus reducing the possibilities of condensation. On the right, a tortuous flow path allows for air to cool down and condensate. Hence, the necessity of standards specific for hygrothermal performance, where the object of assessment is a component of the whole building, commonly the roof or walls, and not the whole building.

ASHRAE Standard 160 (2016) indicates that if the airtightness of the envelope is known, that airflow should be used to calculate the air flow rate through the envelope. If the airtightness is not known, then an air leakage rate of 0.016 L/sm^2, or 0.084 L/sm^2 should be used for airtight and standard construction respectively. Those values are based on the minimum leakage rate for an air barrier and rigid sheathing at 5 Pa. Nevertheless ASHRAE Standard 160 (2016) does not specify exactly how to deal with the airflow

A study by Zirkelbach, Künzel, Schafaczek, & Borsch-Laaks (2009) mentions three classes for building airtightness, measured as Air Changes per hour at 50 Pa differential (n_{50}) or as m^3 per hour per m^2 of envelope at 50 Pa differential (q_{50}). Class A corresponds approximately to the future requirement of DIN 4108 Part 7 (DIN 2011) for a building with controlled ventilation with heat recovery ($n_{50} = 1.0$ [1/h], or $q_{50} = 1$ [m^3/hm^2]) and Class B reflects the minimum requirements of the bonus scheme of the German EnEV (Germany 2013) for an airtight building ($n_{50} = 3.0$ [1/h] or $q_{50} = 3$ [m^3/hm^2]). Class C corresponds approximately to the aforementioned North American requirement according to (J. W. Lstiburek 2005) ($n_{50} = 5.0$ [1/h] or $q_{50} = 5$ [m^3/hm^2]). Zirkelbach proposed a factor of 1/15 for the airtightness of the wall component, obtaining component airflow rates of q_{50} equals 0.07, 0.2 and 0.33 [m^3/hm^2] for class A, B and C respectively.

Additionally, other standards specify maximum airflow rates for materials, assemblies, and buildings such as the Air Barrier Association of America (ABAA) (Air Barrier Association of America 2009) in its point 1.4 – Performance Requirements:

 a. Materials: Materials used for the air barrier system in the opaque envelope shall have air permeance not to exceed (0.02 $L/s.m^2$ @ 75 Pa).

 b. Assemblies of materials and components: shall have air permeance not to exceed (0.2 $L/s.m^2$ @ 75 Pa).

 c. The entire building: The air leakage of the whole building shall not exceed 2.0 $L/s.m^2$ @ 75 Pa) when tested according to ASTM E 779.

Several studies validate or agree with the airflow rates mentioned above. Salonvaara, Karagiozis, & Corning (2013) studied a double stud wall using a Two-Dimensional heat, air, and moisture simulation, with airflow through the cavity based on detailed air leakage characteristics of joints between wall components by Wolf & Tyler (2013a). They determined that there is no need for a stricter air tightness Standard for assemblies than that established by the Air Barrier Association of America (ABAA) (Air Barrier Association of America 2009). It is worth noting that 0.2 L/s.m^2 @ 75 Pa correspond to approximately 0.034 L/s m^2 (using n = 0.65) at 5 Pa which is comparable to the values indicated in ASHRAE Standard 160 (2016). Uvslokk (1996) mentions that the Norwegian Building Research Institute (NBI) recommends an upper limit for air permeance of wind barriers, including joints, of 0.05 m^3/m^2 h Pa (1.4 10^{-5} m3/m2 s Pa). Tuomo Ojanen (1993) as referenced in Uvslokk (1996), concluded the following upper limits for the air permeance of wind barriers:

- 0.036 m^3/m^2 h Pa (1.0 10^{-5} m^3/m^2 s Pa), if strong corner convection is possible. Or,
- 0.09 – 0.11 m^3/m^2 h Pa (2.5-3.0 10^{-5} m^3/m^2 s Pa), if the thermal insulation of the structure is divided into separate structures

Table 8 presents a summary of standards for Component air leakage rates.

Table 8: Moisture Leakage Standards (Component Leakage)

Reference	Component Rates		
	m³/(h·m²) @ 50 Pa	L/(s·m²) @ 75 Pa	L/(s·m²) @ 5 Pa
Class A (Zirkelbach et al., 2009)	0.07	0.025	0.004
Class B (Zirkelbach et al., 2009)	0.20	0.072	0.013
ASHRAE 160 Tight	0.256	0.093	0.016
Class C (Zirkelbach et al., 2009)	0.33	0.119	0.021
The Air Barrier Association of America (ABAA)	0.554	0.20	0.034
ASHRAE 160 Standard	1.350	0.488	0.084

The k_{cl} used in this study corresponds to ASHRAE 160 Standard, ASHRAE 160 Tight and class C. These values mentioned for class C are incorporated in the WTA guideline 6-2 from the Scientific-Technical Association for Building Conservation and Historic Preservation (WTA for

its German acronym) ("WTA" n.d.) as described by Künzel (2014) and referred as k_{cl} WTA in the following sections.

4.3   Pressure Differential Calculation

4.3.1   Stack Pressures

As mentioned in section 2.2.1.1, stack pressures depend on the temperature difference between indoor and outdoor air and the height of the connected air volume in the building. In this research, a height of 6 m was used to calculate the stack pressure; this represents approximately a two-story building height. The following figure present the outdoor temperature for the five cities selected.
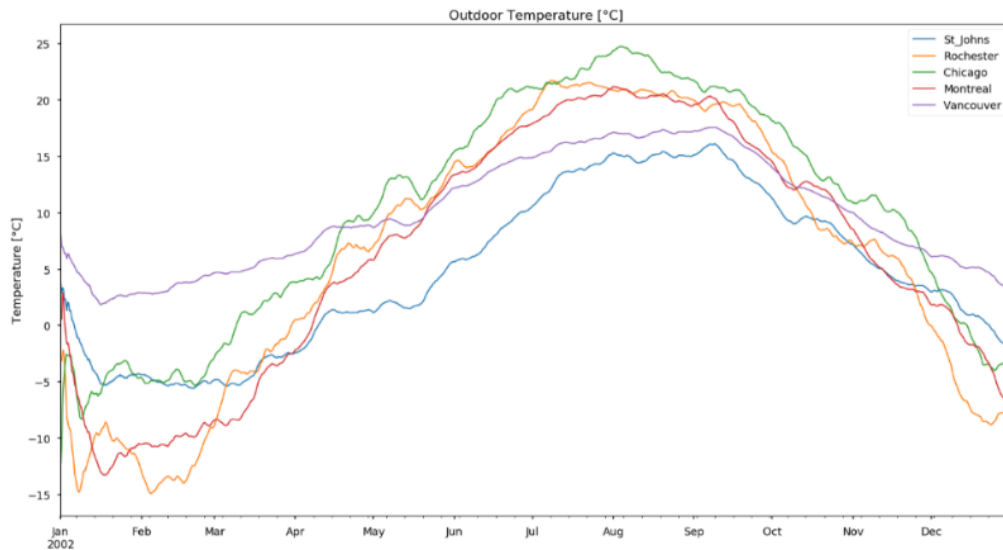
Figure 12: Outdoor Temperature for selected cities

Cities with higher variations in outdoor temperatures, like Rochester or Montreal, will show higher variations in stack pressures. While cities with milder weather, like Vancouver, present lower variations in stack pressures as it can be seen in the following table.

Table 9: Mean stack pressure for each city

City	Stack Pressure [Pa]			
	mean	max	min	Std.
Rochester	-1.99	0	-7.4	1.5
Montreal	-1.98	0	-6.4	1.4
Chicago	-1.59	0	-5.6	1.2
St. Johns	-2.09	0	-4.9	1.0
Vancouver	-1.47	0	-3.4	0.6

4.3.2 Wind Pressure

Sheltering level.

As described in section 2.2.1.2 for low-rise buildings the terrain roughness accounts for a significant fraction of wind sheltering. Hence, no additional sheltering factors will be considered for the simulations. The assumption will limit the validity of cases such as low-rise buildings closely surrounded by tall trees or high rise buildings but will provide a good estimation for most general situations.

As shown in Table 2 in section 2.2.1.2, four terrain categories are defined. In this study, all the categories are simulated, providing a broad range of wind pressures for each city.

Selection of *Cp* Model and *S* Ratio and Wall Orientation

Section 3.1 presented two different parametric models available to calculate C_p coefficients. Both models take into account the wind angle of incidence and the depth to width ratio of the building. This section discusses the selection of the model and the S ratio to perform the following analysis.

The following figure shows both models with different S ratios of 1/2.5, 1/1.5, 1, 1.5, and 2.5 for different angles of incidence. It can be seen that the models follow a similar trend.
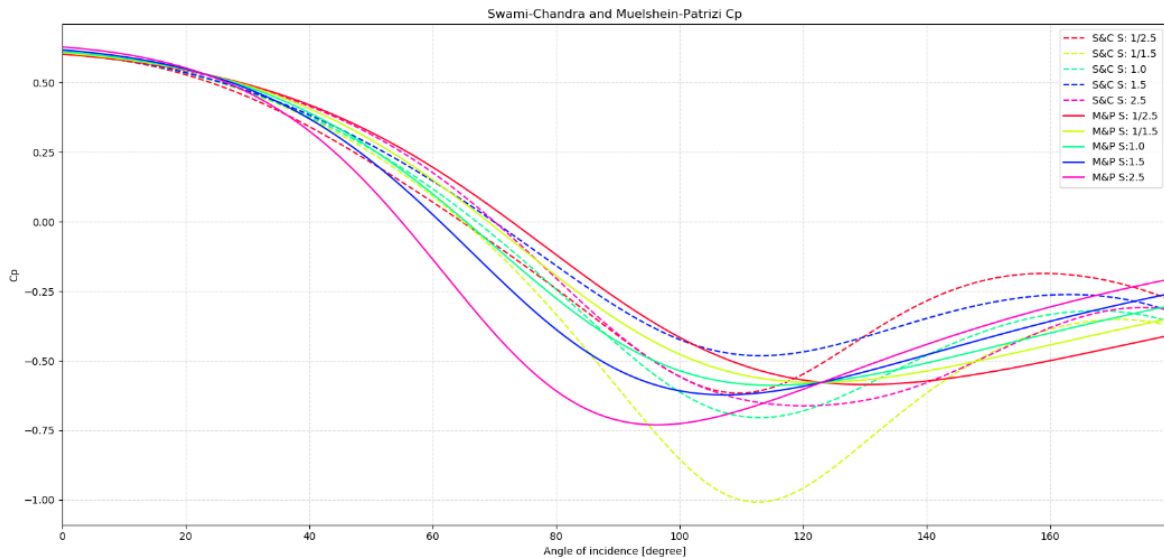
Figure 13: Parametric models for surface-averaged C_p for walls

A preliminary analysis is done to evaluate the wall orientation that generates the highest negative pressures; this is done by optimizing the angle of incidence of the wall for each of the two models and five different S ratios: 1, 0.67, 0.4 1.5 and 2.5. For each model and S ratio the hourly pressures obtained are added. The minimum total pressures for a year is found by solving the optimization problem with the wall orientation as the only variable. Adding the pressures acting on the wall during the year allows to estimate which orientation is subject to the highest mean exfiltration.

For each of the cities, models, and S ratios, the resulting maximum negative annual pressures and the wall orientation that produces it, are shown on Table 10 for the maximum wind pressure orientation, and Table 11 for the North orientation. In both tables the maximum negative wind pressures and the orientations that produces it is coloured red, and the minimum negative wind pressure and the orientations that produces it is coloured blue.

Table 10: Total annual pressure for each model, S, and maximum pressure orientation, for terrain category 1.

Orientation		Maximum. Wind Pressure Orientation									
Model		S&C					M&P				
S		1.0	0.67	0.4	1.5	2.5	1.0	0.67	0.4	1.5	2.5
St. Johns	Orientation	33	27	22	55	38	42	48	53	33	19
	Pressure [Pa]	-11,935	-16,704	-8,366	-7,849	-12,274	-11,711	-11,808	-12,183	-11,927	-13,084
Rochester	Orientation	62	62	62	62	63	63	63	64	63	63
	Pressure [Pa]	-12,401	-17,559	-9,640	-8,112	-12,138	-11,491	-10,928	-10,464	-12,318	-14,008
Chicago	Orientation	80	80	88	80	80	86	83	75	96	106
	Pressure [Pa]	-6,159	-8,703	-4,423	-3,928	-6,075	-5,855	-5,731	-5,769	-6,221	-7,326
Vancouver	Orientation	327	323	327	329	325	325	328	334	324	323
	Pressure [Pa]	-2,403	-3,673	-1,758	-1,286	-2,219	-2,308	-2,062	-1,876	-2,687	-3,509
Montreal	Orientation	105	107	107	102	103	103	99	96	106	115
	Pressure [Pa]	-5,879	-8,137	-4,226	-3,875	-5,894	-5,708	-5,643	-5,692	-5,915	-6,546

	Orientation	North Orientation									
	Model	S&C					M&P				
	S	1.0	0.67	0.4	1.5	2.5	1.0	0.67	0.4	1.5	2.5
St. Johns	Orientation	0	0	0	0	0	0	0	0	0	0
	Pressure [Pa]	-9,988	-14,712	-7,452	-5,930	-9,496	-9,371	-8,719	-8,220	-10,370	-12,486
Rochester	Orientation	0	0	0	0	0	0	0	0	0	0
	Pressure [Pa]	-3,451	-5,576	-1,758	-1,351	-3,147	-3,546	-3,385	-3,427	-3,978	-5,240
Chicago	Orientation	0	0	0	0	0	0	0	0	0	0
	Pressure [Pa]	-3,778	-5,744	-2,479	-1,996	-3,576	-3,595	-3,430	-3,372	-3,923	-4,745
Vancouver	Orientation	0	0	0	0	0	0	0	0	0	0
	Pressure [Pa]	-2,153	-3,383	-1,418	-1,064	-2,038	-2,045	-1,897	-1,802	-2,296	-2,870
Montreal	Orientation	0	0	0	0	0	0	0	0	0	0
	Pressure [Pa]	-3,109	-5,047	-2,005	-1,414	-2,936	-2,913	-2,663	-2,488	-3,318	-4,223

It is worth noting that the terrain category selected does not change the orientation that produces the maximum negative wind pressure. Of course, the annual pressures increase with higher terrain categories, but the ranking for the models, S ratio and the orientation are the same.

It is also noticeable that for the case of maximum wind pressure orientation, the orientation of the wall does not differ too much by changing the model or the S ratio. For St Johns the orientations that maximize the negative pressures are between 19° and 55° across all S ratios and the two models, representing the highest range of variation. For Rochester the wall orientations range from 62° to 64°. For Chicago, between 75° and 106° for the M&P model, but varies only between 80° and 88° for the S&C model. In Vancouver the wall orientation varies between 323° and 329°, and finally for Montreal the variation is between 102° and 115°.

It is important to notice that varying the S ratio can reduce the annual pressure by about 55% in the case of S&C for the maximum wind pressure orientation and by 68% for North orientation. M&P offers less variation for the S ratio selected being about 25% for maximum wind pressure and 35% for North orientation. In order to evaluate the maximum possible effects of wind, the S&C model with S=0.667 is considered for the rest of the analysis.

Table 12 shows the mean wind pressure for each city, both wall orientations (θ_w) and both C_{pi}

Table 12: Mean wind pressures

| City | θ_w | Maximum Wind Pressure | | | | | | | | North | | | | | | | |
| | C_{pi} | -0.2 | | | | 0 | | | | -0.2 | | | | 0 | | | |
	T_{cat}	1	2	3	4	1	2	3	4	1	2	3	4	1	2	3	4
Chicago		-0.5	-1.5	-3.1	-4.4	-1.0	-2.8	-6.0	-8.6	-0.2	-0.5	-1.0	-1.5	-0.7	-1.9	-4.0	-5.6
Montreal		-0.5	-1.4	-3.0	-4.3	-0.9	-2.7	-5.6	-8.0	-0.1	-0.4	-0.9	-1.3	-0.6	-1.6	-3.5	-5.0
Rochester		-1.3	-3.6	-7.6	-10.9	-2.0	-5.7	-12.1	-17.3	0.1	0.3	0.6	0.9	-0.6	-1.8	-3.8	-5.5
St_Johns		-1.0	-2.9	-6.2	-8.8	-1.9	-5.5	-11.5	-16.4	-0.8	-2.3	-4.8	-6.9	-1.7	-4.8	-10.1	-14.5
Vancouver		-0.1	-0.4	-0.8	-1.2	-0.4	-1.2	-2.5	-3.6	-0.1	-0.3	-0.6	-0.9	-0.4	-1.1	-2.3	-3.3

Notice Rochester for North orientation and C_{pi} = -0.2 with mean positive pressures, meaning that for this orientation the wind effect produces infiltration, thus reducing the stack effect exfiltration. The positive pressures are produced by winds blowing in the S-E direction as can be seen in the wind rose in Figure 7.

4.3.3 Total Pressure Differential

The previous sections showed the steps followed to calculate stack and wind pressures. This section shows the results after adding them and deleting positive pressures in the outcome; this is done to consider only exfiltration across the wall.

The mean values for the total pressure are presented in the following table.

Table 13: Mean Total Pressure for C_{pi} and Orientation

| City | θ_w | Maximum Wind Pressure | | | | | | | | North | | | | | | | |
| | C_{pi} | -0.2 | | | | 0 | | | | -0.2 | | | | 0 | | | |
	T_{cat}	1	2	3	4	1	2	3	4	1	2	3	4	1	2	3	4
Chicago		-2.2	-3.7	-6.2	-8.3	-2.7	-4.8	-8.5	-11.6	-1.9	-2.9	-4.8	-6.4	-2.3	-3.9	-6.8	-9.2
Montreal		-2.6	-3.8	-6.0	-7.9	-3.0	-4.9	-8.2	-10.9	-2.3	-3.2	-5.0	-6.4	-2.6	-4.1	-6.7	-8.9
Rochester		-3.3	-6.1	-11.1	-15.1	-4.0	-8.0	-14.9	-20.5	-2.2	-3.1	-5.1	-6.8	-2.7	-4.6	-8.0	-10.8
St. Johns		-3.4	-6.1	-11.0	-14.9	-4.1	-8.2	-15.3	-21.0	-3.2	-5.8	-10.3	-14.0	-3.9	-7.7	-14.3	-19.7
Vancouver		-1.7	-2.3	-3.4	-4.3	-1.9	-2.9	-4.6	-6.0	-1.7	-2.2	-3.4	-4.3	-1.9	-2.8	-4.6	-6.0

It is possible to observe that most of the values on Table 13 are within the range of estimated and measured operational pressures for buildings, which is generally estimated to be about 5 [Pa]. A study by Kalamees et al. (2010) for example measured pressures in a detached house and found that on average pressures ranged from 1 to 7 [Pa] at the ceiling level of the top floor and in the range of -3 to -15 [Pa] at the floor level of the ground floor.

4.4   Ventilated Air Cavity and Rain-screen

The idea behind the pressure equalized rain-screen (PER) has been discussed since the first half of the '60s (Birkeland 1962; Garden 1963) as referenced by Burgess & McCardle (2000) and Salonvarra, Karagiozis, Pazera, & Miller (2007). The objective of a PER is to allow for rapid equalization of wind pressure acting over the cladding and the pressure on the cavity and thus diminishing the risk of raindrops being carried toward the interior cavity. Hence, most of the pressure acting on the rain-screen will be transferred towards the air barrier assembly, which is designed and structurally supported to transmit peak and sustained wind loads towards the structural elements of the building (Quirouette 1985). A field study by Ganguli & Dalgliesh (1988) measured pressure difference across air barrier and rain-screen assembly of precast wall panels of a 27-story office building in downtown Montreal and confirmed that most of the wind pressure acting on the cladding is transmitted to the air barrier.

Although the PER concept has been in use for a long time, there are still many unknowns regarding several parameters related to wind and building pressurization that affect the pressure equalization performance. As mentioned by Kumar (2000), one particular area that needs research is the prediction of the cavity pressures. The specific design of the rain-screen will dictate how effective and responsive the pressure equalization is to the fluctuating pressures of wind.

In this study, it is assumed that the Pressure equalized rain-Screen is perfect, which means that the pressure acting on the rain-screen is precisely the same as that on the air barrier.

Although it has been shown that the presence of a Cavity Ventilation behind the rain screen improves the moisture removal in the wall, the significant deviation in the cavity air exchange rate used in numerical simulation makes the modelling uncertain.

The rate of air cavity ventilation fond in studies range from 1.5 to 500 *ACH*, in most cases, with extreme values of up to 1500 *ACH*. Air Cavity rates in Brick Veneer is in the lower values of the range, between 1.5 and 6 *ACH*, and walls with board sheathing in general ranging between 50 and 500 *ACH*.

Stovall & Karagiozis (2004) developed a parametric model to estimate cavity ventilation rates depending on temperature and wind speeds for brick walls. The study shows values of *ACH* for the cavity ventilation between 50 and 400 *ACH* for winds up to 4 m/s. Additionally, they found that there is no significant difference in ventilation rates when the cavity depth varies from 19 mm to 50 mm. Finally, they found that the ventilation slot size is the controlling factor of the airflow rate for the cases studied, with the airflow varying proportionally to the slot height. Langmans, Desta, Alderweireldt, & Roels (2015) found that 70% of the time the cavity ventilation rate was between 160 and 616 *ACH* for walls with siding and between 1.7 and 6 *ACH* for Brick veneer walls. Van Belleghem, Steeman, Janssens, & De Paepe (2015) evaluated three inlet air velocities of 0.1, 0.2, and 0.3 m/s which correspond to ventilation rates of, 144, 288 and 432 *ACH* respectively, and mention that ventilation velocities of 0.1 m/s or higher, are rare in brick veneer cavity walls.

Karagiozis & Künzel (2010) found that measured velocities on the leeward side were lower but more constant than those measured on the windward side of the building. Simpson (2010) Monitored hygrothermal variables in twelve wall specimens with different cavity ventilation characteristics and used those measurements to predict average *ACH* rates on the cavity walls. The results showed that the average predicted *ACH* for Brick veneer is around 5 *ACH* and between 90 and 320 for walls with fibre cement board. Lepage, Schumacher, & Lukachko (2013) simulated High R-Value walls with fibre cement cladding using *ACH* 20 in the air cavity. Falk, Molnár, & Larsson (2014) simulated sheathing drying times for two different ventilation rates of 284, 101 and concluded that there is practically no difference in the drying time when the average ventilation rate is higher than 100 *ACH*. In a study of the ventilation drying process, Falk & Sandin (2013) measured cavity *ACH* rates in the range 75-310. Fox (2014) used a ventilation rate ranging from 0 to 400 *ACH* for simulations and to determine which average rate best approximated the measured data obtained in experiments.

Finally, Vanpachtenbeke, Langmans, Roels, & Van Acker (2015), remark contradicting studies, some of them favouring the presence of cavity ventilation and others questioning its effectiveness to improve the drying of the wall. Furthermore, it is also discussed the considerable variability on the *ACH* rates assumed in different studies and pointed to the evident need of including a variable ventilation rate for the simulation that takes into consideration the physical complexity of the process to allow a correct implementation in HAM simulations.

All the studies presented in this section permit to assume that the airflow rate on the ventilation cavity can be within the range of 0 to 300 *ACH*. For this thesis 4 values will be assumed for the ACH_{cav} parameter 0, 10, 100 and 300 *ACH*.

4.5   Wall Assembly

A wood frame wall with mineral wool insulation in the cavity is used to evaluate the effect of wind on the hygrothermal performance. Figure 14 illustrates the simulated wall:

Cement Board 8 mm
Air gap 25 mm
WRB (Tyvek)(sd = 0.088)
OSB 11 mm
Mineral Wool (variable)
PE-foil 6 mils (sd=55.8)
Gypsum Board 13 mm
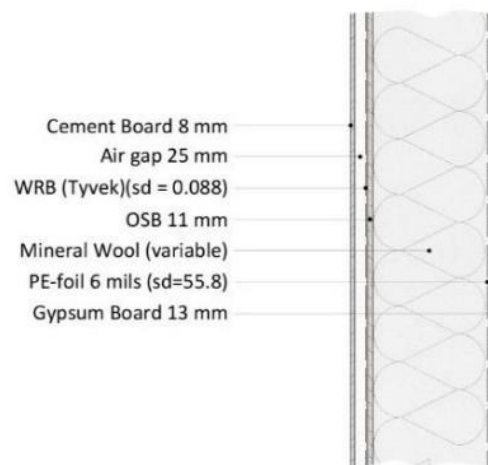
Figure 14: Wall Section and material layers

4.5.1 Material Properties

Material properties are obtained through the DELPHIN material database that is available within the software.

Table 14: Material properties

Material	Thickness	Thermal conductivity	Moisture storage function					Water vapor resistance factor	Density	Open porosity	Water absorption coefficient
	[mm]	λ [W/m·K]	ω [kg/m³]					μ [-]	ρ [kg/m³]	[m³/m³]	A_w [kg/m²·s^{0.5}]
			RH: 33	55	75	97	99				
Cement Board	8	0.313	25.9	38.7	66.4	133.3	136.1	26.4	1158.7	0.6	0.014
Air Gap	25	0.138	-	-	-	-	-	0.4	1.3	1.0	-
WRB (Tyvek) (sd=0.088)	-	-	-	-	-	-	-	470.0	-	-	-
OSB	11	0.130	62.6	75.6	90.6	153.1	198.5	165.0	595.0	0.9	0.002
Mineral Wool	120 240 314 420	0.040	0.2	0.3	0.3	0.5	600.2	1.0	134.0	0.9	-
PE-foil 6 mils (sd=55.8)	-	-	-	-	-	-	-	366141.7	-	-	-
Gypsum Board	13	0.177	3.9	6.6	7.9	14.9	41.4	11.0	745.1	0.7	0.179

According to Section 3.2.3 a "sensitive" sensitivity class will be used for the OSB sheathing.

4.5.2 *RSI*-value

Following the material properties shown in the previous point, the total *RSI*-value of an open section of the wall can be calculated. Table 15 shows the total *RSI*-value for the wall.

Table 15: Total RSI value of the open section of the wall

Material	Thickness	Thermal conductivity	*RSI*		Total *RSI* value
	[mm]	λ [W/m·K]	[m²·K/W]		[m²·K/W]
Cement Board	8	0.313	0.03		
Air Gap	25	0.138	0.18		
WRB (Tyvek) (sd=0.088)	-	-	0.00		Total *RSI* value
OSB	11	0.130	0.08		[m²·K/W]
Mineral Wool	120	0.040	3.00		3.4
	240		6.00		6.3
	314		7.85		8.0
	420		10.50		10.7
PE-foil 6 mils (sd=55.8)	-	-	0.00		
Gypsum Board	13	0.177	0.07		

As previously stated, the cities selected are categorized according to ASHRAE 90.2 (2002) climate zones as zone 5 or 6. The following table presents minimum R-values for those zones according to ASHRAE 90.2 (2002) and the NECB (NRCC 2017).

Table 16: Minimum Requirements for insulation

	RSI value [m²·K/W]	
	ASHRAE 90.2 (2002)	**NECB (2017)**
	Nominal Cavity insulation	Overall Thermal Resistance of Above-ground Opaque Building Assemblies
Zone 5	2.6	3.6
Zone 6	3.7	4.0

According to these standards, the three higher selected *RSI*-values of insulation are above the requirements and the lower R-value selected would comply with ASHRAE 90.2 (2002) zone 5 but would fall just below the other Standards.

4.6 Boundary Conditions for Hygrothermal Modelling
Boundary Exchange Coefficients

The initial temperature for the materials is set to 12°C, and the initial relative humidity is set to 80% according to the default values in DELPHIN. Initial moisture content is determined by the software according to those values. Boundary exchange coefficients are those used by default in DELPHIN and are shown in Table 17.

Table 17: Boundary exchange coefficients

\	Name	Value	Unit
α_{ex}	Exterior heat transfer coefficient	25	W/m·K
α_{in}	Interior heat transfer coefficient	8	W/m·K
	Reflection coefficient of the surrounding ground (albedo)	0.2	-
α_s	Short-wave radiation absorptivity	0.6	-
α_l	Long-wave radiation emissivity	Not considered	
β_{ex}	Exterior vapour transfer coefficient	3.00E-08	s/m
β_{in}	Interior vapour transfer coefficient	2.00E-06	s/m
	Rain factors	Not considered	

Rain deposition is not considered because it acts in the opposite direction of the winds that generate exfiltration. In any case, the inclusion of rain deposition would definitely increase the moisture in the OSB, as shown by different studies (Cornick et al. 2009; Blocken & Carmeliet 2004; Künzel 2006). HAM modelling tools require hourly datasets of rainfall, which can be challenging to obtain, and the additional requirement of coincident wind and rain data makes it even more problematic (Cornick et al. 2009). Moreover, a study by Blocken & Carmeliet (2000) demonstrated that averaging errors produced in hourly wind and rain data could produce significant errors in wind-driven rain amounts, and they suggested that a ten-minute data would be required to minimize errors, which makes this data very difficult to obtain.

Long-wave radiation is not considered because the weather files available did not include the atmospheric counter-radiation data required for modelling it. The inclusion of longwave radiation can have positive or negative effects, depending on the value of the surface emissivity, as shown by Künzel et al. (2012).

Indoor and Outdoor conditions

Hygrothermal performance assessment and the design of building envelopes should focus on the expected and normal use of buildings. Even in buildings with the highest standards and performance, excessive indoor humidity caused by unexpected moisture loads and not counterbalanced by additional ventilation can create moisture problems like condensation or even mould growth if the conditions are sustained or frequent. However, these cases should be the exception, and if the design was provided with adequate safety margins, the hygrothermal performance should be guaranteed (Künzel 2005).

Several references find that Indoor relative humidity fluctuates between 30% and 40% in winter and between 50% and 60% in summer. (Künzel 2005; Straube & Schumacher 2001; Holm, Kilian, & Janssen 2007).

Künzel (2005) mentions that mainly because materials at a distance of more than 10 mm are not affected by hourly fluctuations of indoor relative humidity, only daily or monthly mean values are required to assess hygrothermal performance of building envelope.

The interior climate is defined using a model based on ISO 13788 (2012) Standard. The method is described in Annex A of the standard provides a simplified approach that allows the calculation of indoor temperature and relative humidity based on the exterior ambient temperature. The model is intended for dwellings or offices in the absence of well-controlled internal air conditions.

By default, DELPHIN defines the limits interior Temperature to the range 20-25 °C and relative humidity to the range of 35%-65%, which corresponds to a "Normal Occupancy" pattern according to ISO 13788 (2012). The model linearly increases the interior temperature from 20°C when the outdoor temperature is 10°C to a temperature of 25°C when the outdoor temperature reaches 20°C. The same happens with the relative humidity, staying at the lower limit of 35% when the exterior temperature is below -10°C and linearly increasing up to 65% until the exterior temperature reaches 20°C. Figure 15 shows the interior climate depending on the outdoor temperature.
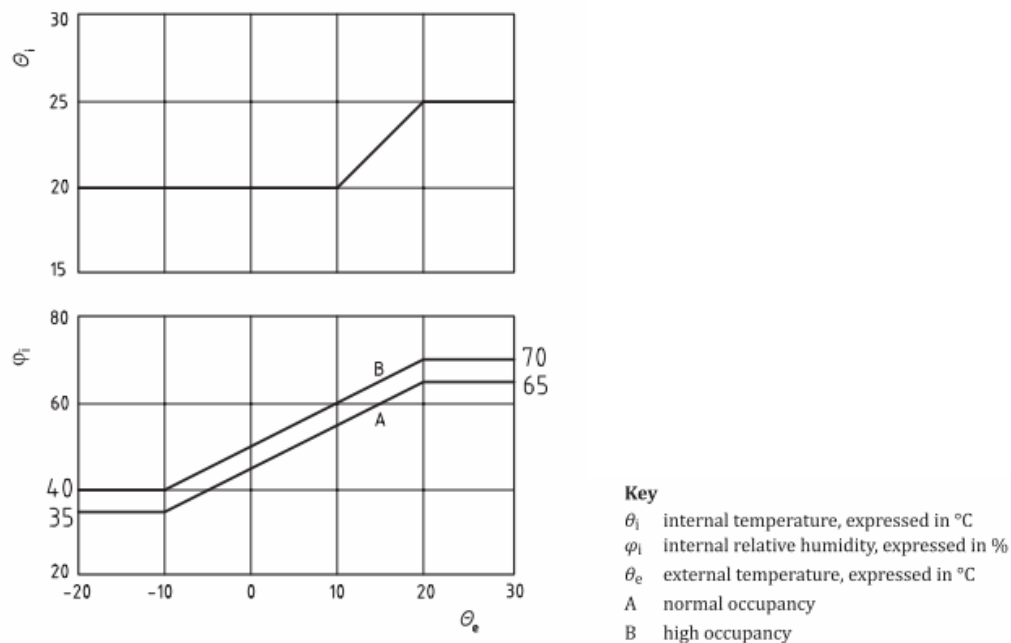
Figure 15: Daily mean internal air temperature and humidity in dwellings and office buildings depending on the daily mean external air temperature. Source ISO 13788 (2012).

The outdoor climate is obtained through TMY weather files. Temperature, relative humidity, and solar radiation are shown in the following graphs. Running average of 720 hours (one month) is used in the charts.
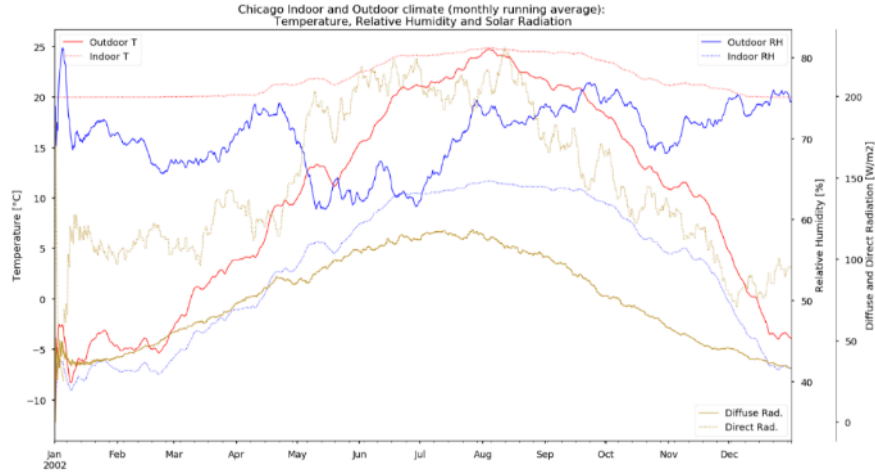
Figure 16: Chicago Indoor and Outdoor Climate (monthly running average)
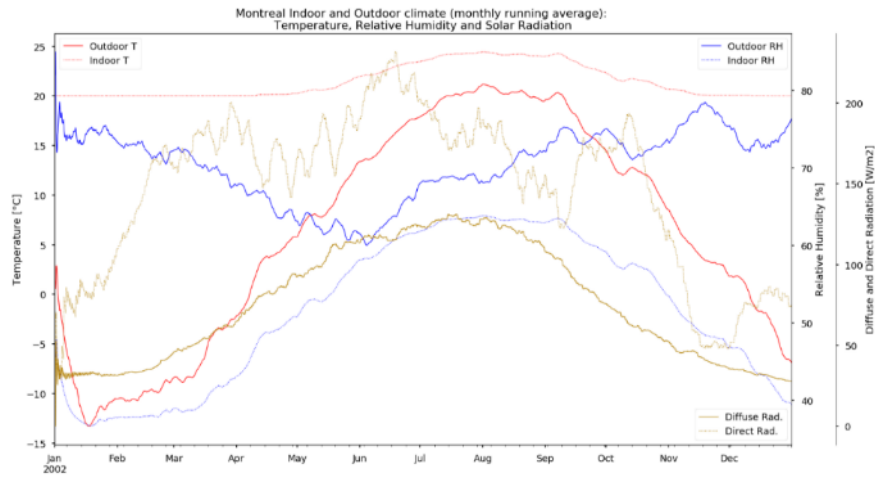
Figure 17: Montreal Indoor and Outdoor Climate (monthly running average)
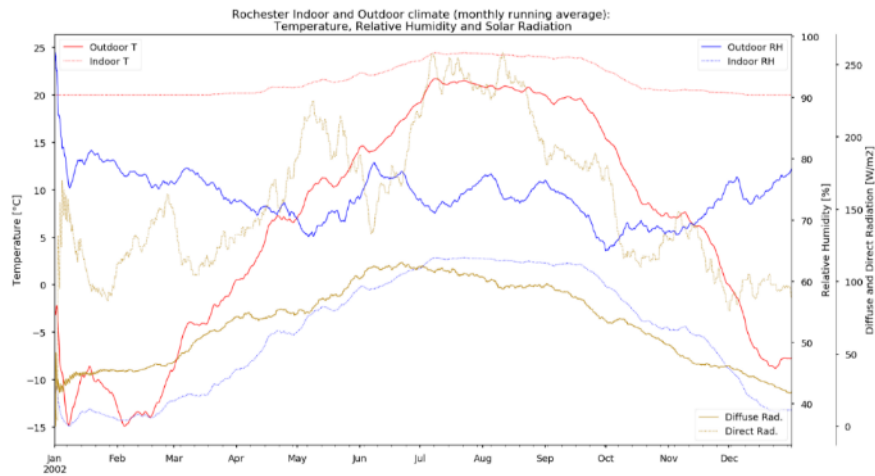
Figure 18: Rochester Indoor and Outdoor Climate (monthly running average)

51
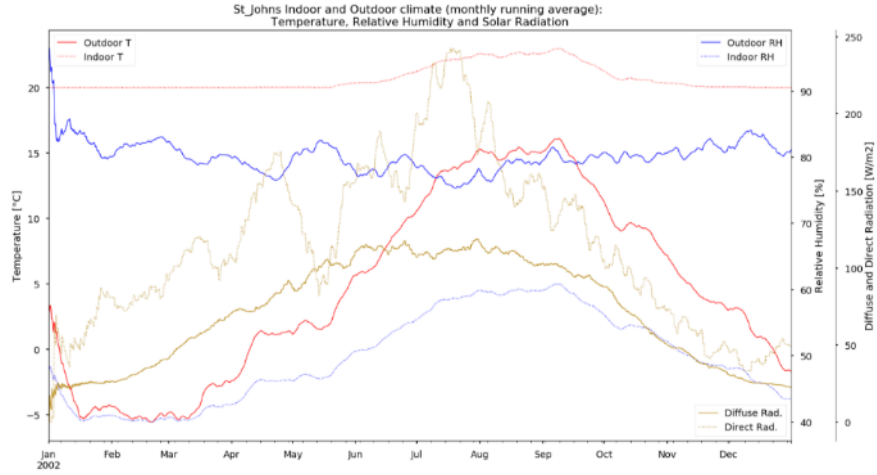
Figure 19: St. Johns Indoor and Outdoor Climate (monthly running average)
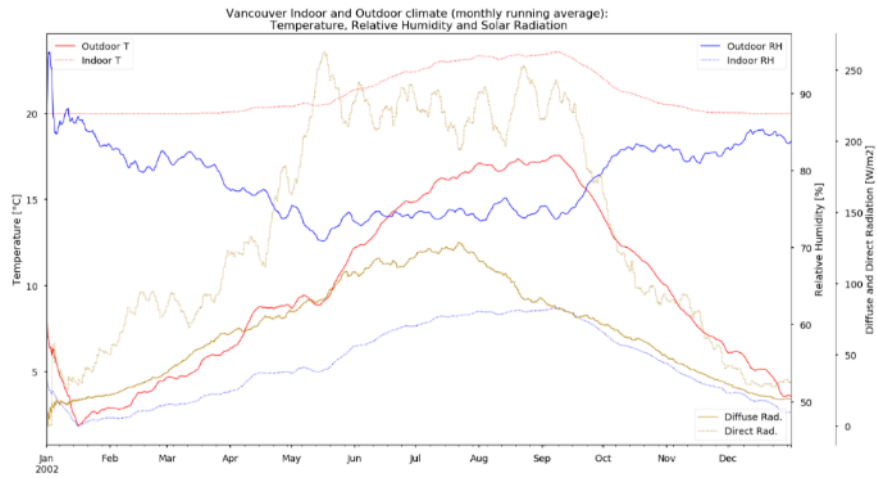
Figure 20: Vancouver Indoor and Outdoor Climate (monthly running average)

5 Results and Analysis

The following section will describe the effect that each of the six parameters described in Section 3.2 has over the hygrothermal performance of the wall in each of the selected cities. In general, the six parameters can be categorized into two groups. The first with parameters directly related to the pressure differential and the airflow through the wall, and the second, with the parameters that are associated with the wall design. Table 18 shows the parameters within these categories. It can be argued that the k_{cl} parameter (moisture permeability) is related to both, the wall design and the airflow through the envelope, but because of its relation with the pressure differential according to equation [9], it is classified under that category.

Table 18: Parameters and values used in simulations

Pressure differential / Airflow				Wall design		
Case type:	k_{cl} [m³/(m²·h·Pa)]:	Terrain category:	C_{pi}:	Orientation:	*RSI* value [W/m²·K]:	Cavity ACH rate [1/h]:
a) Tight	-	-	-	a) Maximum Wind Pressure b) North	a) 3 b) 6 c) 7.85 d) 10.5	a) 0 b) 10 c) 100 d) 300
b) Stack		-	-			
c) Wind	a) ASHRAE Standard: 0.06 b) ASHRAE tight: 0.01 c) WTA: 0.007	a) 1 b) 2 c) 3 d) 4	a) -0.2 b) 0.0			

All the results are analyzed in regard to the performance indicators defined in 3.2. For clarity in the visualization of the results, relative humidity, and moisture content graphs are plotted as a rolling average of 720 hours (1 month), this allows smoothing the hourly variations while showing the general trends.

Moreover, due to the significant number of cases, the results are grouped to facilitate the analysis. When one or more of the parameters are being examined, the outcome of all the cases with those parameters in common is averaged into one result, i.e. if the parameter being analyzed is the *RSI* value, four lines will be shown, each line representing the averaged results of all the cases containing each of the *RSI* values. While this will not show the exact results, it shows the overall effect of the parameter being analyzed. A colour map with the mean *RH* of each case is provided in the following section to analyze in more detail the results.

5.1 Results for the Combination of All Parameters

This section describes, from a general perspective, the results obtained. Due to the complexity of analyzing and comparing the time series of the results, the mean relative humidity and a colour scheme representing mould index are used to obtain some preliminary conclusions that will be further explored and explained in the following sections.

The initial inspection of the results shows that only with an ASHRAE Standard k_{cl} the variation of the results is significant; therefore, only those results will be analyzed in more detail in this section. From this result, it is evident the absolute relevance of air infiltration over the hygrothermal performance, as all the other parameters analyzed produced minor variations in the performance indicators.

The following tables present the mean absolute relative humidity for each of the cases simulated corresponding to k_{cl} ASHRAE Standard. Additionally, the cases are coloured according to the scheme defined in section 3.2.3 for the mould index:

- Light green. mould index less than 1
- Dark green mould index between 1 and 2
- Yellow mould index between 2 and 3
- Red mould index higher than 3

Table 19: Mean relative humidity for Chicago

City	Orientation	RSI-value	k_cl / Case / T_cat / C_pi / ACH_cav	Tight	Stack	ASHRAE Standard Wind 1 (-0.2)	1 (0)	2 (-0.2)	2 (0)	3 (-0.2)	3 (0)	4 (-0.2)	4 (0)
Chicago	Max. Wind Pressure	3	0	61.7	65.7	66.5	67.0	68.1	69.2	70.5	72.2	72.1	74.3
			10	59.5	63.6	64.5	65.0	66.2	67.3	68.6	70.4	70.2	72.5
			100	55.9	60.5	61.4	61.9	63.1	64.4	65.8	67.8	67.5	70.0
			300	57.4	62.1	63.1	63.6	64.9	66.2	67.7	69.7	69.5	72.0
		6	0	63.1	67.4	68.3	68.8	69.9	71.0	72.3	74.1	73.9	76.3
			10	61.1	65.4	66.3	66.9	68.0	69.2	70.5	72.4	72.2	74.6
			100	57.4	62.2	63.1	63.7	65.0	66.3	67.7	69.7	69.5	72.1
			300	58.8	63.7	64.7	65.3	66.7	68.0	69.5	71.5	71.3	74.0
		7.85	0	63.5	67.8	68.7	69.2	70.3	71.5	72.7	74.5	74.3	76.8
			10	61.5	65.9	66.8	67.3	68.5	69.7	70.9	72.8	72.6	75.2
			100	57.8	62.6	63.6	64.2	65.5	66.8	68.2	70.2	70.0	72.7
			300	59.1	64.1	65.2	65.8	67.1	68.5	69.9	72.0	71.7	74.5
		10.5	0	63.9	68.2	69.1	69.6	70.7	71.8	73.1	74.9	74.7	77.3
			10	61.8	66.3	67.2	67.7	68.9	70.1	71.3	73.3	73.0	75.6
			100	58.2	63.0	64.0	64.6	65.9	67.2	68.6	70.6	70.4	73.1
			300	59.5	64.5	65.5	66.1	67.5	68.8	70.3	72.4	72.1	75.0
	North	3	0	67.2	71.9	72.1	72.7	73.2	74.4	75.2	77.0	76.6	78.7
			10	66.0	70.7	70.9	71.5	72.0	73.2	74.0	75.9	75.5	77.6
			100	63.2	68.1	68.3	68.9	69.4	70.7	71.5	73.5	73.1	75.4
			300	63.5	68.5	68.7	69.4	69.9	71.2	72.1	74.2	73.7	76.0
		6	0	69.0	73.9	74.2	74.7	75.3	76.5	77.3	79.1	78.7	80.9
			10	67.7	72.7	72.9	73.5	74.1	75.3	76.1	78.0	77.6	79.8
			100	64.8	70.0	70.3	70.9	71.5	72.8	73.7	75.6	75.2	77.5
			300	65.0	70.2	70.5	71.2	71.8	73.2	74.1	76.0	75.6	78.0
		7.85	0	69.4	74.4	74.7	75.3	75.8	77.0	77.8	79.6	79.2	81.5
			10	68.2	73.2	73.5	74.1	74.6	75.9	76.7	78.5	78.1	80.4
			100	65.3	70.5	70.8	71.4	72.0	73.3	74.2	76.1	75.7	78.1
			300	65.4	70.7	71.0	71.7	72.3	73.6	74.6	76.5	76.1	78.5
		10.5	0	69.9	74.9	75.2	75.7	76.3	77.5	78.3	80.0	79.7	82.0
			10	68.6	73.7	74.0	74.6	75.1	76.3	77.1	78.9	78.5	80.9
			100	65.7	70.9	71.3	71.9	72.5	73.8	74.7	76.6	76.2	78.6
			300	65.8	71.1	71.4	72.1	72.7	74.1	75.0	76.9	76.5	79.0

For Chicago, it is possible to observe differences of up to 10.5% between the cases including wind and those considering just the stack effect. The maximum difference is produced for maximum wind pressure orientation, *RSI* 10.5, Cavity *ACH* 300 and terrain category 4 with C_{pi} equal to 0. Nevertheless higher *RH* are obtained for the North orientation, being on average 5.6% higher.

It can be observed that only in the case of terrain category 4 and C_{pi} equal to 0, there is a risk of mould represented by a mould index higher than 3 (red colour). However, although the *RH* is higher for the North oriented wall there are more cases of Mould index higher than 2 (yellow or red) for the maximum wind pressure orientation, 12 red and 13 yellow versus eight red and six

yellow, respectively. The higher number of cases with a mould index greater than 2 for maximum wind pressure orientation, can be explained by the higher surface temperatures due to the higher solar radiation, as it will be demonstrated later.

Table 20: Mean relative humidity for Montreal

City	Orientation	RSI-value	kcl / Case / T$_{cat}$ / C$_{pi}$ / ACH$_{cav}$	Tight	Stack	1 (-0.2)	1 (0)	2 (-0.2)	2 (0)	3 (-0.2)	3 (0)	4 (-0.2)	4 (0)
Montreal	Max. Wind Pressure	3	0	61.6	68.1	68.9	69.4	70.4	71.7	72.8	74.9	74.5	77.3
			10	59.8	66.5	67.3	67.9	68.9	70.3	71.4	73.6	73.1	76.0
			100	56.2	63.6	64.5	65.1	66.2	67.7	68.9	71.2	70.8	73.8
			300	57.3	65.0	66.0	66.6	67.8	69.3	70.6	73.0	72.5	75.6
		6	0	63.6	70.3	71.1	71.7	72.6	73.9	75.0	77.3	76.9	79.9
			10	61.9	68.8	69.6	70.2	71.2	72.5	73.6	75.9	75.5	78.6
			100	58.0	65.6	66.5	67.2	68.3	69.8	71.1	73.5	73.0	76.2
			300	58.8	66.8	67.8	68.5	69.6	71.2	72.5	75.0	74.5	77.8
		7.85	0	64.1	70.8	71.6	72.2	73.1	74.4	75.6	77.9	77.4	80.5
			10	62.4	69.3	70.1	70.7	71.7	73.0	74.2	76.5	76.1	79.2
			100	58.4	66.1	67.0	67.7	68.8	70.3	71.6	74.0	73.6	76.8
			300	59.3	67.3	68.2	68.9	70.1	71.7	73.0	75.5	75.0	78.4
		10.5	0	64.6	71.3	72.1	72.6	73.6	74.9	76.0	78.4	78.0	81.1
			10	62.8	69.8	70.6	71.2	72.1	73.5	74.7	77.1	76.6	79.8
			100	58.8	66.5	67.4	68.1	69.2	70.7	72.0	74.5	74.1	77.4
			300	59.6	67.6	68.6	69.3	70.5	72.0	73.4	76.0	75.5	78.9
	North	3	0	65.1	72.7	72.8	73.4	73.8	75.2	76.0	78.0	77.5	80.0
			10	64.1	71.8	71.9	72.5	73.0	74.3	75.1	77.1	76.6	79.1
			100	61.9	69.9	70.0	70.6	71.1	72.5	73.3	75.4	74.9	77.5
			300	62.1	70.3	70.4	71.1	71.6	73.0	73.9	76.1	75.5	78.2
		6	0	67.3	75.0	75.1	75.8	76.2	77.5	78.2	80.2	79.7	82.4
			10	66.3	74.1	74.2	74.9	75.3	76.6	77.3	79.4	78.9	81.5
			100	64.0	72.1	72.2	72.9	73.3	74.7	75.5	77.6	77.1	79.8
			300	63.9	72.3	72.4	73.1	73.6	75.0	75.9	78.0	77.5	80.3
		7.85	0	67.9	75.6	75.7	76.3	76.8	78.0	78.8	80.8	80.3	83.0
			10	66.9	74.7	74.8	75.4	75.9	77.1	77.9	80.0	79.4	82.1
			100	64.5	72.7	72.8	73.4	73.9	75.2	76.0	78.2	77.6	80.4
			300	64.4	72.8	73.0	73.6	74.1	75.5	76.4	78.5	78.0	80.8
		10.5	0	68.4	76.1	76.2	76.8	77.2	78.5	79.2	81.3	80.8	83.6
			10	67.5	75.2	75.3	75.9	76.3	77.6	78.4	80.5	79.9	82.7
			100	65.0	73.1	73.2	73.9	74.4	75.7	76.5	78.6	78.1	80.9
			300	64.9	73.3	73.4	74.1	74.6	76.0	76.8	79.0	78.4	81.3

Montreal show results comparable to the cases in Chicago, which can be summarized as follows:

- Higher *RH* for the North oriented cases
- Higher mould Index for the Maximum wind pressure orientation cases
- Risk of mould (red) for cases with terrain category 4 and *C*$_{pi}$ = 0, and minor risk (yellow) for terrain category 3 and *C*$_{pi}$ =0.

Both cities, Chicago and Montreal present medium wind speed as defined in Section 4.1, and although there is an increase in the mean *RH* when considering the wind effect, with maximum differences of about 11% when compared to simulations considering only stack effect, only for cases located in terrain category 4 the inclusion of wind is translated into a mould Index higher than 3.

Table 21: Mean relative humidity for Rochester

City	Orientation	R-value	kcl / Case / Tcat / Cpi / ACHcav	Tight	Stack	ASHRAE Standard Wind							
						1		2		3		4	
						-0.2	0	-0.2	0	-0.2	0	-0.2	0
Rochester	Max. Wind Pressure	3	0	66.9	74.4	76.4	77.3	79.4	81.3	84.0	87.2	87.3	91.8
			10	65.4	73.0	75.0	75.9	78.1	80.0	82.7	86.0	86.1	90.4
			100	62.6	70.4	72.6	73.5	75.8	77.8	80.6	83.9	84.0	88.3
			300	63.4	71.4	73.5	74.5	76.9	78.9	81.8	85.1	85.2	89.5
		6	0	68.9	76.4	78.3	79.2	81.5	83.4	86.3	90.0	90.1	95.0
			10	67.4	75.0	77.0	77.8	80.1	82.2	85.0	88.6	88.8	93.8
			100	64.6	72.4	74.5	75.4	77.8	79.9	82.9	86.4	86.5	91.2
			300	65.2	73.2	75.3	76.2	78.7	80.9	83.9	87.5	87.6	92.2
		7.85	0	69.5	77.0	78.8	79.7	82.0	84.0	86.9	90.7	90.8	95.6
			10	68.0	75.6	77.5	78.3	80.7	82.7	85.6	89.4	89.5	94.6
			100	65.1	72.9	75.0	75.9	78.3	80.5	83.5	87.1	87.2	92.0
			300	65.8	73.7	75.7	76.7	79.2	81.4	84.4	88.1	88.2	93.0
		10.5	0	70.1	77.4	79.3	80.1	82.5	84.5	87.5	91.4	91.5	96.1
			10	68.6	76.0	77.9	78.8	81.2	83.2	86.2	90.0	90.2	95.2
			100	65.6	73.4	75.4	76.3	78.8	81.0	84.0	87.7	87.9	92.8
			300	66.2	74.1	76.1	77.1	79.6	81.9	84.9	88.7	88.8	93.7
	North	3	0	68.5	76.3	76.0	77.1	76.8	78.9	79.0	81.9	80.6	84.1
			10	67.3	75.2	74.8	75.9	75.7	77.8	77.9	80.8	79.5	83.0
			100	64.8	72.8	72.4	73.5	73.3	75.5	75.6	78.6	77.3	80.9
			300	65.2	73.4	73.0	74.1	74.0	76.1	76.3	79.3	77.9	81.7
		6	0	70.7	78.4	78.1	79.2	79.0	81.0	81.1	84.1	82.7	86.5
			10	69.5	77.3	77.0	78.0	77.9	79.9	80.0	83.0	81.6	85.4
			100	66.8	74.8	74.5	75.6	75.5	77.5	77.7	80.8	79.4	83.3
			300	67.2	75.2	74.9	76.0	75.9	78.0	78.1	81.3	79.8	83.9
		7.85	0	71.4	79.0	78.7	79.7	79.6	81.5	81.7	84.7	83.3	87.1
			10	70.1	77.8	77.5	78.6	78.5	80.4	80.5	83.6	82.2	86.1
			100	67.4	75.4	75.1	76.1	76.0	78.1	78.2	81.4	79.9	83.9
			300	67.7	75.7	75.4	76.5	76.4	78.5	78.6	81.8	80.4	84.4
		10.5	0	71.9	79.5	79.2	80.2	80.1	82.0	82.2	85.2	83.8	87.7
			10	70.7	78.3	78.0	79.0	78.9	80.9	81.0	84.2	82.7	86.6
			100	68.0	75.8	75.5	76.6	76.5	78.5	78.7	81.9	80.4	84.5
			300	68.2	76.1	75.8	76.9	76.8	78.9	79.1	82.3	80.8	84.9

Rochester presents results contrary to what was obtained in the previous cities. In this case, the higher *RH* is obtained for the maximum wind pressure orientation, showing that a different orientation from the North can present a worse situation. Moreover, the combined higher relative

humidity and higher sun radiation that this orientation receives increases drastically the mould Index, with 81 cases in red and 9 in yellow for the maximum wind pressure orientation, versus 24 in red and 7 in yellow for the North orientation. For the maximum wind pressure orientation, even some cases in an urban setup (terrain category 2) showed an elevated risk of presenting mould when compared with an evaluation that does not include wind pressures.

An explanation for higher *RH* for the maximum wind orientation can be found by re-assessing the wind rose presented in Figure 7 as will be discussed later in section 5.3.1.

Table 22: Mean relative humidity for St. Johns

City	Orientation	R-value	k_{cl} / Case / T_{cat} / C_{pi} / ACH_{cav}	Tight	Stack	ASHRAE Standard Wind 1 (-0.2)	1 (0)	2 (-0.2)	2 (0)	3 (-0.2)	3 (0)	4 (-0.2)	4 (0)
St Johns	Max. Wind Pressure	3	0	72.1	77.5	79.4	80.5	82.9	84.9	87.3	91.1	90.7	95.9
			10	70.7	76.2	78.1	79.3	81.7	83.8	86.2	90.0	89.6	94.9
			100	67.4	73.1	75.2	76.4	79.0	81.2	83.8	87.8	87.4	92.8
			300	67.8	73.8	75.9	77.2	79.8	82.2	84.9	89.0	88.6	94.2
		6	0	74.4	80.1	82.0	83.1	85.3	87.5	90.2	94.5	94.1	97.8
			10	73.1	78.8	80.8	81.9	84.1	86.4	89.1	93.5	93.1	97.6
			100	69.7	75.7	77.8	79.0	81.5	83.8	86.7	91.2	90.8	96.7
			300	69.9	76.1	78.3	79.5	82.1	84.5	87.6	92.2	91.8	97.4
		7.85	0	75.1	80.8	82.6	83.7	85.9	88.1	91.0	95.4	95.0	97.9
			10	73.7	79.5	81.4	82.5	84.7	87.0	89.9	94.4	94.0	97.8
			100	70.3	76.4	78.4	79.6	82.1	84.5	87.5	92.2	91.7	97.3
			300	70.4	76.7	78.9	80.1	82.7	85.2	88.3	93.0	92.6	97.6
		10.5	0	75.6	81.3	83.2	84.2	86.4	88.8	91.7	96.2	95.8	98.0
			10	74.3	80.0	81.9	83.0	85.3	87.6	90.6	95.3	94.9	97.9
			100	70.8	76.9	79.0	80.1	82.6	85.1	88.2	93.0	92.5	97.5
			300	70.9	77.2	79.4	80.6	83.2	85.7	88.9	93.8	93.3	97.8
	North	3	0	73.2	78.9	80.5	81.7	83.9	85.9	88.2	91.8	91.4	96.3
			10	72.3	77.9	79.6	80.8	83.0	85.1	87.4	91.1	90.7	95.7
			100	69.6	75.5	77.2	78.5	80.9	83.0	85.5	89.3	88.9	94.1
			300	69.7	75.8	77.6	78.9	81.4	83.6	86.1	90.1	89.7	95.2
		6	0	75.7	81.6	83.2	84.3	86.4	88.6	91.1	95.3	94.8	98.0
			10	74.8	80.7	82.4	83.5	85.6	87.8	90.4	94.6	94.2	97.9
			100	72.0	78.1	79.9	81.1	83.4	85.6	88.4	92.7	92.3	97.5
			300	71.8	78.2	80.1	81.3	83.7	86.0	88.8	93.3	92.8	97.7
		7.85	0	76.4	82.3	83.9	85.0	87.1	89.3	91.9	96.1	95.7	98.1
			10	75.4	81.4	83.1	84.1	86.3	88.5	91.2	95.5	95.1	98.0
			100	72.6	78.8	80.6	81.8	84.0	86.3	89.1	93.6	93.2	97.7
			300	72.4	78.8	80.7	81.9	84.2	86.6	89.5	94.2	93.7	97.9
		10.5	0	77.0	82.9	84.5	85.5	87.6	89.9	92.6	96.8	96.4	98.1
			10	76.0	82.0	83.6	84.7	86.8	89.1	91.9	96.3	95.8	98.1
			100	73.2	79.4	81.2	82.3	84.5	86.9	89.8	94.5	94.0	97.9
			300	72.9	79.4	81.2	82.4	84.7	87.2	90.2	94.9	94.4	98.0

St. Johns presented results with similar trends to those obtained for Chicago and Montreal, but the higher wind speeds in this city increase the *RH* generating mould Index higher than 3 for all the cases simulated under terrain category 3 and 4 and showing that some cases in terrain category 2 develop a mould Index between 2 and 3. In cities with high wind speeds like Rochester or St. Johns, it can be observed that wind-induced exfiltration has significant effects, and that it drastically increases the mould Index when compared to simulations considering only stack effect.

Table 23: Mean relative humidity for Vancouver

City	Orientation	R-value	k_{cl} / Case / T_{cat} / C_{pi} / ACH_{cav}	Tight	Stack	ASHRAE Standard Wind 1 -0.2	0	-0.2	0	-0.2	0	-0.2	0
Vancouver	Max. Wind Pressure	3	0	70.0	71.4	71.5	71.7	71.8	72.2	72.4	73.1	72.9	73.9
			10	68.8	70.2	70.3	70.4	70.6	71.0	71.2	71.9	71.7	72.7
			100	66.7	68.2	68.3	68.4	68.6	69.0	69.2	70.0	69.7	70.7
			300	67.7	69.3	69.4	69.6	69.8	70.2	70.4	71.2	71.0	72.1
		6	0	71.6	73.2	73.4	73.5	73.7	74.1	74.4	75.2	75.0	76.0
			10	70.4	72.0	72.2	72.3	72.5	73.0	73.2	74.0	73.8	74.9
			100	68.3	70.0	70.1	70.3	70.5	70.9	71.2	72.0	71.8	72.9
			300	69.2	71.0	71.1	71.3	71.5	72.0	72.3	73.2	72.9	74.1
		7.85	0	72.0	73.7	73.8	74.0	74.2	74.6	74.9	75.7	75.5	76.6
			10	70.8	72.5	72.6	72.8	73.0	73.5	73.7	74.6	74.3	75.4
			100	68.7	70.4	70.6	70.7	70.9	71.4	71.7	72.6	72.3	73.4
			300	69.5	71.4	71.5	71.7	71.9	72.4	72.7	73.6	73.4	74.6
		10.5	0	72.3	74.1	74.2	74.4	74.6	75.1	75.3	76.2	75.9	77.0
			10	71.1	72.9	73.0	73.2	73.4	73.9	74.1	75.0	74.8	75.9
			100	69.0	70.8	70.9	71.1	71.3	71.8	72.1	73.0	72.7	73.9
			300	69.9	71.7	71.9	72.1	72.3	72.8	73.1	74.0	73.8	75.0
	North	3	0	72.2	73.6	73.6	73.8	73.9	74.2	74.4	75.0	74.9	75.7
			10	71.3	72.8	72.8	72.9	73.0	73.3	73.6	74.2	74.0	74.8
			100	69.6	71.1	71.1	71.3	71.4	71.7	72.0	72.6	72.4	73.3
			300	70.2	71.8	71.8	72.0	72.1	72.5	72.7	73.4	73.2	74.1
		6	0	73.8	75.5	75.5	75.7	75.8	76.2	76.5	77.2	77.0	77.9
			10	73.0	74.7	74.7	74.8	75.0	75.3	75.6	76.3	76.1	77.1
			100	71.2	73.0	73.0	73.1	73.3	73.7	73.9	74.7	74.5	75.4
			300	71.7	73.5	73.5	73.7	73.8	74.3	74.5	75.3	75.1	76.1
		7.85	0	74.3	76.0	76.0	76.2	76.3	76.7	77.0	77.7	77.5	78.5
			10	73.4	75.2	75.2	75.3	75.5	75.9	76.1	76.8	76.7	77.6
			100	71.6	73.4	73.4	73.6	73.7	74.2	74.4	75.2	75.0	76.0
			300	72.1	74.0	74.0	74.2	74.3	74.7	75.0	75.8	75.6	76.6
		10.5	0	74.6	76.5	76.5	76.6	76.8	77.2	77.4	78.2	78.0	79.0
			10	73.8	75.6	75.6	75.8	75.9	76.3	76.6	77.3	77.1	78.1
			100	72.0	73.8	73.8	74.0	74.1	74.6	74.8	75.6	75.4	76.4
			300	72.4	74.3	74.3	74.5	74.7	75.1	75.4	76.2	76.0	77.1

Finally, in cities with wind speeds considered slow like Vancouver there is practically no effect by the wind. The *RH* increases but to a maximum amount of 3%, which does not translate into an increased risk for mould development.

5.2 Moisture Flow Parameters

Moisture flow is defined by the pressure differential across the envelope and the moisture permeability (k_{cl}). As described previously, pressure differential varies depending on the stack pressure, wind pressure, and wind-induced internal pressure coefficient. Three different values for k_{cl} were defined in section 2.3.2. The following section discusses the effect of those parameters.

5.2.1 Effect of Terrain Category and Moisture Leakage

This section discusses the effects of the terrain category (T_{cat}) and the moisture leakage parameter (k_{cl}). Each colour represents one of the three k_{cl}, ASHRAE Standard in reds, ASHRAE Tight in blues and WTA in greens; the dotted line represents the reference tight case, segmented lines represent the cases where only stack effect is considered, and continuous line the cases where wind effect is included. Finally, each terrain category is represented as a shade of the corresponding color, with darker color showing terrain category 4 and lighter colour representing terrain category 1.
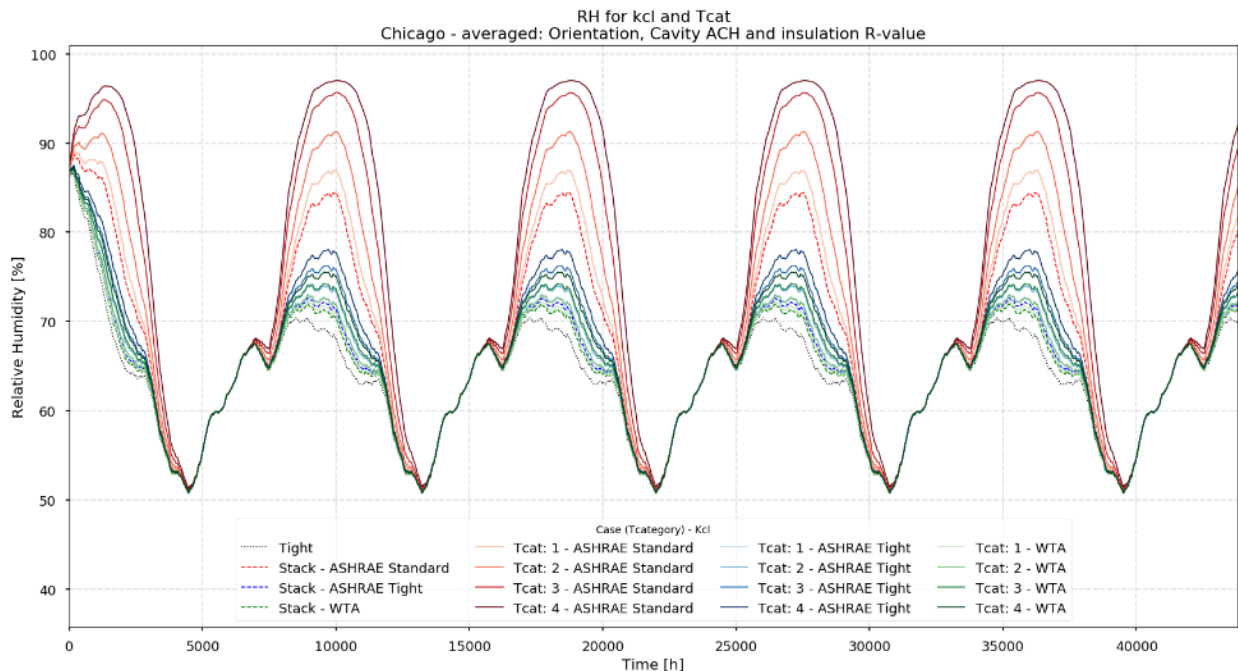
Figure 21: Chicago relative humidity for different k_{cl} and Terrain category.

60

Figure 21 shows the 5-year simulation for Chicago. It can be seen that for the lower k_{cl}'s (ASHRAE Tight and WTA) the difference in relative humidity between the model considering just the stack effect and the model including wind are minor. For ASHRAE Tight the mean difference ranges between 0.19% for T_{cat} 1 and 1.95% for T_{cat} 4. For WTA the difference ranges between 0.13% and 1.4% for T_{cat} 1 and for T_{cat} 4 respectively. Those differences increase up to 0.9% and 7.24% for T_{cat} 1 and for T_{cat} 4 respectively when using ASHRAE Standard k_{cl}. Peak differences reached up to 2.5% for T_{cat} 1 and up to 20% for T_{cat} 4. The difference in *RH* are observable for approximately 6 moths, reaching zero during the rest of the year.
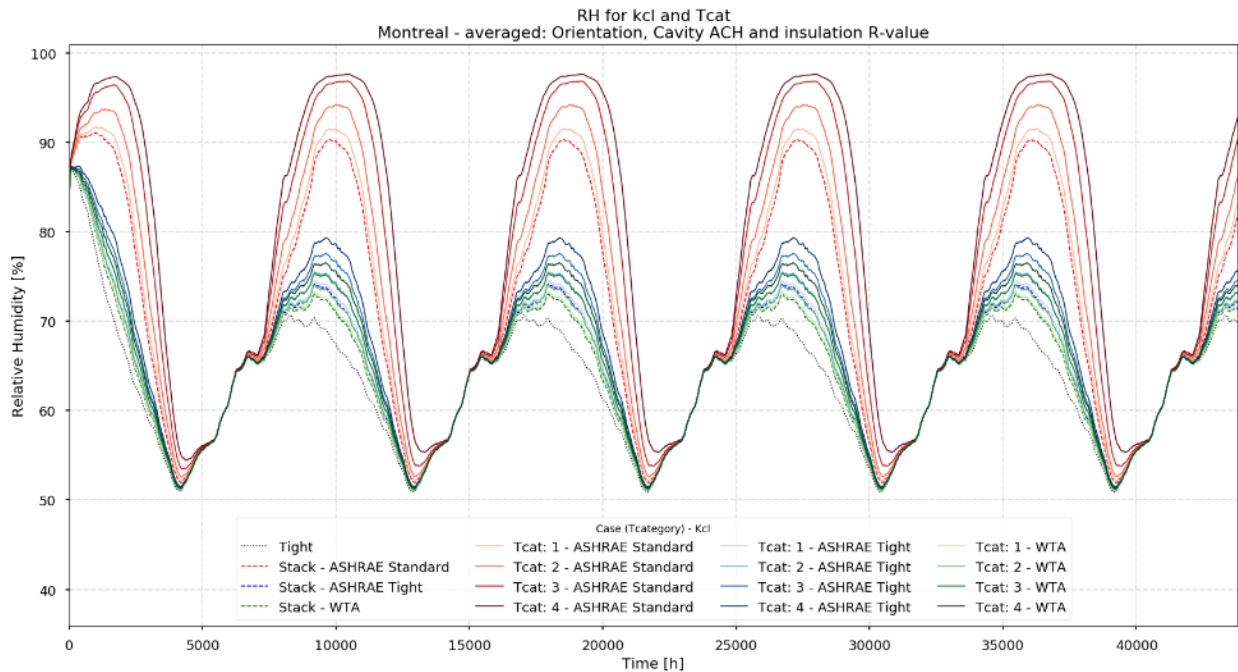
Figure 22: Montreal relative humidity for different k_{cl} and Terrain category.

Montreal shows a similar behaviour to Chicago. In this city the differences between the results with stack pressure and those including wind are also in the range of 0.14% - 1.61% for WTA and 0.19% - 2.21% for ASHRAE Tight k_{cl}. For ASHRAE Standard k_{cl} the results are also comparable to Chicago, the difference ranges between 0.81% and 7.48% for the extreme T_{cat}. The peak differences also can reach up to 20% for T_{cat} 4.
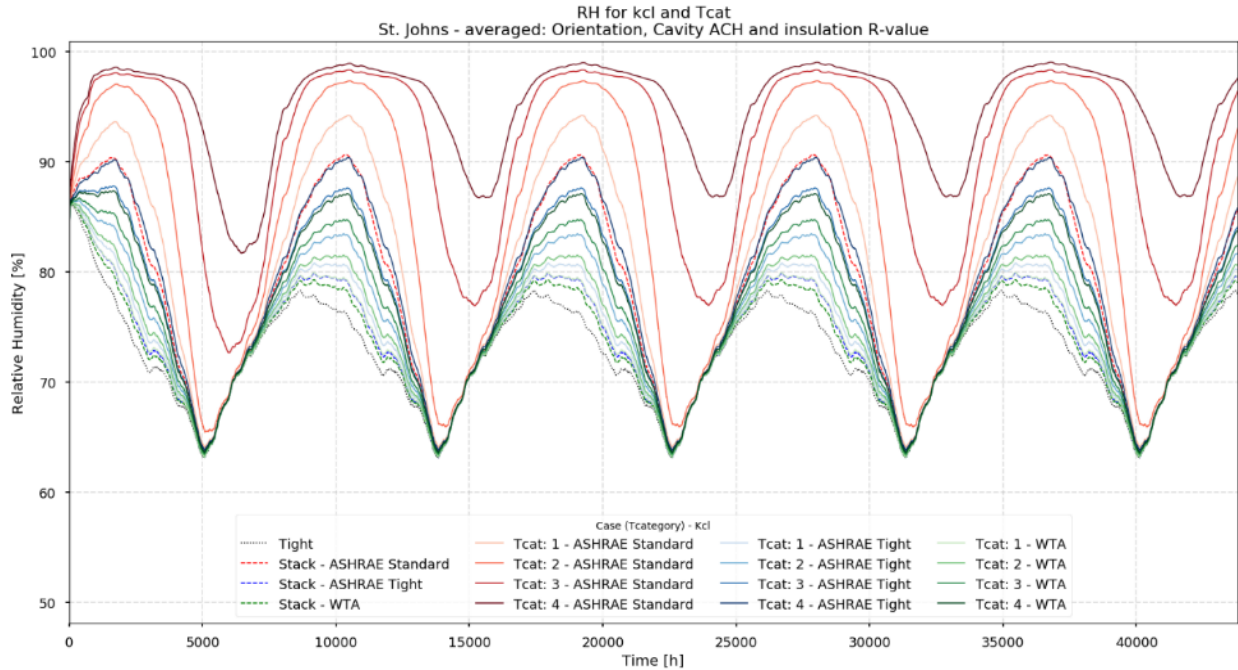
Figure 23: St Johns relative humidity for different k_{cl} and Terrain category.

The 5-year simulation for St. Johns shows larger variations in comparison to the previous cities (Chicago and Montreal). In this city, the mean difference between the simulations considering wind and those including only stack effect is 2.45% for T_{cat} 1 and 16.42% for T_{cat} 4 for ASHRAE Standard k_{cl}. For ASHRAE Tight that mean difference ranges between 0.57% and 5.19% and for WTA between 0.41% and 3.84%. Notably for St. Johns the peak differences reach up to 30% for T_{cat} 4 and are sustained above 15% difference for more than 3 month. That greater difference and the longer periods with much higher *RH* explain the higher mould Index obtained for most of the terrain categories when wind was considered in the analysis.
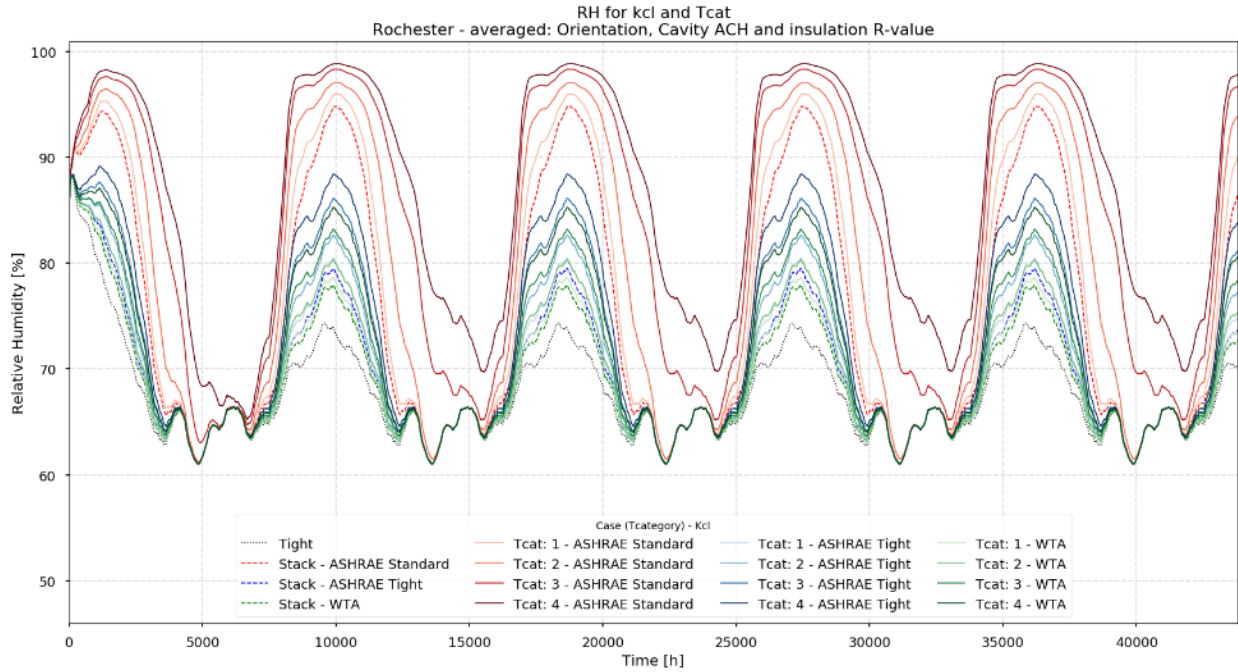
Figure 24: Rochester relative humidity for different k_{cl} and Terrain category.
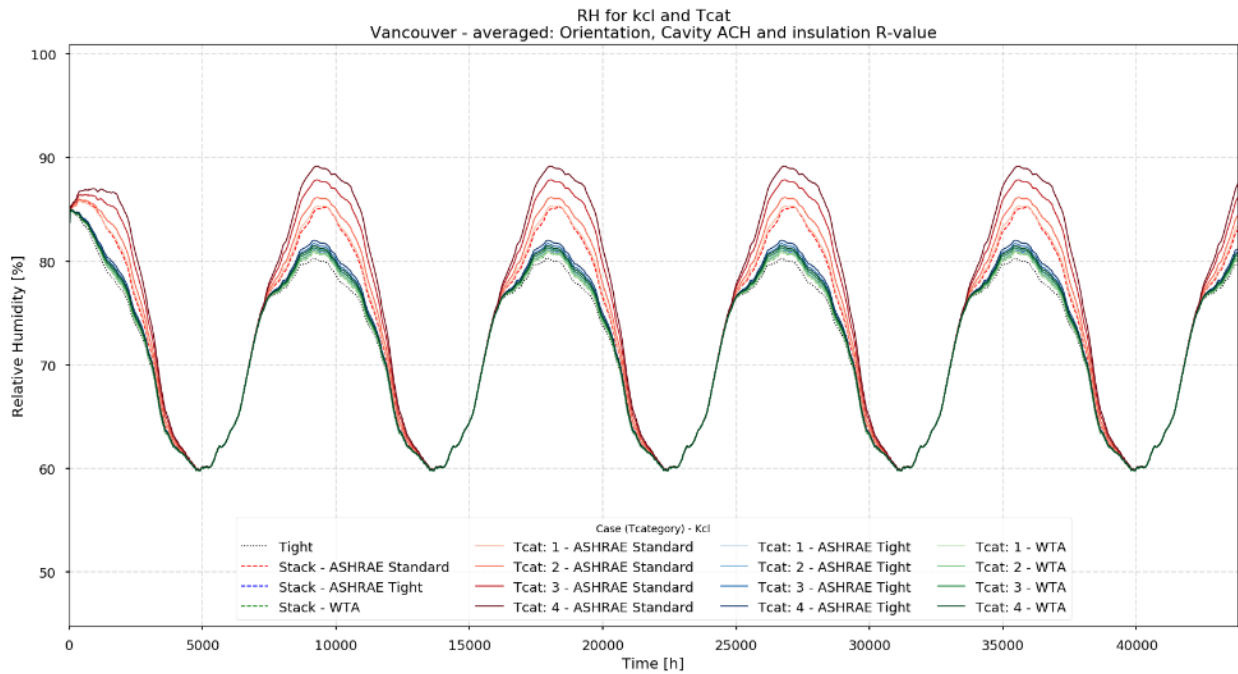
Figure 25: Vancouver relative humidity for different k_{cl} and Terrain category.

Figure 24 for Rochester presents variations between 0.28% and 2.99 for WTA, 0.39% and 3.97% for ASHRAE Tight and 1.33% and 11.35% for ASHRAE Standard k_{cl}. Considering ASHRAE Standard k_{cl} peak differences reach 25% for T_{cat} 4, 21% for T_{cat} 3, 12.5% for T_{cat} 2 and abot 3%

for T_{cat} 1. Also for ASHRAE Standard k_{cl} differences in *RH* are sustained through time for T_{cat} 3 and T_{cat} 4, while for T_{cat} 1 and 2, there is no difference during the driest period.

Finally, Figure 25 for Vancouver presents only minor differences when wind is considered in the simulation. The mean difference between stack and wind cases only reaches 2.15% for T_{cat} 4 and ASHRAE Standard k_{cl}. The peak difference is only 5% for T_{cat} 4 and ASHRAE Standard.

It is worth noticing that for each of the cities all the cases using WTA or ASHRAE tight k_{cl} are located between the cases considering stack pressure and ASHRAE Standard k_{cl} (segmented red line), and the reference tight case (dotted black line). This shows the importance of the airtightness, i.e. if the building is tighter than ASHRAE Standard (has a k_{cl} lower than 0.06 m³/hm²Pa) then assuming an ASHRAE Standard k_{cl} and only the stack effect for simulation will account for even the worst-case wind scenario of a lower k_{cl}.

5.2.2 Effect of Wind-Induced Internal Pressure

Following what was discussed in the previous point, only ASHRAE Standard k_{cl} is used to demonstrate the effect of C_{pi} on the relative humidity. All other cases will be between the stack and tight cases shown on the following plots. Here, each T_{cat} is shown in a different color, and the different C_{pi} are annotated with a different line style, dotted line for C_{pi} = -0.2 and continuous line for C_{pi} = 0.

The results for terrain categories showed in the previous point represent the average of the results shown in the following graphs. It can be seen that the effect of the C_{pi} is relevant for cities with high wind speeds, where it can be seen that during the drying period the differences are drastically increased. For cities with mid and low wind speeds, the differences are much lower, and there is practically no difference in the drying period.
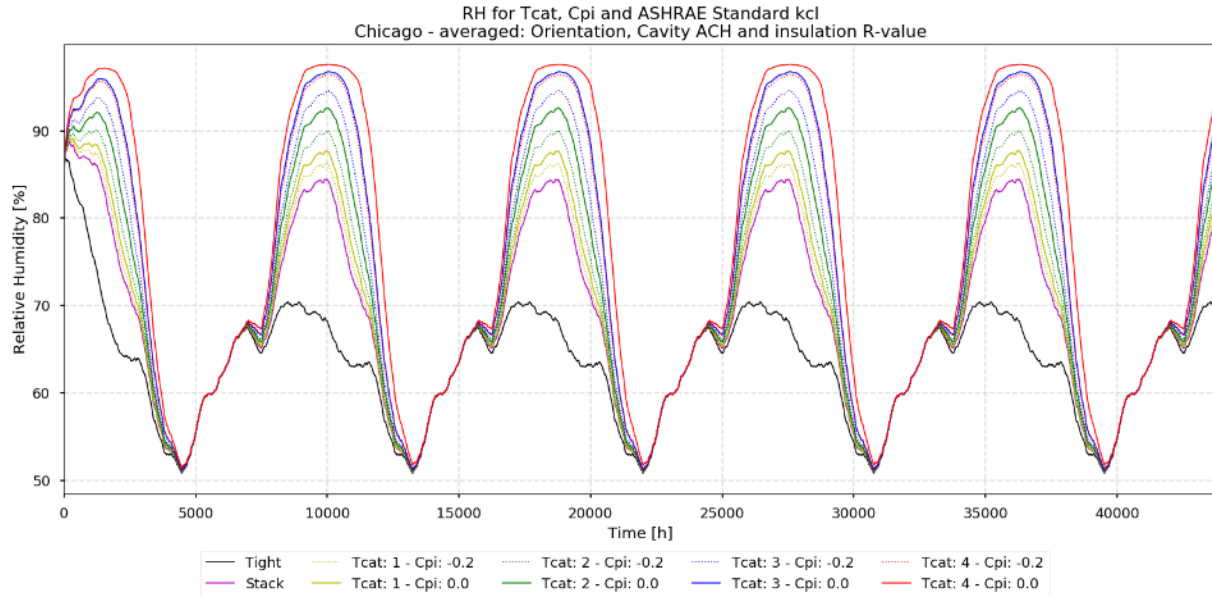
Figure 26: Chicago – RH for ASHRAE Standard k_{cl} and different C_{pi}, other parameters averaged.
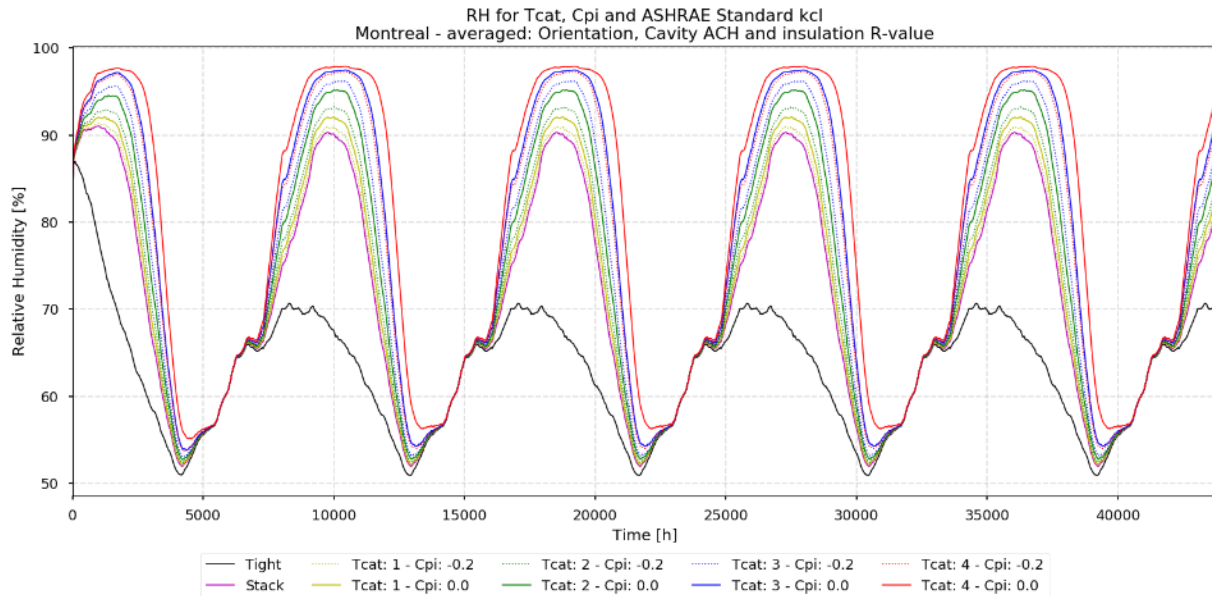
Figure 27: Montreal – RH for ASHRAE Standard k_{cl} and different C_{pi}, other parameters averaged.

For Chicago and Montreal the difference between the results with both C_{pi} is about 0.6% for T_{cat} 1 and less than 3% for T_{cat} 4. Also there is little or no difference during the drying period.
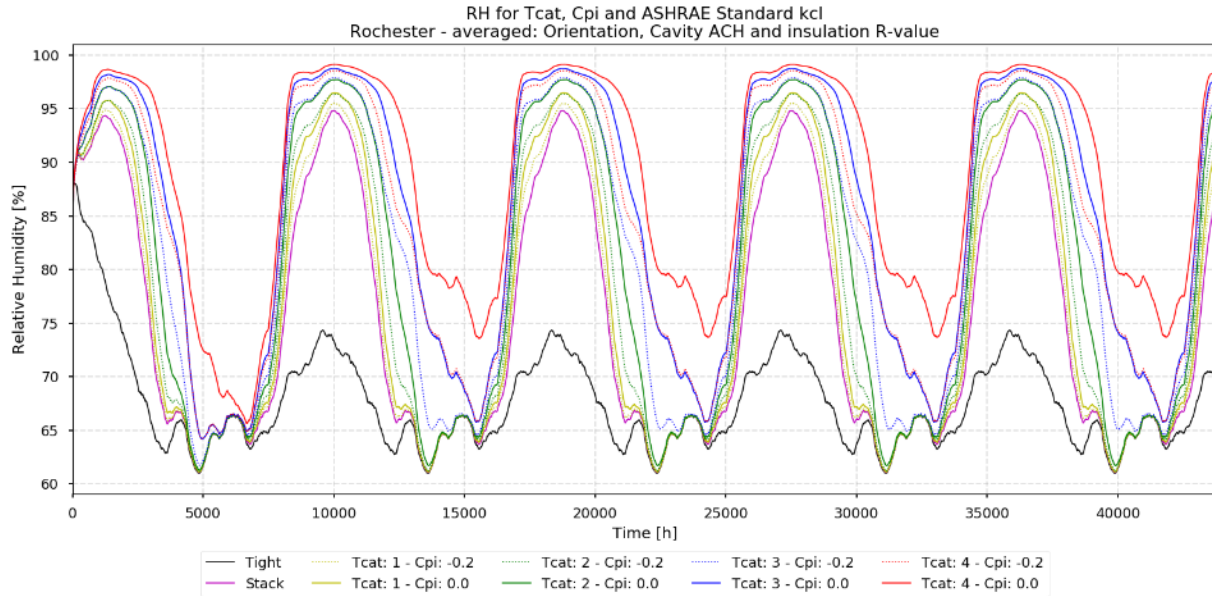
Figure 28: Rochester – RH for ASHRAE Standard k_{cl} and different C_{pi}, other parameters averaged.

Contrary to Chicago and Montreal, Rochester shows a great difference during the drying period, although that difference is only noticeable for terrain categories 3 and 4. To visualize the differences during the drying period Figure 29 shows a zoom to one year of the simulation.
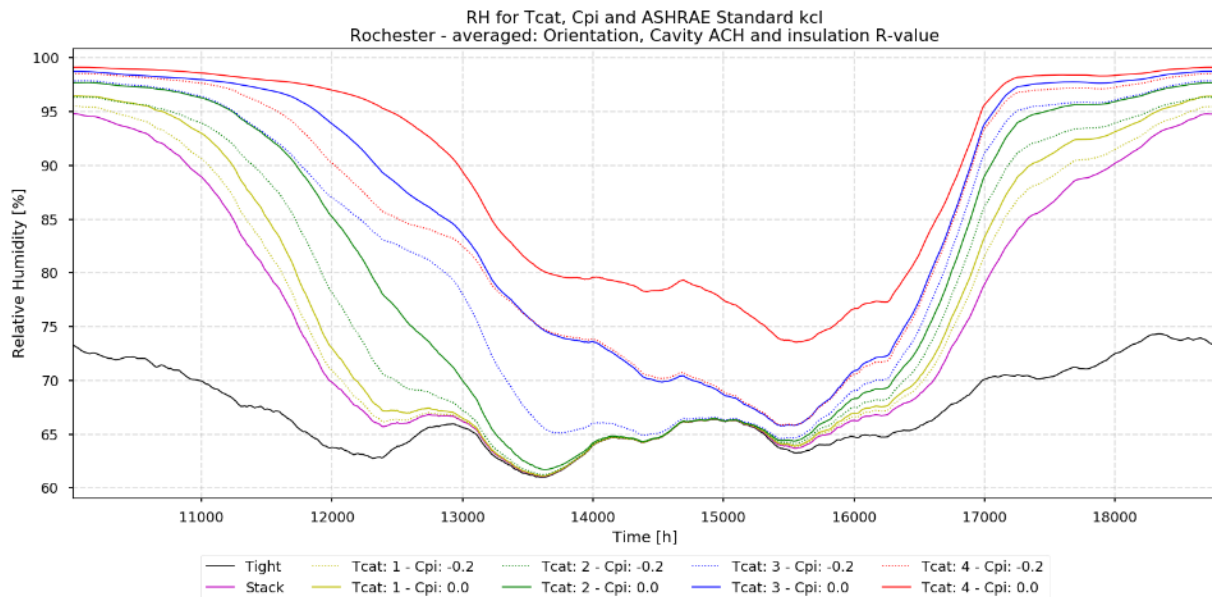
Figure 29: Rochester drying period – RH for ASHRAE Standard k_{cl} and different C_{pi}, other parameters averaged.

For Rochester the differences between $C_{pi}=0$ and $C_{pi}=-0.2$ go up to about 10% during September-October (15000 – 15600 h) for terrain category 4 and around 10% during the end of July (13500 h) for terrain category 3, the difference decreases as the terrain category is 2 or 1.

66
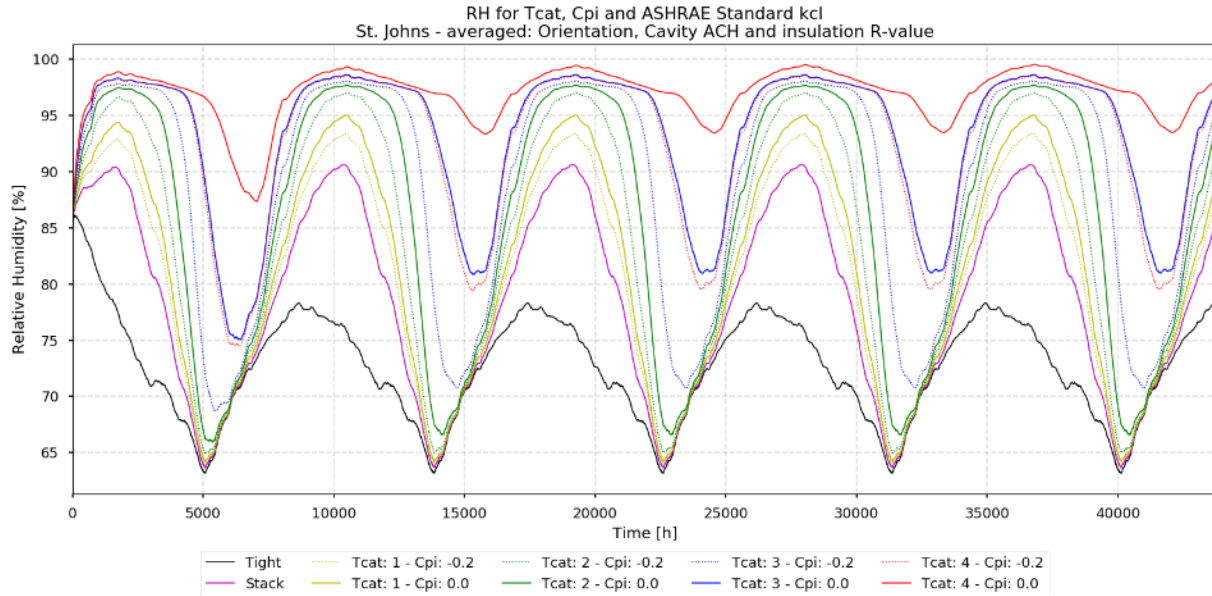
Figure 30: St. Johns – RH for ASHRAE Standard k_{cl} and different C_{pi}, other parameters averaged.

Similar to Rochester, the difference in *RH* for St. Johns considering the two values for C_{pi} is greater for the drying period. Figure 31 provides a zoom to a year period.
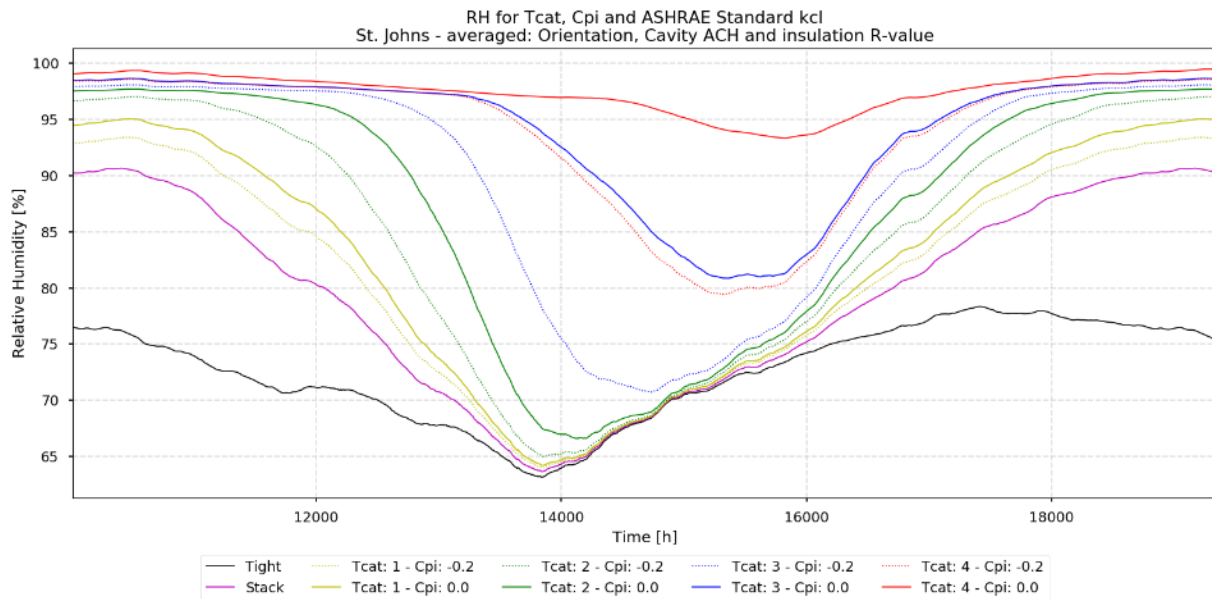
Figure 31: St. Johns drying period – RH for ASHRAE Standard k_{cl} and different C_{pi}, other parameters averaged.

For St Johns, the difference is about 14% during October (15600 h) for terrain category 4 and goes up to about 16% from August (14200 h) to September (15000 h) for terrain category 3. This extended period with higher humidity can prove prejudicial as can be seen in the higher mould index presented in Section 5.1.

67

The highest difference during the drying period for Rochester and St. can be explained because the exfiltration flow generated in this windy cities when using C_{pi}=0 is high enough to continually generate condensation on the wall sheathing, reducing the drying capacity of the wall.
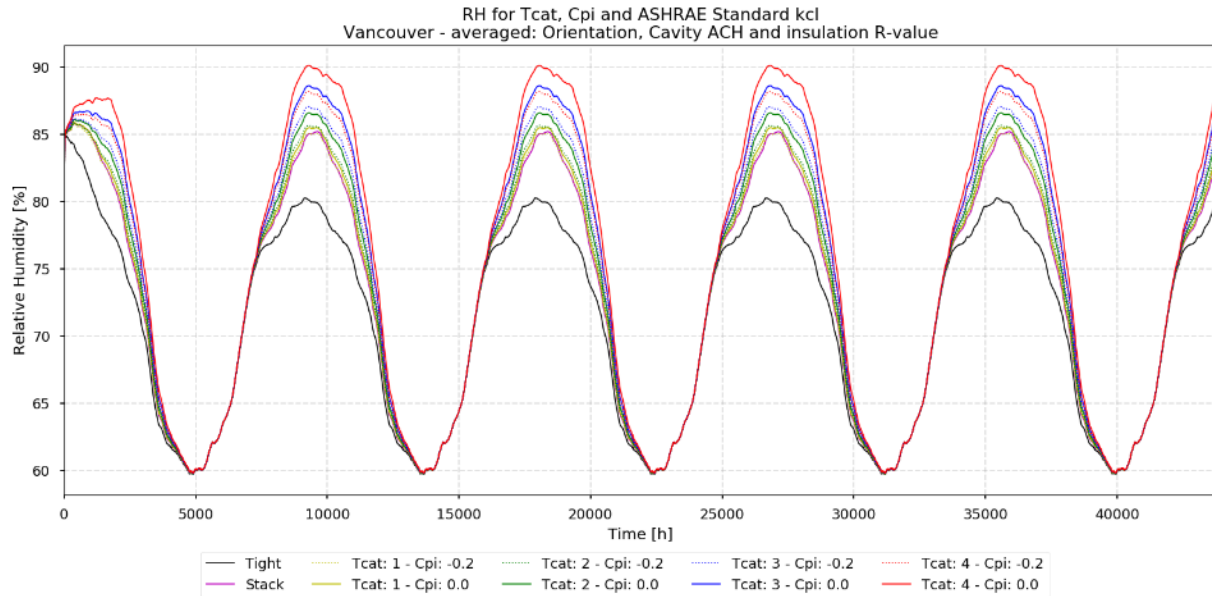
Figure 32: Vancouver – RH for ASHRAE Standard k_{cl} and different C_{pi}, other parameters averaged.

The difference between the results for different C_{pi} for Vancouver is minor reaching a maximum of only 2.5%. With the results shown in this section it can be appreciated that the importance of the C_{pi} is dependent on the wind speeds. With higher wind speeds, the difference in the RH obtained with $C_{pi} = 0$ and $C_{pi} = -0.2$ will be higher than that obtained for lower wind speeds.

5.3   Wall Design Parameters

Wall orientation, *RSI* value, and cavity ventilation rate parameters are proper of the design of the wall and do not affect, or are affected by the wind. Although in reality, the cavity ventilation rate will depend on the wind speed and direction, in this research, it was treated as an independent variable.

5.3.1 Effect of Orientation

The following graphs demonstrate the effect of the orientation of the wall over the hygrothermal performance. Blue lines show north-oriented wall and red lines correspond to maximum wind

pressure orientation. The different moisture leakage parameters (k_{cl}) are shown with different shades of the corresponding color. The results considering only stack pressures is shown in a segmented line style, and the continuous line shows the results when wind is included.

For all locations except for Rochester, the relative humidity is higher for north orientation cases in comparison to the orientation that produces the maximum wind pressure over the wall. In general, this could be expected as other orientations different from the north will receive more solar radiation, thus providing an enhanced drying capacity.
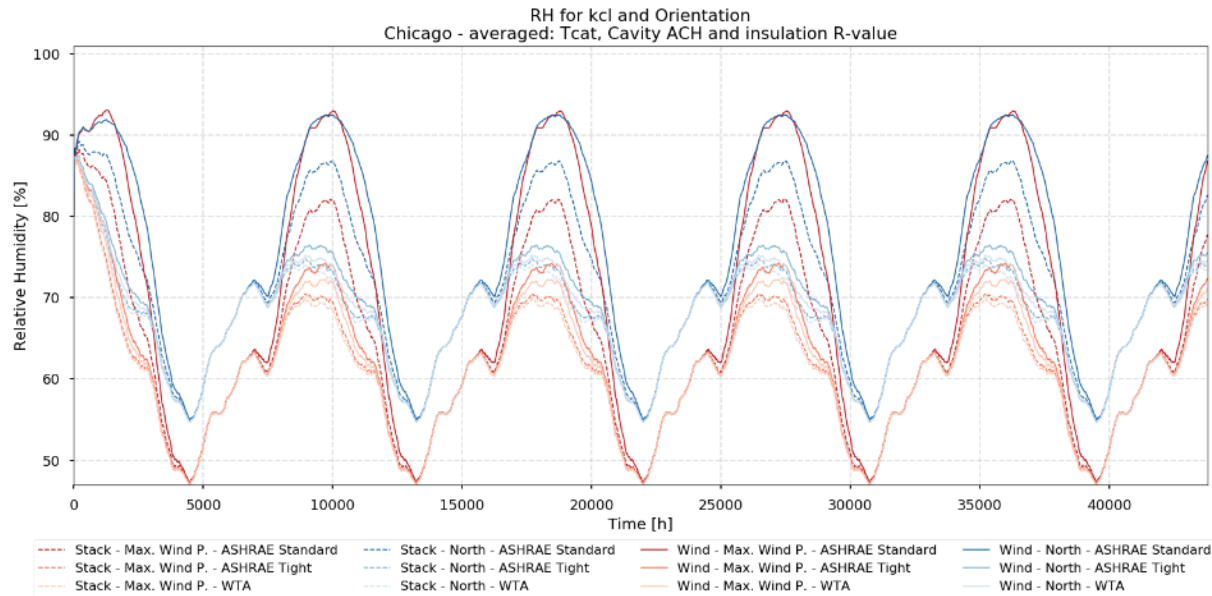
Figure 33: Chicago – RH for k_{cl} and Orientation.

For Chicago the North orientation presents a *RH* about 7% higher than maximum wind pressure orientation during the drying period, independently from the k_{cl} and if wind is considered or not. During the wetting period the difference between each k_{cl} are visible. When wind and ASHRAE Standard k_{cl} are considered there is practically no difference in the maximum *RH* obtained, when only stack pressures are considered (segmented lines) the difference between both orientations reaches about 5%, being higher for the North orientation.
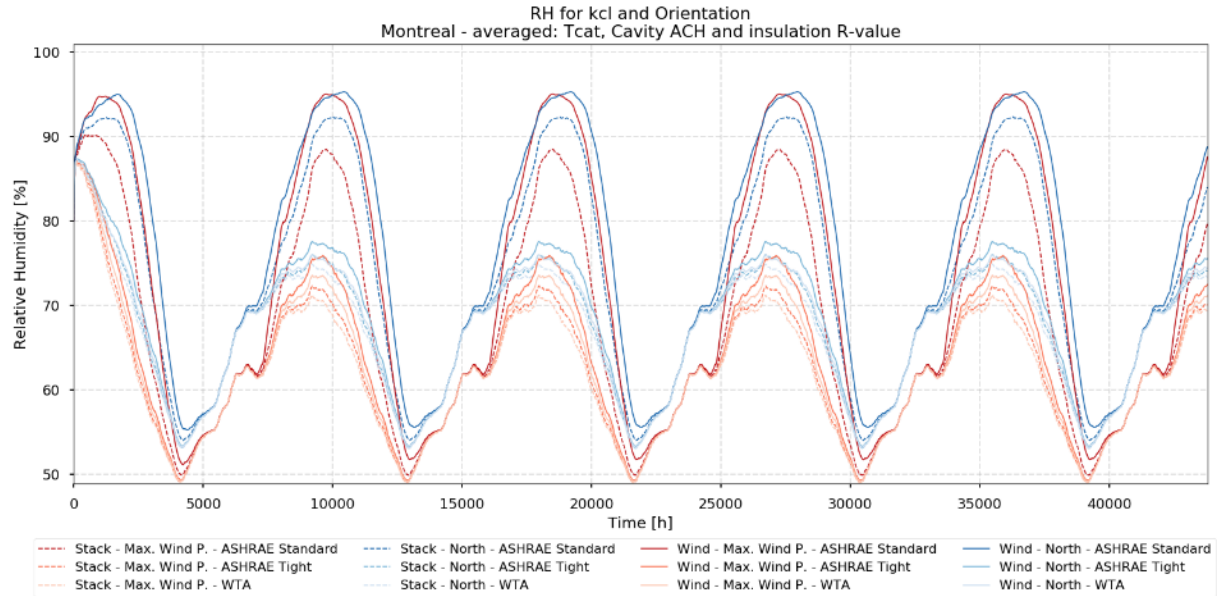
Figure 34: Montreal – RH for k$_{cl}$ and Orientation.

Montreal has a similar behaviour to Chicago, but the differences between both orientations are minor, being around 3% higher for North orientation, independently from the *k$_{cl}$*. When only stack pressures are considered (segmented lines) the difference between both orientations reaches about 4%, being higher for the North orientation.
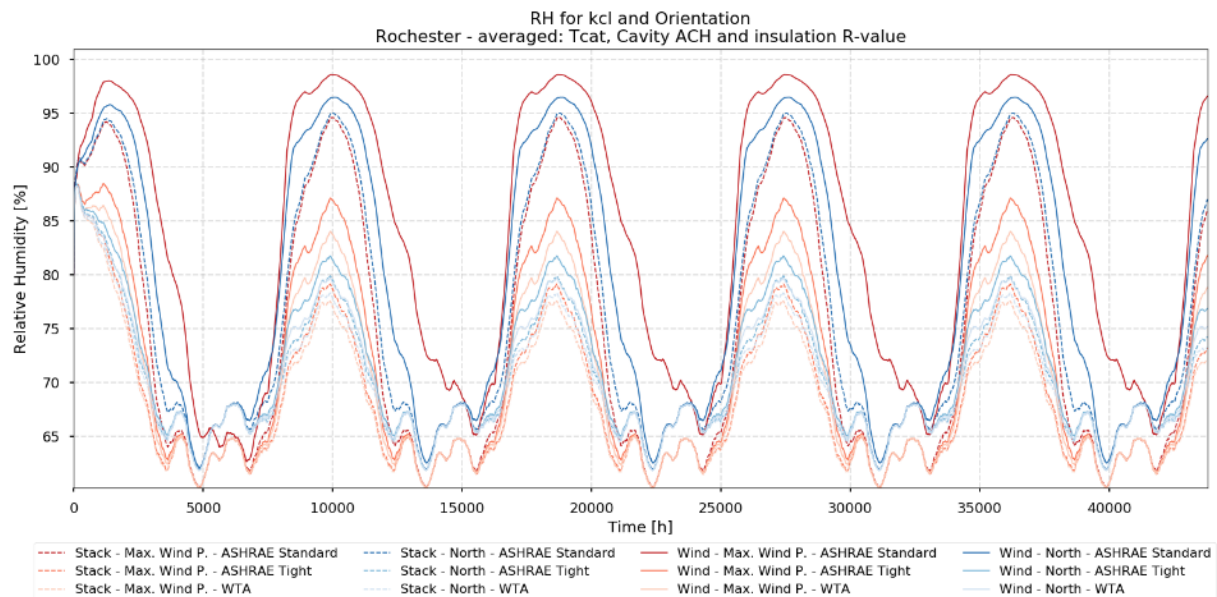
Figure 35: Rochester – RH for k$_{cl}$ and Orientation.

For Rochester contrary to the rest of the cities, when wind is considered in the hygrothermal analysis the *RH* for the maximum wind orientation is higher than the *RH* for the North orientation. This difference can be explained by the S-E wind blowing in the city (see Figure 7), which counteracts the winds blowing to the north thus reducing the total pressure affecting the wall, whereas the maximum wind orientation maximizes the effect of both wind directions, increasing the moisture deposition on the wall. Additionally, this orientation receives more solar radiation, which increases the temperature of the wall sheathing, and when it is combined with the higher relative humidity generates mould index higher than 3. The *RH* for the maximum wind pressure orientation is between 2% and 10% higher than for the North orientation.
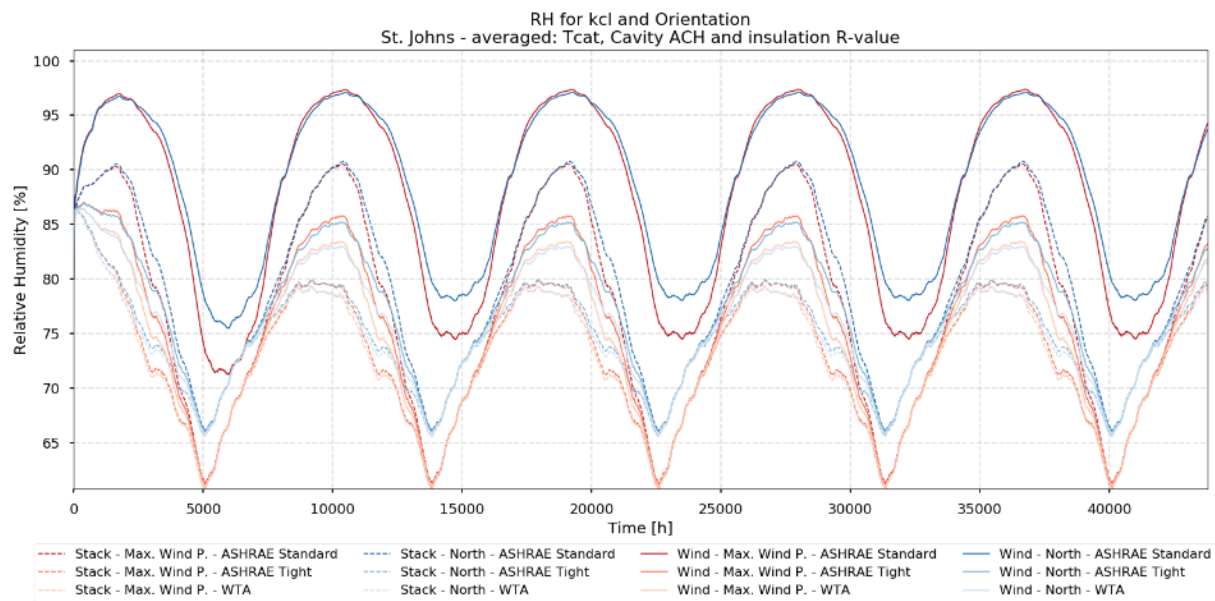
Figure 36: St. Johns – RH for k_{cl} and Orientation.

Figure 36 for St. Johns shows that the North oriented wall has higher *RH* than when oriented towards the maximum wind pressure, with a difference of around 5% noticeable mostly during the drying period and independently from the k_{cl} assumed or if wind or only stack effect are considered. This similitude between orientations was observed previously in section 5.1, where there was little difference in the mean *RH* or mould Index between both orientations.
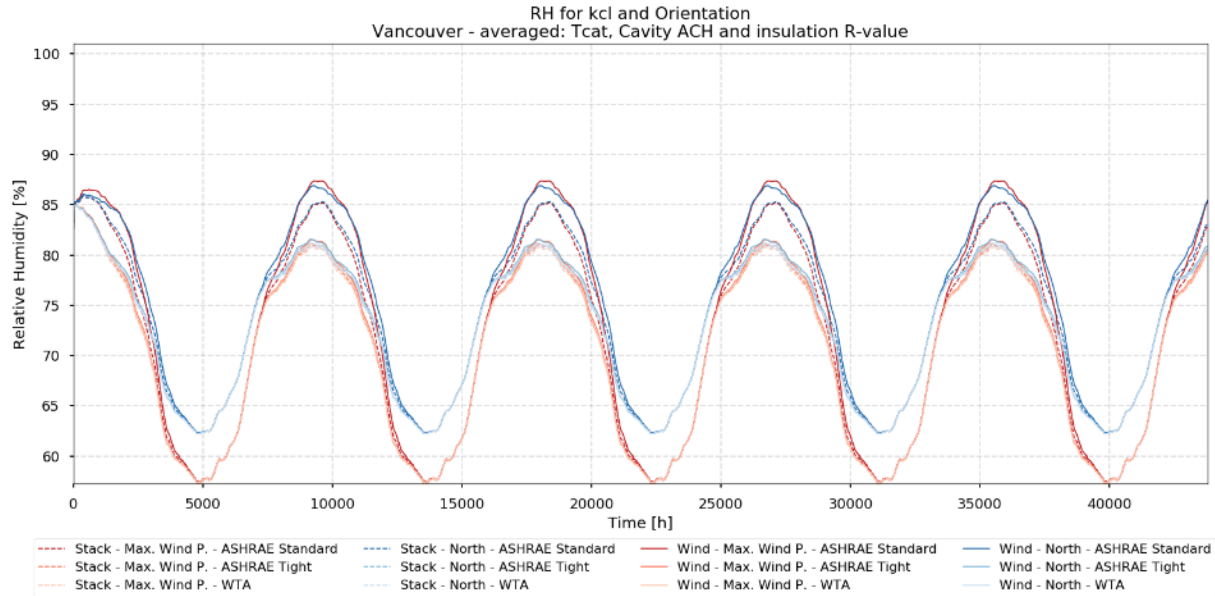
Figure 37: Vancouver – RH for k_{cl} and Orientation.

Figure 37 for Vancouver also shows a difference of about 5% between both orientations for the driest period and practically no difference at other times.

5.3.1.1 Mould Index – Effect of Orientation, Terrain Category and Internal Pressure Coefficient

The previous sections had demonstrated the effect of Orientation, Terrain category and C_{pi} over the hygrothermal performance, showing that they are especially relevant in cities with high wind speeds. All these three parameters have a more significant effect than the level of insulation and the airflow rate of the ventilation cavity, parameters that will be discussed in the following sections.

As briefly mentioned in section 5.1, the terrain category and C_{pi} has a proportional relationship with the relative humidity, i.e. the higher the terrain category and C_{pi}, the higher will be the relative humidity of the surface. While the Orientation, because the combined effect of sun and wind has an effect that is city dependent. Section 5.1 showed different behaviour of the mould Index for Rochester in comparison with the other cities. The following figures show the mould Index depending on the Orientation, Terrain category and C_{pi} for each of the cities.

72
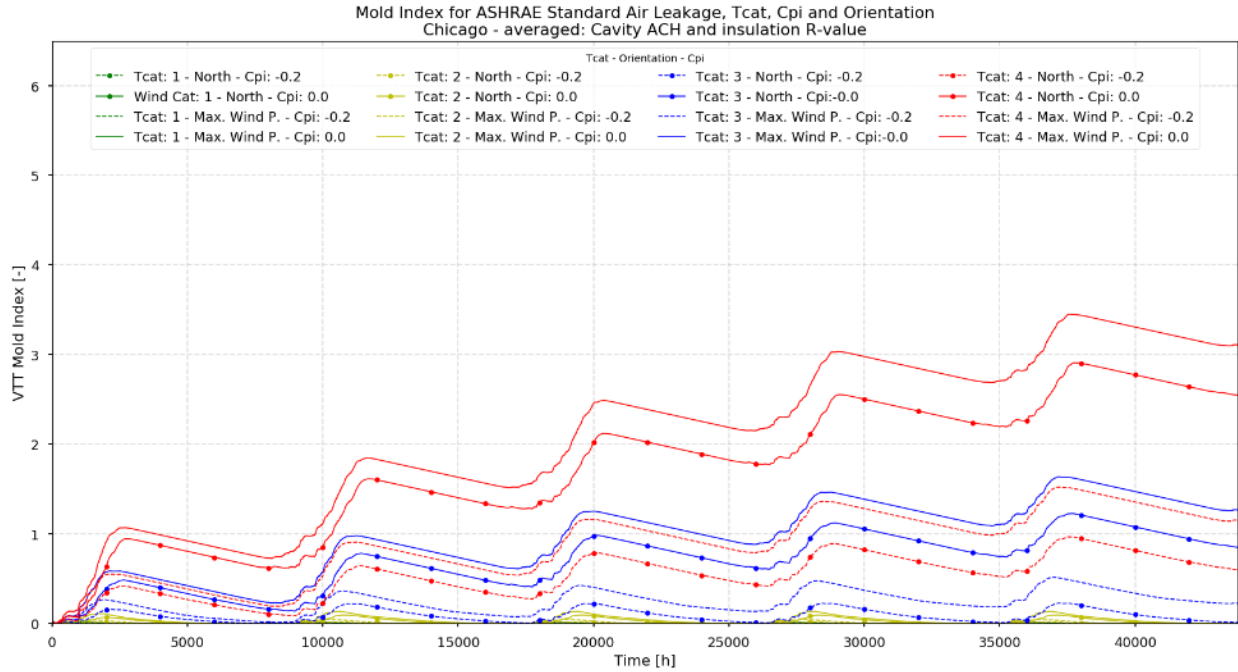
Figure 38: Chicago - Mould index for ASHRAE Standard k_{cl}, Orientation, Terrain category and C_{pi}. Ventilation ACH rate and RSI-value averaged.
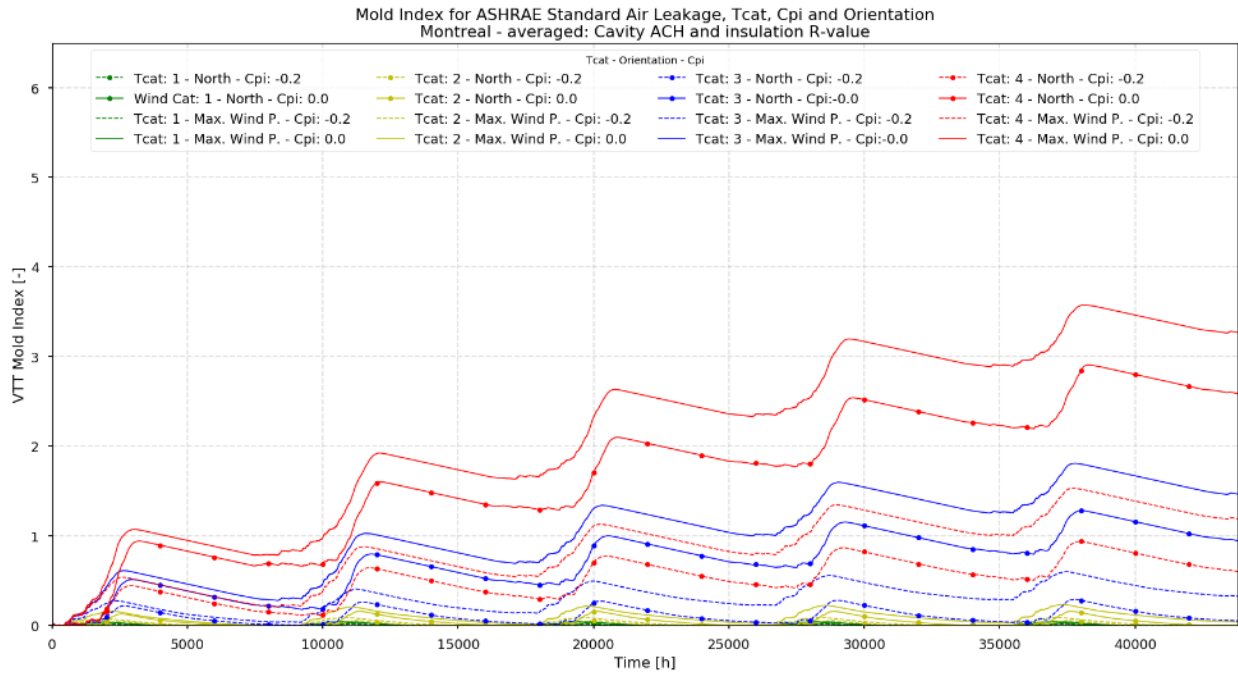
Figure 39: Montreal – Mould index for ASHRAE Standard k_{cl}, Orientation, Terrain category and C_{pi}. Ventilation ACH rate and RSI-value averaged.

As seen in the previous sections Chicago and Montreal presented moderate effects in all the parameters related to the airflow (k_{cl}, C_{pi}, T_{cat}) and orientation, this is reflected in the mould index

curves. For these cities only the case with higher exfiltration (T_{cat} = 4 and C_{pi} =0) presented a mould index higher than 3 as can be seen in Figure 38 and 39. For both cities the average mould Index is higher for the maximum wind orientation than for the North orientation but the difference is only about 0.5 mould Index.
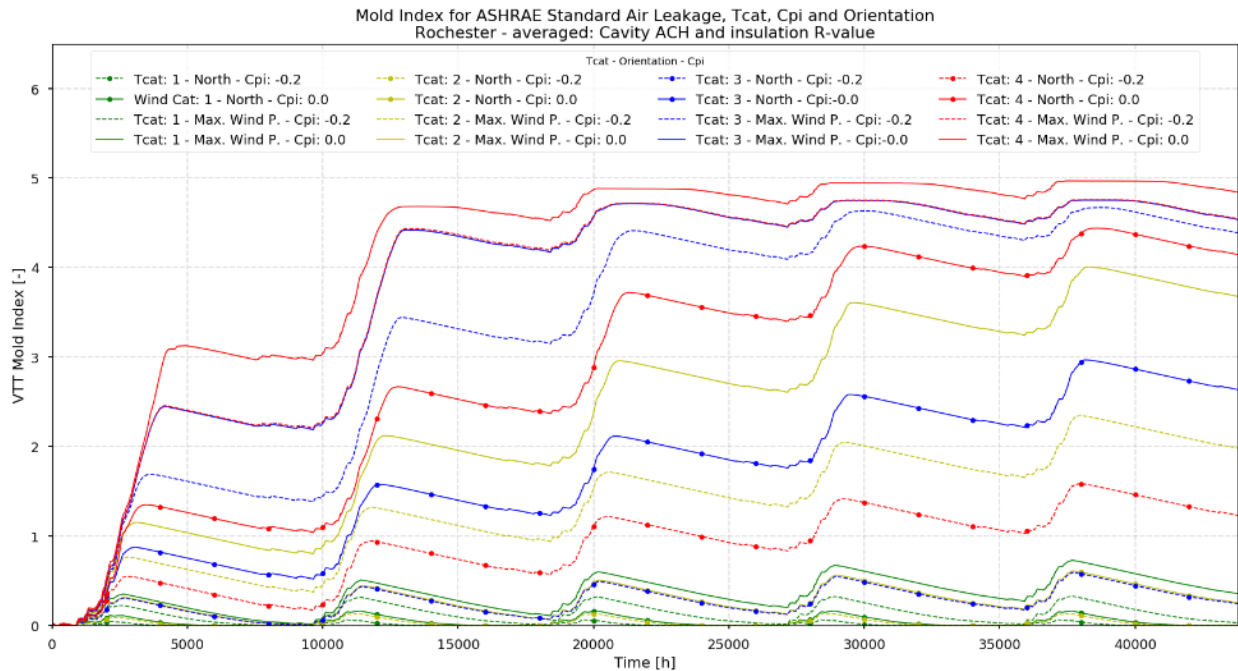
Figure 40: Rochester – Mould index for ASHRAE Standard k_{cl}, Orientation, Terrain category and C_{pi}. Ventilation ACH rate and RSI-value averaged.

For Rochester, the highest mould Index is generated for cases positioned towards the maximum wind pressure orientation as mentioned in previous sections. Due to the higher wind speeds that induce higher exfiltration rates, more cases develop a mould index higher than 3. It is also appreciable the difference in mould index between both orientations, for example if T_{cat} 2 and C_{pi} 0 are considered it can be seen that the maximum wind orientation developed a maximum mould Index of 4, and for the North orientation the maximum mould Index was close to 0.5.

Figure 41 for St. Johns shows practically the same result between both orientations with a difference of less than 0.1 mould Index independent from the T_{cat}. The effect of the C_{pi} is appreciable for T_{cat} 2, generating a difference of about 1.5 mould Index, for the other T_{cat} the difference is not noticeable because the mould Index reaches its extreme vales.
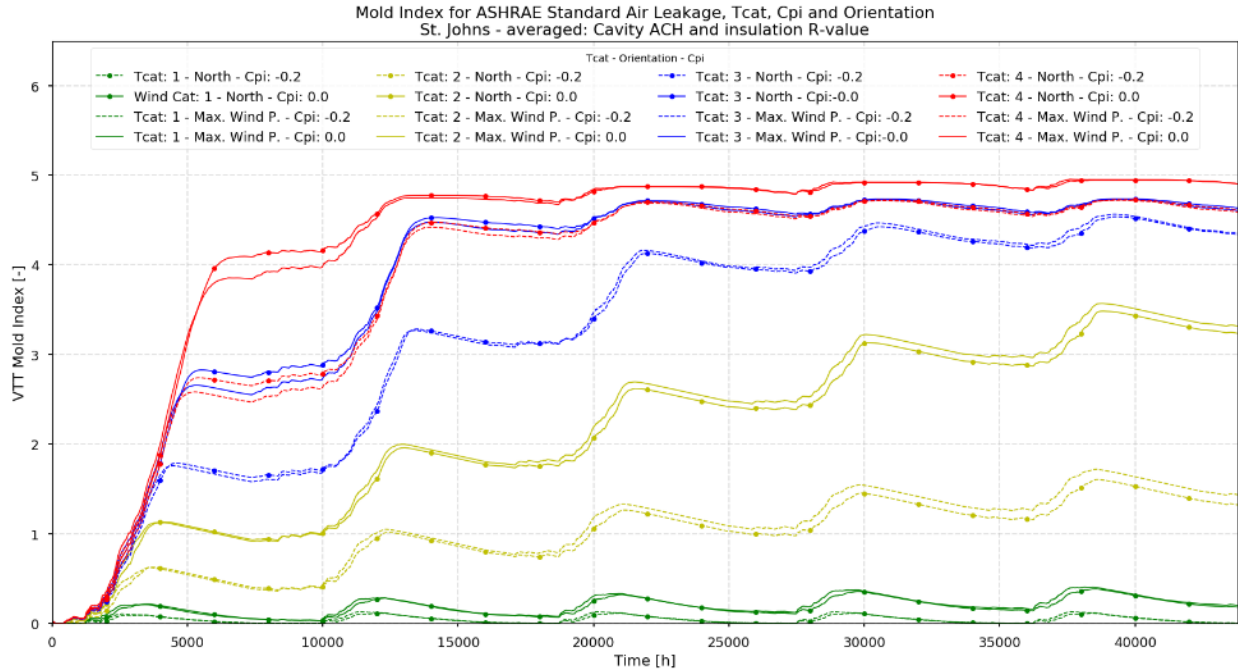
Figure 41: St. Johns– Mould index for ASHRAE Standard k_{cl}, Orientation, Terrain category and C_{pi}. Ventilation ACH rate and RSI-value averaged.
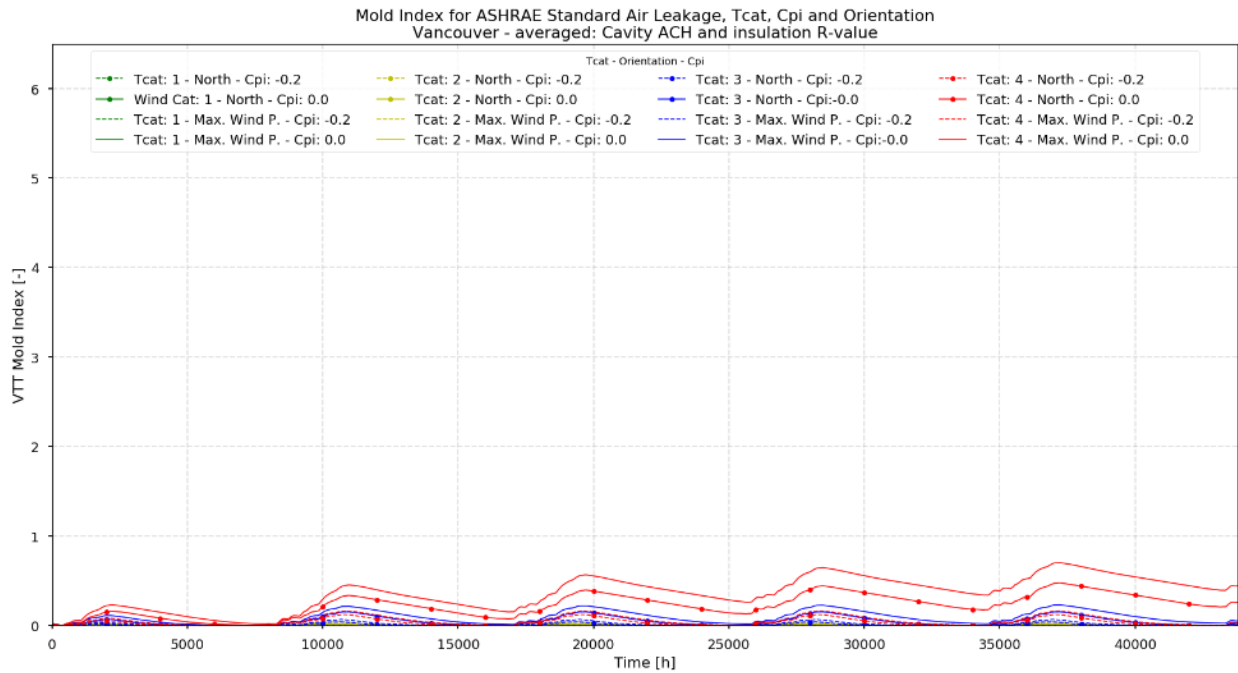
Figure 42: Vancouver – Mould index for ASHRAE Standard k_{cl}, Orientation, Terrain category and C_{pi}. Ventilation ACH rate and RSI-value averaged.

Vancouver due to the slower wind speeds present mould Index lower than 1. Appendix I presents the maximum mould Index for each of the simulations for further details.

5.3.2 Effect of *RSI*-value

The following graphs show the effect of increasing insulation over the hygrothermal performance of the wall. Only ASHRAE Standard is shown due to the smaller difference in the results when using more tighter k_{cl}'s. The different levels of insulation are shown with different intensities of each corresponding color, lighter colors meaning lower *RSI* values and darker colours showing higher *RSI* values.

Increasing the *RSI*-value of the wall insulation generate higher relative humidity. With more insulation, the exterior OSB sheathing remains colder because the heat flow from the interior is restricted by the higher thermal resistance. The effect of the *RSI*-value is more evident in cities like St. Johns or Rochester, and at higher T_{cat}, were the wall is not able to dry out to levels comparable to when only stack effect is considered in the analysis.
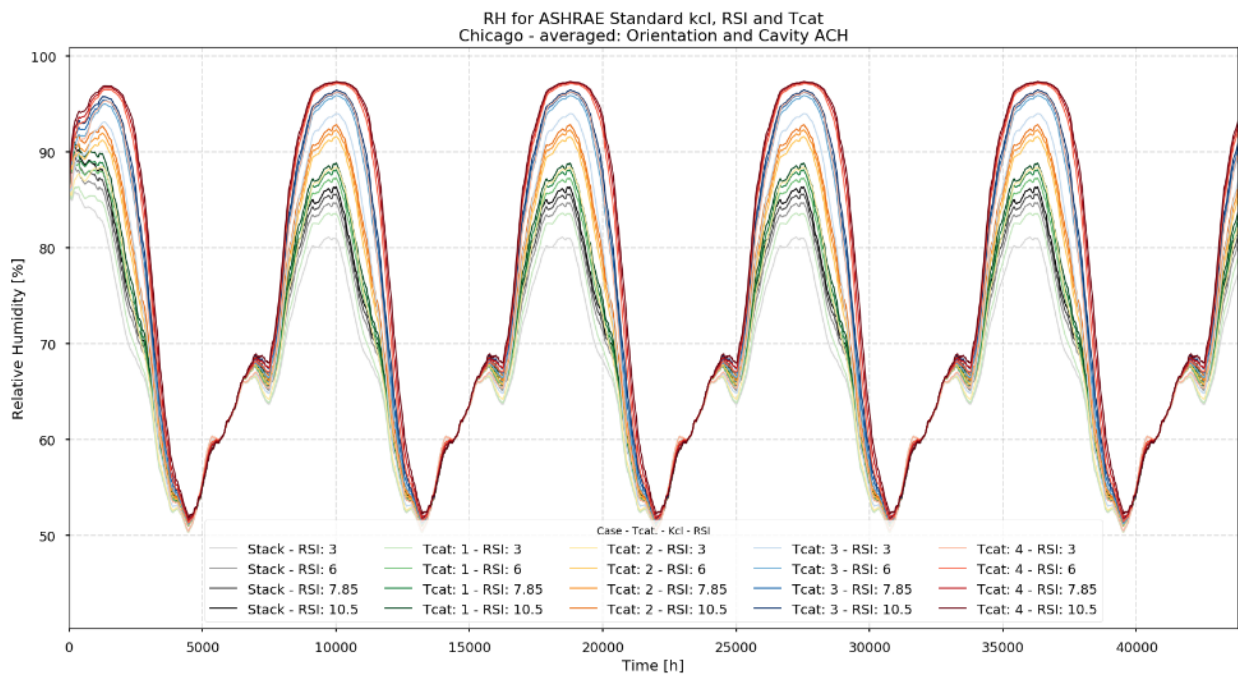
Figure 43: Chicago – RH for different Insulation level and Terrain category (ASHRAE Standard k_{cl})
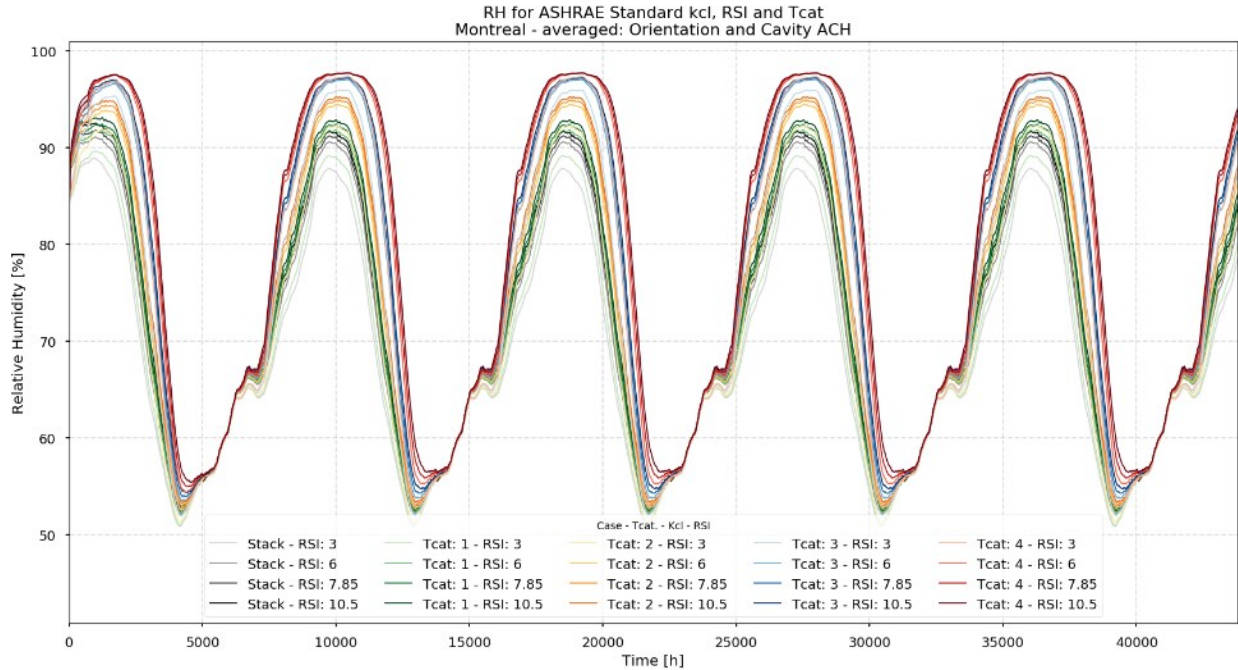
Figure 44: Montreal – RH for different Insulation level and Terrain category (ASHRAE Standard k_{cl})

Montreal and Chicago show a very similar trend for the variation of *RSI*. The maximum RH reaches a maximum when the *RSI* is higher, but the difference between the maximum reached, when *RSI* is 3 and *RSI* is 10.5 is less than 5%. As the terrain category increases the air exfiltration and the moisture deposition, the relative humidity reaches values closer to 100%, at this point, the differences between different *RSI* are almost none as can be seen for Tcat = 4 where the curves are close together. A better resolution of the effect of the *RSI*-value can be observed in Appendix V, where the moisture content is shown.
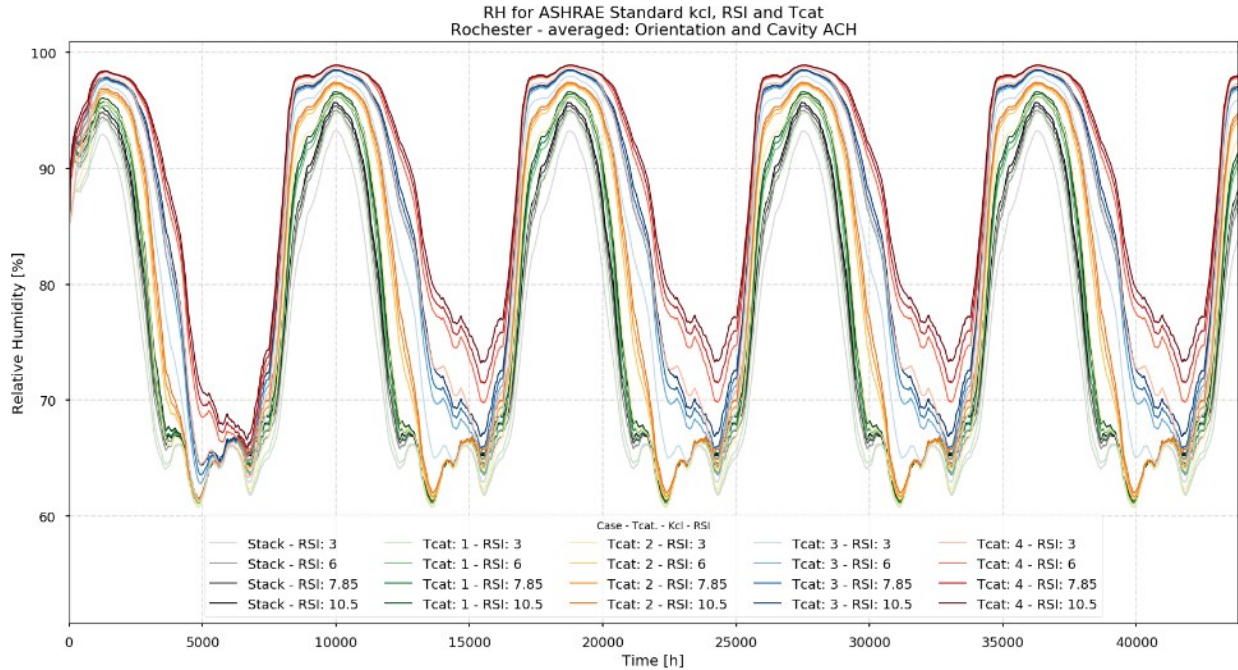
Figure 45: Rochester – RH for different Insulation level and Terrain category (ASHRAE Standard k_{cl})
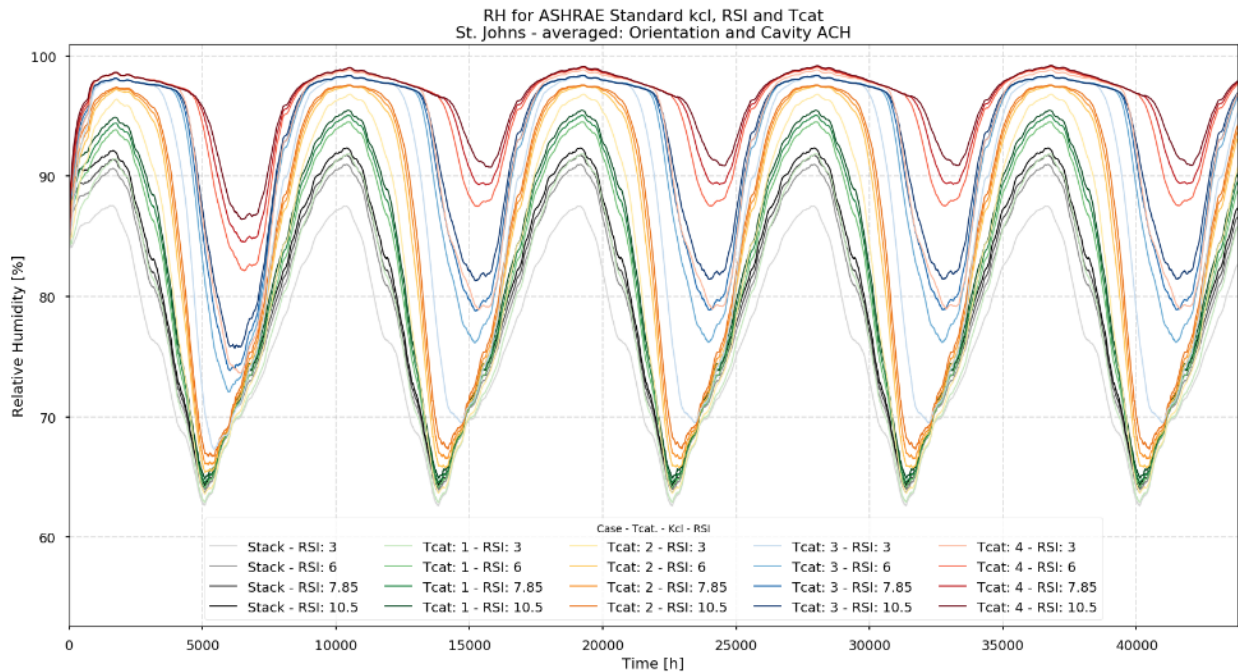
Figure 46: St. Johns – RH for different Insulation level and Terrain category (ASHRAE Standard k_{cl})

For Rochester and St. Johns the difference between different *RSI* is greater in comparison with the two previous cities. The difference is clearly noticeable during the drying period, were for T_{cat} 3 and 4 the difference between *RSI* 3 and *RSI* 6 is about 5% for Rochester and up to 8% for St. Johns.

78

For T_{cat} 1 and 2 the difference between *RSI* is similar to that observed for Montreal and Chicago. The greater difference observed in the cities with higher wind speeds (Rochester and St. Johns) can be explained by the increased moisture deposition due to the higher levels of exfiltration, with higher moisture content it takes longer time to dry the wall.
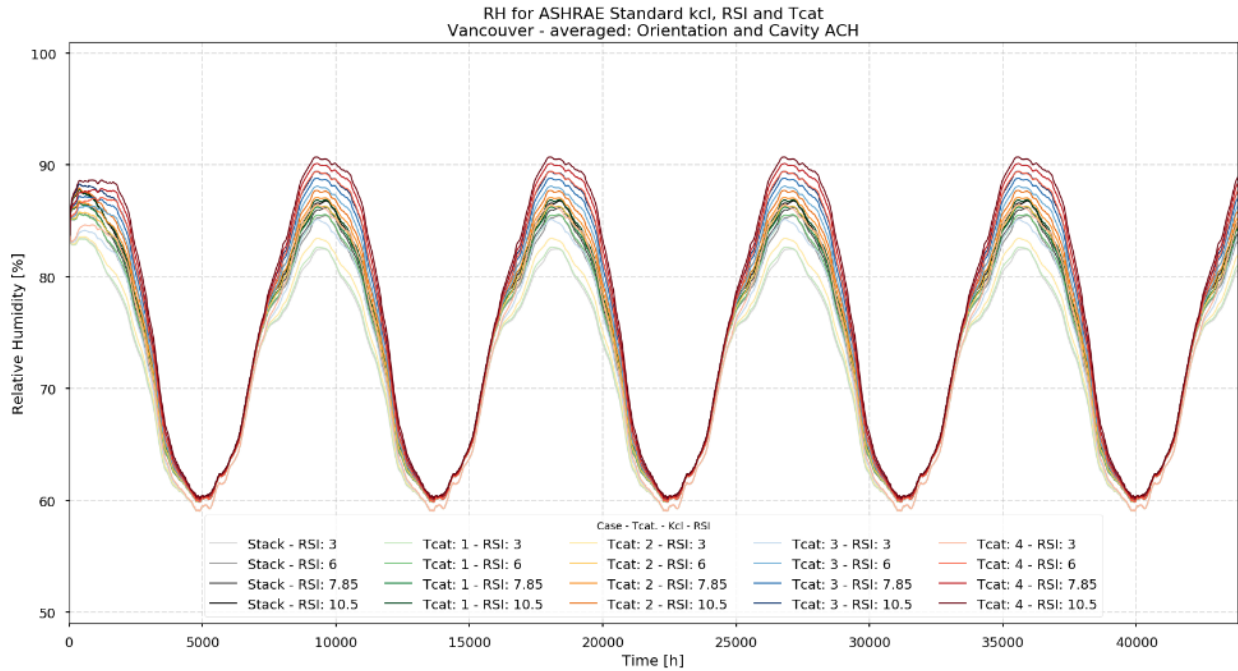
Figure 47: Vancouver – RH for different Insulation level and Terrain category (ASHRAE Standard k_{cl})

Vancouver due to the lower moisture deposition presents minimal difference between the various *RSI* used in the parametric study.

5.3.3 Effect of Cavity Air Change Rate

The following graphs show the effect of the airflow rate in the air cavity. Only ASHRAE Standard k_{cl} is shown, with lighter colors represent a lower air change, and the darker colours represent a higher airflow rate.

Although the difference in the results between cases with different air changes in the ventilation cavity is small, around 4%, it is interesting to notice that an *ACH* rate of 100 was found to produce the lower mean relative humidity in the parametric study context.
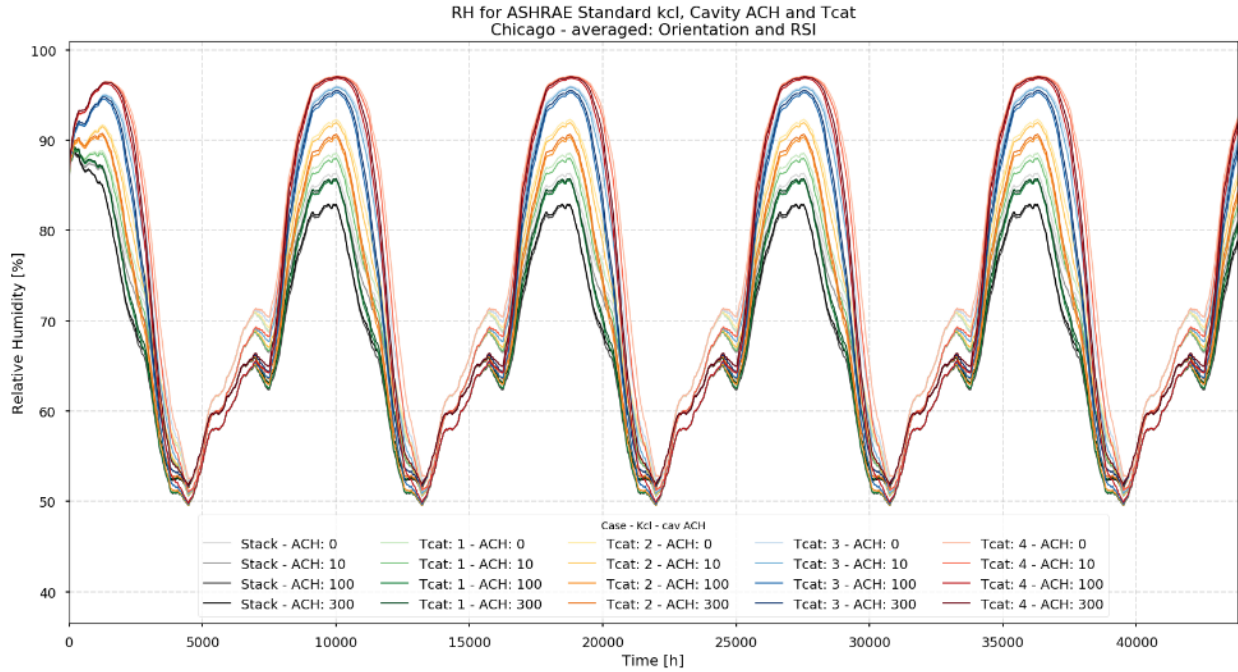
Figure 48: Chicago – RH for different cavity ACH rate and Terrain category (ASHRAE Standard k$_{cl}$)
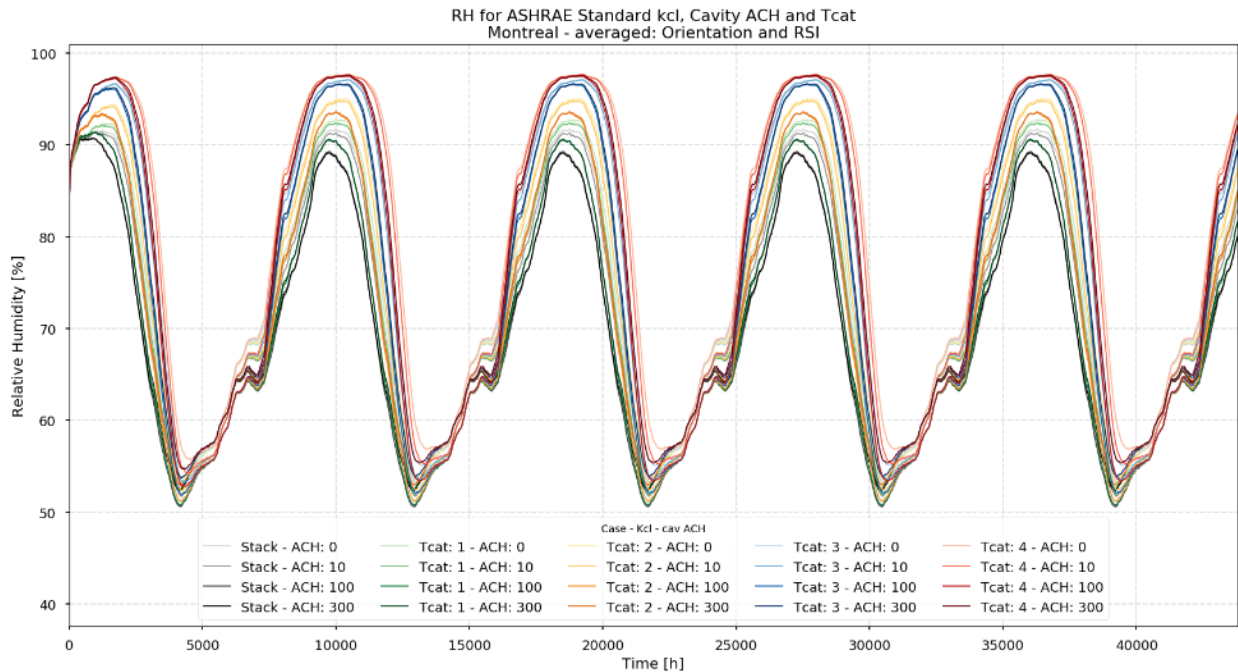
Figure 49: Montreal – RH for different cavity ACH rate and Terrain category (ASHRAE Standard k$_{cl}$)

For cities with medium wind speed (Montreal and Chicago) the variation in *RH* due to different ACH rates in the ventilation cavity is very minor, being less than 2% different. Similar to section 5.3.2 when the effect of the *RSI*-value was studied, the resolution at higher *RH* can be better

visualized in the Appendix VI – Terrain Category and Cavity Air Change Rate, where *MC* is shown.
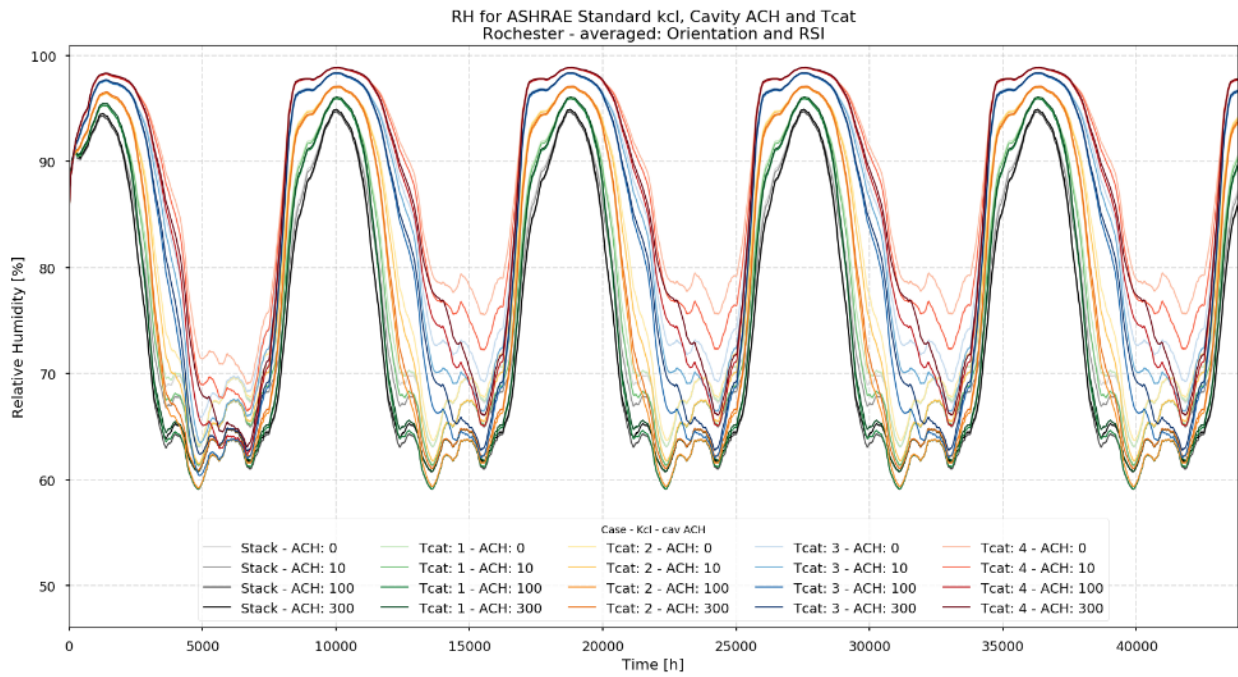
Figure 50: Rochester – RH for different cavity ACH rate and Terrain category (ASHRAE Standard k_{cl})
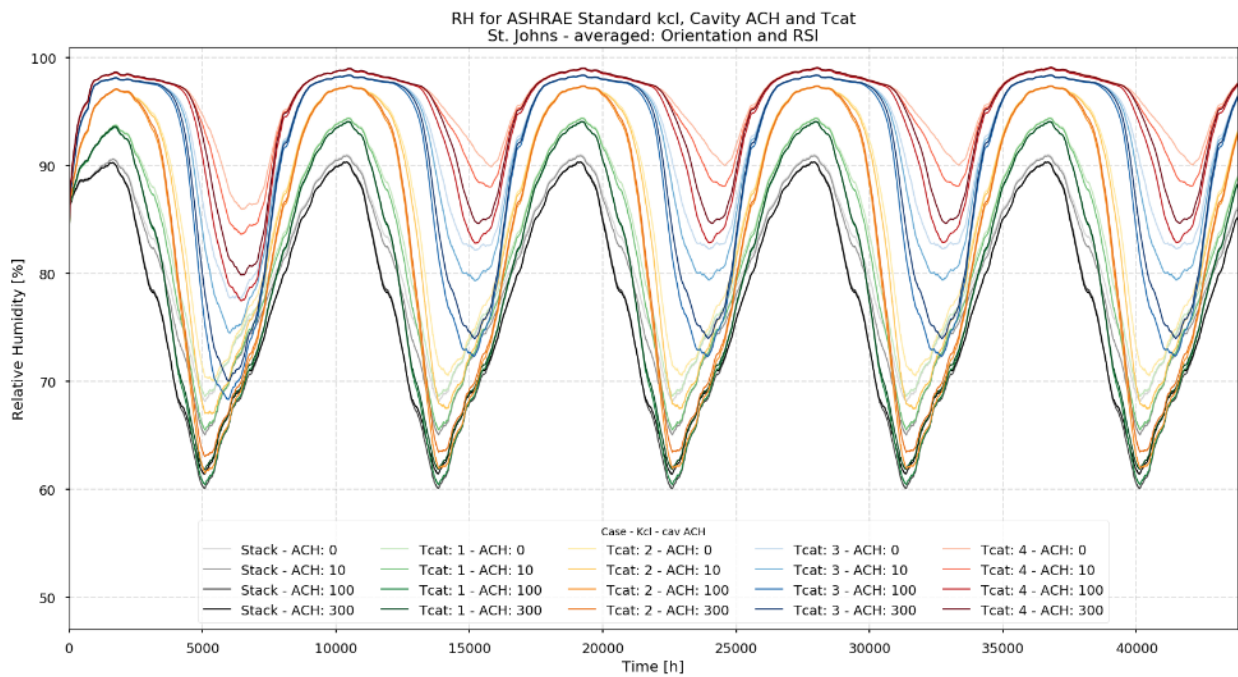
Figure 51: St. Johns – RH for different cavity ACH rate and Terrain category (ASHRAE Standard k_{cl})

81

Similar to what was observed for the *RSI* effect, a clear difference between the different ACH rates can be observed during the dryer period. For T_{cat} 3 or 4 differences of about 8 to 10% can be observed. Also, in both cities it can be seen that a ventilation cavity rate of 100 has the lower *RH*. This suggest that the drying capacity of the wall does not improve with higher ventilation rates.
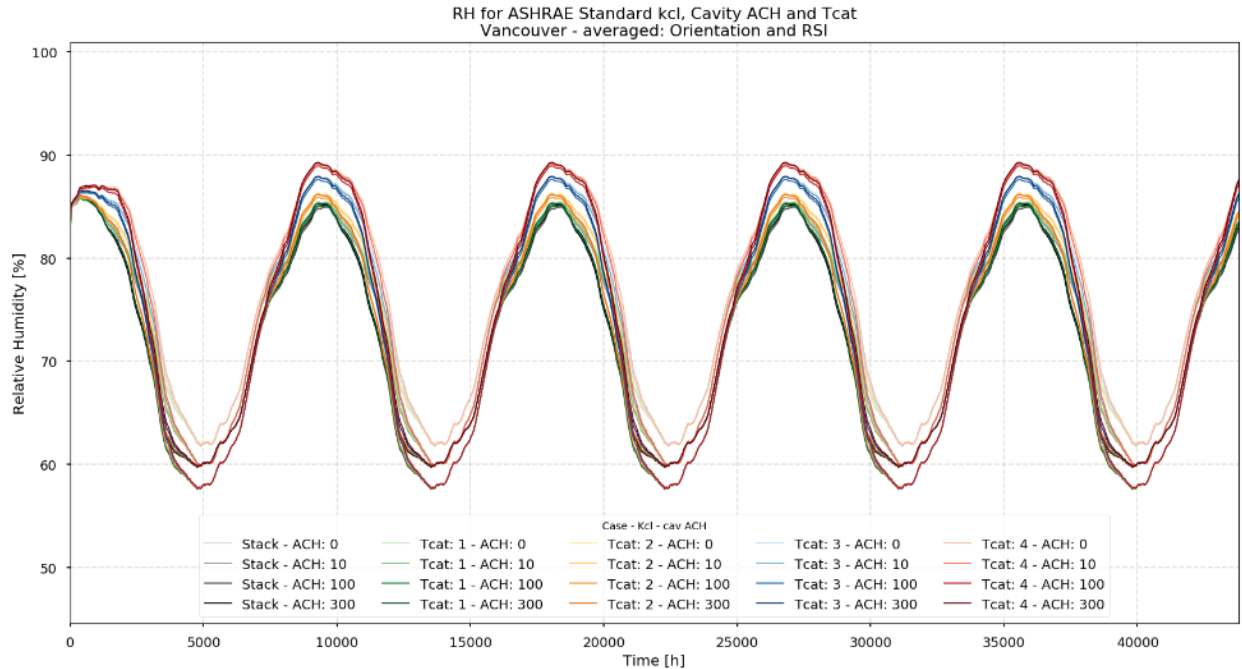
Figure 52: Vancouver – RH for different cavity ACH rate and Terrain category (ASHRAE Standard k_{cl})

Vancouver does not present notable differences between the 4 values for the ventilation rate in the cavity. In general it was observed that a minimum *RH* is achieved when 100 ACH is considered for all the cities.

6 Summary of Results

This section summarizes the findings discussed in Section 5.

With the exception of the results for Rochester, north-oriented walls presented a higher relative humidity than walls oriented towards the direction that maximized wind pressure differentials. However, when using the mould Index as the performance indicator, all cases oriented towards the maximum wind pressure orientation presented higher mould Index. The higher mould Index present in orientations different from the North could be explained by the fact that those orientations have a higher surface temperature generated by the increased solar radiation, which reduces the critical relative humidity (shown in Figure 4), thus increasing the number of hours of favourable conditions to develop Mould.

It was found that orientations other than North can have a higher RH and mould potential. Specifically for Rochester, it was found that the RH for North orientation was between 2% to 10% lower than for the maximum wind pressure orientation. This case can occur when the North orientation is subject to continuous positive pressure acting on the surface, which will reduce the exfiltration due to the stack effect and the moisture deposition.

Higher levels of insulation (RSI-value), are detrimental for the hygrothermal performance. In the presence of high levels of air leakage, additional insulation reduces the thermal energy that reaches the wall sheathing, generating a colder surface, increasing the relative humidity and reducing the drying capacity. On the other hand, the cavity ventilation airflow rate (ACH_{cav}), is favourable for the drying process. A maximum drying of the sheathing was found with a ventilation cavity rate of 100 ACH. Higher ventilation cavity rates cool down the sheathing increasing the relative humidity. Both parameters (RSI-value and ACH_{cav}) generated lower changes in the hygrothermal performance indicators in comparison to the parameters related to airflow and orientation.

For large density locations (terrain category 1) wind effect could be disregarded for all cities considered in this study. The variation in the relative humidity was lower than 3.4% for all the cases when compared to the case including only stack-induced pressure differential.

Table 24 shows the percentage of cases that are under a certain category of the mould index. Simulations considering just the stack effect have a mould index lower than 2, but when wind is included in the analysis up to 60% of the cases for St. Johns and 41% of the cases develop a mould index higher than 3. For Montreal and Chicago about 10% of cases develop mould index higher than 3. Finally, the inclusion of wind does not have an influence over the mould Index for Vancouver.

Table 24: Summary of results. Percentage of cases under mould category

Mould Index	% of cases (ASHRAE Standard k_{cl})									
	St Johns		Rochester		Chicago		Montreal		Vancouver	
	Stack	Wind	Stack	Wind	Stack	Wind	Stack	Wind	Stack	Wind
0-2	100%	34%	100%	53%	100%	85%	100%	83%	100%	100%
2-3	0%	6%	0%	6%	0%	7%	0%	9%	0%	0%
≥ 3	0%	59%	0%	41%	0%	8%	0%	9%	0%	0%

7 Conclusions

Although air leakage rates used for hygrothermal analysis account for wind, those rates are commonly taken from energy-related Standards which do not differentiate between infiltration and exfiltration processes and are usually assumed to be a constant value, which might be over simplistic and under some conditions produce underestimation of the air exfiltration.

Through a parametric study this thesis has qualitatively illustrated that wind-induced exfiltration can have a significant effect on the hygrothermal performance of walls of low-rise buildings, and that under some wind speeds and some wall orientation, if wind is ignored mould risk can be underestimated. Not accounting for the wind could lead to an underestimation of the mould index, which can lead to the selection of an envelope design that will not perform as expected or predicted by simulation. The parametric study showed that the evaluated wall assembly have a higher risk of developing mould in cities with higher wind speeds in comparison to cities with lower wind speeds.

Based on the parametric study, this research quantified certain wind speeds under which mould is more likely to be underestimated if wind is not considered in the hygrothermal analysis. This conclusion is based on the limited work of this study, both the selected performance indicators and the corresponding numerical values are not meant to be definitive but rather as a demonstration that a guideline similar to Table 25 is worthwhile to be developed.

Table 25: Recommendation for the inclusion of wind-induced exfiltration for hygrothermal analysis based on limited work of this study

Annual mean wind speed	Recommendation for hygrothermal analysis
≥ 5.7 m/s	Consider wind-induced exfiltration
≈ 4.5 m/s	Consider wind-induced exfiltration if T_{cat} is 3 or 4
≤ 3 m/s	Wind-induced exfiltration can be disregarded.

Readers are welcomed to refer section 8 to see the proposed future work to develop a similar guideline to what was presented in this thesis.

The case study for Rochester city illustrated that wall orientations other than the North can develop higher mould index. This case suggests that when wind is considered for the calculation of air

exfiltration, it is of importance to analyze which wall orientation will increase the mould growth risk.

Moisture leakage (k_{cl}) was found to be the most influential parameter in this parametric study. The two lowest values used for this parameter did not present a single case with a mould index higher than 1, while the highest k_{cl} produced 23% of the cases with a mould Index higher than 3. Additionally, as a consequence of the relationship between k_{cl} and the pressure differential, the airflow related parameters, namely T_{cat} and C_{pi}, demonstrated higher variation in the performance as indicated by *RH*, *MC* and mould Index, when compared to those produced by the parameters that define the wall design, namely, *RSI*-value and ACH_{cav}. Due to the lower thermal energy flow in designs with higher insulation levels, hygrothermal performance indicators are worse in those designs, although it will only be problematic if high levels of exfiltration are present. Also, ventilating the air cavity improves the drying capabilities of the assembly, the parametric study suggested that ventilation rates higher than 100 *ACH* do not improve the drying effect under the boundary conditions of the case study. Finally, the wall orientation is the only parameter that is location-dependent because it is related to the wind direction distribution and speed of each particular city.

All things considered, this study illustrated that under some wind conditions, it is worthwhile to include wind-induced air exfiltration for hygrothermal modelling. A recommendation for when it can be influential to include wind-induced exfiltration for hygrothermal performance of walls to avoid underestimating the mould index, relative humidity and moisture content was presented.

8 Contribution and Future Research

Contribution:

- This study has qualitatively illustrated the influence of wind-induced exfiltration on the hygrothermal performance of wood-framed walls on low-rise buildings. It was shown that under some wind conditions the mould Index of walls was underestimated when wind-induced exfiltration was not considered in the analysis.
- By quantifying the effects of wind-induced exfiltration on the hygrothermal performance of walls across five cities it was possible to provide general guidelines for when it is recommended to consider wind-induced exfiltration in the hygrothermal analysis for practice purposes. Future research can expand and develop a similar guideline.

Future Research:

- This workflow can be used to develop a design tool to inform practitioners when they should consider wind for the hygrothermal analysis.
- In order to assess the hygrothermal performance of wooden assemblies in high-rise buildings, where wind effect is more pronounced, it would be necessary to modify the workflow presented in this study. Storey compartmentalization affects stack pressures, mechanical equipment is almost always included in high-rise buildings, and different wind pressure coefficient models for high-rise buildings would be required. Nevertheless, with the corresponding modifications for pressure differential calculation, it would be possible to assess the hygrothermal performance of high-rise buildings using a similar approach to the one presented in this study.

9 References

Air Barrier Association of America. (2009). *ABAA 014400 THE AIR BARRIER SYSTEM SPECIFICATION*. Retrieved from http://www.airbarrier.org/technical-information/master-specification/

Allen, C. (1984). Computer-friendly method for the representation of surface wind pressure data. *In: AIVC, Wind Pressure Workshop Proceedings AIC-TN-13.1-84. Brussels: AIVC*.

Antretter, F., Karagiozis, A., TenWolde, A., & Holm, A. (2007). Effects of Air Leakage of Residential Buildings in Mixed and Cold Climates. *Thermal Performance of Exterior Envelopes of Whole Buildings X*.

ASHRAE 90.2. (2007). ASHRAE Standard 90.2-2007: Energy-Efficient Design of Low-Rise Residential Buildings. *ASHRAE Standard*.

ASHRAE Fundamentals. (2017). ASHRAE Fundamentals. *Ashrae Handbook*.

ASHRAE Standard 160. (2009). *ASHRAE Standard 160-2009 - Criteria for Moisture-Control Design Analysis in Buildings*.

ASHRAE Standard 160. (2016). *ASHRAE Standard 160-2016 - Criteria for Moisture-Control Design Analysis in Buildings.pdf*.

Baskaran, B. A., & Brown, W. C. (1995). *Dynamic Evaluation of the Building Envelope for Wind and Wind-Driven Rain Performance*. *18*(january), 261–275.

Birkeland, O. (1962). Curtain Walls. *Oslo, Norwegian Building Research Institute Handbook 11b*.

Blocken, B., & Carmeliet, J. (2000). "Driving Rain on Building Envelopes—II. Representative Experimental Data for Driving Rain Estimation." *J. Build. Phys.*, *Vol. 24,* 89–110.

Blocken, B., & Carmeliet, J. (2004). A review of wind-driven rain research in building science. *Journal of Wind Engineering and Industrial Aerodynamics*, *92*(13), 1079–1130. https://doi.org/10.1016/j.jweia.2004.06.003

Blocken, B., Stathopoulos, T., & Carmeliet, J. (2007). CFD simulation of the atmospheric boundary layer: wall function problems. *Atmospheric Environment*, 41:238–52.

Bomberg, M., Kisilewicz, T., & Nowak, K. (2016). Is there an optimum range of airtightness for a building? *Journal of Building Physics*, *39*(5), 395–421. https://doi.org/10.1177/1744259115603041

Borsch-Laaks, R., Zirkelbach, D., Künzel, H. M., & Schafaczek, B. (2009). Creating drying reserves! Consideration of convective moisture stresses for the evaluation of wooden constructions. *1130542 4th International Symposium on Building and Ductwork Air Tightness - BUILDAIR (Former European Blower Door Symposium), 1-2 October 2009, Berlin, Germany*.

Bre, F., Gimenez, J. M., & Fachinotti, V. D. (2018). Prediction of wind pressure coefficients on building surfaces using artificial neural networks. *Energy and Buildings*, *158*, 1429–1441. https://doi.org/10.1016/j.enbuild.2017.11.045

Burgess, J. C., & McCardle, G. (2000). Building cladding air pressure equalisation investigations - Comparison between field results and a numerical model. *Building and Environment*, *35*(3), 251–256. https://doi.org/10.1016/S0360-1323(99)00022-0

CMHC. (2007). *Research report Air Leakage Control Manual Existing Multi-Unit Residential Buildings*.

Cornick, S., Dalgliesh, W. A., Maref, W., Mukhopadhyaya, P., Kumaran, M. K., & Dean, S. W. (2009). Sensitivity of Hygrothermal Analysis to Uncertainty in Rain Data. *Journal of ASTM International*, *6*(4), 102032. https://doi.org/10.1520/JAI102032

Cóstola, D., Blocken, B., & Hensen, J. L. M. (2009). Overview of pressure coefficient data in building energy simulation and airflow network programs. *Building and Environment*, *44*(10), 2027–2036. https://doi.org/10.1016/j.buildenv.2009.02.006

Defraeye, T., Blocken, B., & Carmeliet, J. (2011). Convective heat transfer coefficients for exterior building surfaces: Existing correlations and CFD modelling. *Energy Conversion and Management*, *52*(1), 512–522. https://doi.org/10.1016/j.enconman.2010.07.026

DELPHIN. (2018). Dresden, Germany: Dresden University of Technology.

Derome, D., Kubilay, A., Defraeye, T., Blocken, B., & Carmeliet, J. (2017). Ten questions concerning modeling of wind-driven rain in the built environment. *Building and*

Environment, *114*, 495–506. https://doi.org/10.1016/j.buildenv.2016.12.026

Desmarais, G. (2000). *Impact of added insulation on the hygrothermal performance of leaky exterior wall assemblies*.

Desmarais, G., Derome, D., & Fazio, P. (2000). Mapping of Air Leakage in Exterior Wall Assemblies. *Journal of Building Physics*, *24*(2), 132–154. https://doi.org/10.1106/BWH8-9D3J-R939-957E

DIN. *DIN 4108-7 - Thermal insulation and energy economy in buildings - Part 7: Air tightness of buildings - Requirements, recommendations and examples for planning and performance*. , (2011).

Djebbar, R., Reenen, D. Van, & Kumaran, M. (2001). *Environmental Boundary Conditions for Long-term Hygrothermal Calculations*.

Domhagen, F., & Wahlgren, P. (2017). Consequences of Varying Airtightness in Wooden Buildings. *Energy Procedia*, *132*, 873–878. https://doi.org/10.1016/j.egypro.2017.09.688

Eldin, A. (2007). A parametric model for predicting wind-induced pressures on low- rise vertical surfaces in shielded environments. *Solar Energy*, 81:52–61.

EnergyPlus. (2018). *Engineering Reference -EnergyPlus*. U.S. Department of Energy.

Falk, J., Molnár, M., & Larsson, O. (2014). Investigation of a simple approach to predict rainscreen wall ventilation rates for hygrothermal simulation purposes. *Building and Environment*, *73*, 88–96. https://doi.org/10.1016/j.buildenv.2013.11.025

Falk, J., & Sandin, K. (2013). Ventilated rainscreen cladding: A study of the ventilation drying process. *Building and Environment*, *60*, 173–184. https://doi.org/10.1016/j.buildenv.2012.11.015

Fox, M. J. (2014). *Hygrothermal Performance of highly insulated wood frame walls with air leakage: Field Measurements and Simulations*.

Fox, M. J., Straube, J., Ge, H., & Trainor, T. (2014). *Field Test of hygrothermal performance of highly insulated wall assemblies*. 101–110. Retrieved from http://www.buildingsciencelabs.com/wp-content/uploads/2014/11/CCBST-2014-Fox-

Straube-Ge-Trainor-Highly-Insulated-Walls1.pdf

Ganguli, U., & Dalgliesh, W. A. (1988). *Wind Pressures on Open Rain Screen Walls: Place Air Canada*. *114*(3), 642–656.

Garden, G. K. (1963). Rain penetration and its control. *Canadian Building Digest 40, NRCC*.

Gavanski, E., & Uematsu, Y. (2014). Local wind pressures acting on walls of low-rise buildings and comparisons to the Japanese and US wind loading provisions. *Journal of Wind Engineering and Industrial Aerodynamics*, *132*, 77–91. https://doi.org/10.1016/j.jweia.2014.06.020

Ge, H., Deb Nath, U. K., & Chiu, V. (2017). Field measurements of wind-driven rain on mid-and high-rise buildings in three Canadian regions. *Building and Environment*, *116*, 228–245. https://doi.org/10.1016/j.buildenv.2017.02.016

Ge, H., Wang, R., & Baril, D. (2018). Field measurements of hygrothermal performance of attics in extreme cold climates. *Building and Environment*, *134*, 114–130. https://doi.org/10.1016/J.BUILDENV.2018.02.032

Germany, F. G. of. (2013). Energy Saving Ordinance (residential buildings). Retrieved September 27, 2019, from https://www.bbsr-energieeinsparung.de/EnEVPortal/EN/EnEV/enev_node.html;jsessionid=C30D4457E61283 BCB43D12BD8E14020A.live11291

Ginger, J. D., Mehta, K. C., & Yeatts, B. B. (1997). Internal pressures in a low-rise full-scale building. *Journal of Wind Engineering and Industrial Aerodynamics*, *72*(1–3), 163–174. https://doi.org/10.1016/S0167-6105(97)00241-9

Ginger, John D. (2000). *Internal Pressures and Clading Net Wind Loads on Full-Scale Low-Rise Building*. *126*(April), 538–543.

Gradeci, K., Labonnote, N., Time, B., & Köhler, J. (2017). Mould growth criteria and design avoidance approaches in wood-based materials – A systematic review. *Construction and Building Materials*, *150*, 77–88. https://doi.org/10.1016/j.conbuildmat.2017.05.204

Grimsrud, D. T., Sherman, M. H., Blomsterberg, A. K., & Rosenfeld, A. H. (1979). Infiltration

and Air Leakage Comparisons: Conventional and Energy-Efficient Housing Designs. *Journal of Geophysical Research*, *3*, 1351–1358. Retrieved from https://www.engineeringvillage.com/share/document.url?mid=cpx_946469&database=cpx

Grosso, M. (1992). Wind pressure distribution around buildings: a parametrical model. *Energy and Buildings*, *18*(2), 101–131. https://doi.org/10.1016/0378-7788(92)90041-E

Hens, H. (1995). Heat , Air , and Moisture Transfer in Envelope Parts : the International Energy Agencies Annex 24 Common Exercises. *Thermal Envelopes VI*, 321–334.

Hens, H. (2002). ANNEX 24 - Heat, Air and Moisture Transfer In Highly Insulated Building Envelopes (HAMTIE). *IEA ECBCS Annex*, *24*, 21.

Hens, H. (2015). Combined heat, air, moisture modelling: A look back, how, of help? *Building and Environment*, *91*, 138–151. https://doi.org/10.1016/j.buildenv.2015.03.009

Holm, A., Kilian, R., & Janssen, H. (2007). *Subtask 4 : Moisture-Engineering Application*. (October).

Holmes, J. D. (1983). Wind loads on Low Rise Buildings - A Review. *CSIRO - Division of Building Research*, Vol. 16, pp. 3–26.

Holscher, N., & Niemann, H. (1998). Towards quality assurance for wind tunnel tests: a comparative testing program of the Windtechnologische Gesellschaft. *Journal of Wind Engineering & Industrial Aerodynamics*, 74:599–608.

Hukka, A., & Viitanen, H. (1999). A mathematical model of mould growth on wooden material. *Wood Science and Technology*, *33*(6), 475–485. https://doi.org/10.1007/s002260050131

Hun, D. E., Atchley, J., & Childs, P. (2016). *Air Leakage Rates in Typical Air Barrier Assemblies*. (November).

Ilomets, S., Kalamees, T., & Vinha, J. (2018). Indoor hygrothermal loads for the deterministic and stochastic design of the building envelope for dwellings in cold climates. *Journal of Building Physics*, *41*(6), 547–577. https://doi.org/10.1177/1744259117718442

ISO 13788. (2012). *ISO 13788 - International Standard: Hygrothermal performance of building components and building temperature to avoid critical*.

Janssen, H., Blocken, B., & Carmeliet, J. (2007). Conservative modelling of the moisture and heat transfer in building components under atmospheric excitation. *International Journal of Heat and Mass Transfer*, *50*(5–6), 1128–1140. https://doi.org/10.1016/j.ijheatmasstransfer.2006.06.048

Janssens, A., & Hens, H. (2007). Effects of wind on the transmission heat loss in duo-pitched insulated roofs: A field study. *Energy and Buildings*, *39*(9), 1047–1054. https://doi.org/10.1016/j.enbuild.2006.10.016

Jensen, M., & Franck, N. (1965). Model-scale tests in turbulent wind – Part II. *Copenhagen: The Danish Technical Press;*

Kalamees, T., Alev, Ü., & Pärnalaas, M. (2017). Air leakage levels in timber frame building envelope joints. *Building and Environment*, *116*, 121–129. https://doi.org/10.1016/j.buildenv.2017.02.011

Kalamees, T., Jokisalo, J., Jokiranta, K., Vinha, J., Kurnitski, J., & Eskola, L. (2010). Measured and simulated air pressure conditions in Finnish residential buildings. *Building Services Engineering Research and Technology*, *31*(2), 177–190. https://doi.org/10.1177/0143624410363655

Karagiozis, A. (2014). *The Next Frontier of Building Science : Air Leakage*. Owens Corning.

Karagiozis, A., & Künzel, H. M. (2010). The Effect of Air Cavity Convection on the Wetting and Drying Behavior of Wood-Frame Walls Using a Multi-Physics Approach. *Symposium on "Up Against the Wall": An Examination of Building Envelope Interface*, *6*(10), 48-48–20. https://doi.org/10.1520/stp48942s

Kopp, G. A., Oh, J. H., & Inculet, D. R. (2012). Wind-Induced Internal Pressures in Buildings. *Wind Engineers, JAWE*, *1993*(56), 11–20. https://doi.org/10.5359/jawe.1993.56_11

Kosny, J., Asiz, A., Smith, I., Shrestha, S., & Fallahi, A. (2014). A review of high R-value wood framed and composite wood wall technologies using advanced insulation techniques. *Energy and Buildings*, *72*, 441–456. https://doi.org/10.1016/j.enbuild.2014.01.004

Kumar, K. S. (2000). Pressure equalization of rainscreen walls: a critical review. *Building and Environment*, *35*(2), 161–179.

Künzel, H. M. (2005). Condition to Assess the Moisture Performance of Building Envelope Systems. *Indoor Air*, *no volume*(no issue), 1–26. Retrieved from http://www.hoki.ibp.fraunhofer.de/ibp/publikationen/fachzeitschriften/wksb Raumluftfeuchte1_E.pdf

Künzel, H. M. (2006). Influence of rain water leakage on the hygrothermal performance of exterior insulation systems Sheathing Adhesive Rigid Insulation Board Base Coat with Reinforcing Mesh Finish Coat. *Proceedings of the 8th Nordic Symposium on Building Physics in the Nordic Countries 2008.*, *1*, 253–260.

Künzel, H. M. (2012). Modeling Air Leakage in Hygrothermal Envelope Simulation. *In: Building Enclosure Science & Technology (BEST3) Conference, Atlanta, USA.*

Künzel, H. M. (2014). Accounting for unintended moisture sources in hygrothermal building analysis. *Proc. 10th Nordic Symposium on Building Physics*, 947–952.

Künzel, H. M., Zirkelbach, D., & Schafaczek, B. (2011). Vapour control design of wooden structures including moisture sources due to air exfiltration. *Proceedings 9th Nordic Symposium on Building Physics (NSB)*, 189–196.

Künzel, H. M., Zirkelbach, D., & Schafaczek, B. (2012). Modelling the Effect of Air Leakage in Hygrothermal Envelope Simulation. *Proceedings of the BEST 3*.

Langmans, J., Desta, T. Z., Alderweireldt, L., & Roels, S. (2015). Experimental analysis of cavity ventilation behind residential rainscreen cladding systems. *Energy Procedia*, *78*, 1750–1755. https://doi.org/10.1016/j.egypro.2015.11.290

Langmans, J., Desta, T. Z., Alderweireldt, L., & Roels, S. (2016). Field study on the air change rate behind residential rainscreen cladding systems: A parameter analysis. *Building and Environment*, *95*, 1–12. https://doi.org/10.1016/j.buildenv.2015.09.012

Langmans, J., Klein, R., & Roels, S. (2012). Hygrothermal risks of using exterior air barrier systems for highly insulated light weight walls: A laboratory investigation. *Building and Environment*, *56*, 192–202. https://doi.org/10.1016/j.buildenv.2012.03.007

Lawton, M. (1999). Vancouver's rotting condominium problem - how did we get into this mess? *Journal of Thermal Envelope and Building Science*, *22*(.), 356–363.

https://doi.org/10.1177/109719639902200410

Lepage, R., Schumacher, C., & Lukachko, A. (2013). *Moisture Management for High R-Value Walls Moisture Management*. (November). https://doi.org/DOE/GO-102013-4266

Levitan, M., Holmes, J., Mehta, K. C., & Vann, W. (1991). Field measurements of pressures on the Texas Tech building. *Journal of Wind Engineering & Industrial Aerodynamics*, 38:227–34.

Liddament, M. (1986). Air infiltration calculation techniques – an applications guide. *AIVC*.

Lstiburek, J. (1998). The Pressure Response of Buildings. *Thermal Envelopes VII, Airtightne*.

Lstiburek, J. (2001). *Moisture, Building Enclosures, and Mold*. (December).

Lstiburek, J. (2002). *Moisture Control for Buildings*. (February), 36–41.

Lstiburek, J. (2006). Building Science Digest 109 Pressures in Buildings. *Buildings*, 1–18.

Lstiburek, J. (2009). Building in extreme cold. *ASHRAE Journal*, *51*(2), 56–59.

Lstiburek, J. W. (2005). Understanding air barriers. *ASHRAE Journal*, *47*(7), 24–30.

McClung, R., Ge, H., Straube, J., & Wang, J. (2010). Hygrothermal performance of cross-laminated timber wall assemblies with built-in moisture: field measurements and simulations. *Journal of Cardiothoracic and Vascular Anesthesia*, *71*(24), 95–110. https://doi.org/10.1016/j.buildenv.2013.09.008

Muehleisen, R. T., & Patrizi, S. (2013). A new parametric equation for the wind pressure coefficient for low-rise buildings. *Energy and Buildings*, *57*, 245–249. https://doi.org/10.1016/j.enbuild.2012.10.051

Ng, L. C., Ojeda Quiles, N., Dols, W. S., & Emmerich, S. J. (2018). Weather correlations to calculate infiltration rates for U. S. commercial building energy models. *Building and Environment*, *127*(July 2017), 47–57. https://doi.org/10.1016/j.buildenv.2017.10.029

NRCC. (2017). *National Energy Code of Canada for Buildings*.

Ojanen, T. (1993). Criteria for the Hygrothermal Performance of Wind Barrier Structures. *Proceedings of the 3rd Symposium Building Physics in the Nordic Countries, B. Saxhof, Ed.,*

Thermal Insulation Laboratory, Technical University of Denmark, 643–652.

Ojanen, T., Viitanen, H., Peuhkuri, R., Vinha, J., & Salminen, K. (2010). *Mold Growth Modeling of Building Structures Using Sensitivity Classes of Materials*.

Oxford English Dictionary. (2019). Retrieved from https://www.oed.com/view/Entry/90148?redirectedFrom=hygrothermal#eid1009290

Pallin, S. (2013). *Risk Assessment of Hygrothermal Performance - Building Envelope Retrofit*.

Pallin, S., Hun, D. E., Jackson, R. K., & Desjarlais, A. O. (2015). *Moisture Durability Assessment of Selected Well-insulated Wall Assemblies*.

Pankratz, O., & Holm, A. (2004). *Designing and Testing a Structural Insulated Panel (SIP) with the Help of Hygrothermal Model*.

Passive House Institute. (n.d.). Retrieved June 9, 2019, from https://passivehouse.com/

Pihelo, P., Kikkas, H., & Kalamees, T. (2016). Hygrothermal Performance of Highly Insulated Timber-frame External Wall. *Energy Procedia*, *96*(October), 685–695. https://doi.org/10.1007/s11947-009-0181-3

Quan, Y., Tamura, Y., Matsui, M., Cao, S., & Yoshida, A. (2007). TPU aerodynamic database for low-rise buildings,. *12th International Conference on Wind Engineering*, 2–6. Retrieved from http://www.wind.arch.t-kougei.ac.jp/info center/ windpressure/lowrise/mainpage.html.

Quirouette, R. L. (1985). "The difference between a vapour barrier and an air barrier." *Building Practice Note 54, Div. of Bldg. Res., Nat. Res. Council of Canada, Ottawa*.

Reinhold, T. (1982). Wind tunnel modeling for civil engineering applications. *Cambridge: Cambridge University Press*.

Ricketts, L. (2014). *A Field Study of Airflow in a High-Rise Multi-Unit Residential Building*.

Rode, C., Hens, H., & Janssen, H. (2008). *IEA Annex 41 whole building heat, air moisture response - Closing seminar Nordic Building Physics Conference*.

Said, M. N. A. (2006). *NRC PERD 079 Project Task 2: Literature Review: Building Envelope, Heating, and Ventilating Practices and Technologies for Extreme Climates*. (December).

Salonvaara, M., Karagiozis, A., & Corning, O. (2013). *Acceptable Air Tightness of Walls in Passive Houses*. *c*, 1–35.

Salonvarra, M., Karagiozis, A., Pazera, M., & Miller, W. (2007). Air Cavities Behind Claddings — What Have We Learned ? *Thermal Performance of Exterior Envelopes of Whole Buildings X International Conference*.

Sedlbauer, K. (2001). Prediction of mold fungus formation on the surface of and inside building components.. *Dissertation Universität Stuttgart*.

Sherman, M. H., Modera, M. P., & Grimsrud, D. T. (1980). A predictive air infiltration Model - Field validation and sensitivity analysis. *Energy*, 6. A. 1-6. A. 10. Retrieved from https://www.engineeringvillage.com/share/document.url?mid=cpx_1450605&database=cpx

Simpson, Y. (2010). *Field evaluation of ventilation wetting and drying of rainscreen walls*.

Stathopoulos, T. (1997). Computational wind engineering: past achievements and future challenges. *Journal of Wind Engineering & Industrial Aerodynamics*, 67:509–32.

Stathopoulos, T., Surry, D., & Davenport, A. G. (1979). *Internal pressure characteristics of low-rise buildings due to wind action*.

Stovall, T. K., & Karagiozis, A. (2004). *Airflow in the Ventilation Space behind a rain screen wall*. 11. https://doi.org/10.1016/S0733-8619(03)00096-3

Straube, J., & Lstiburek, J. (2013). *Moisture-Related Durability of Walls with Exterior Insulation in the Pacific Northwest*. Retrieved from http://web.ornl.gov/sci/buildings/conf-archive/2013 B12 papers/211_Smegal.pdf

Straube, J., & Schumacher, C. (2001). The Role of Hygrothermal Modeling in Practical Building Design: Case Stuies by: Civil Engineering Department , University of Waterloo. *Civil Engineering*. Retrieved from jfstraube@uwaterloo.ca cjschuma@uwaterloo.ca

Straube, J., & Smegal, J. (2010). *Building America Special Research Project : High-R Walls Case Study Analysis*. (November).

Swami, M., & Chandra, S. (1987). Procedures for Calculating Natural Ventilation Airflow Rates in Buildings. *ASHRAE Final Report FSEC-CR-163-86*, 130. Retrieved from

http://scholar.google.com/scholar?hl=en&btnG=Search&q=intitle:Procedures+for+Calculati ng+Natural+Ventilation+Airflow+Rates+in+Buildings#0%5Cnhttp://scholar.google.com/sc holar?hl=en&btnG=Search&q=intitle:Procedures+for+calculating+natural+ventilation+airfl

Tamura, Y. (2012). Aerodynamic Database of Low-Rise Buildings. Retrieved June 9, 2019, from http://www.wind.arch.t-kougei.ac.jp/system/eng/contents/code/tpu

TenWolde, A. (1989). Moisture transfer through material and systems in buildings, Water Vapour Transmission Through Building Materials and Systems: Mechanisms and Measurement. *ASTM STP 1039*.

Uvslokk, S. (1996). *The Importance of Wind Barriers for Insulated Timber Frame Constructions*. *1065*(July), 40–62.

Van Belleghem, M., Steeman, M., Janssens, A., & De Paepe, M. (2015). Heat, air and moisture transport modelling in ventilated cavity walls. In *Journal of Building Physics* (Vol. 38). https://doi.org/10.1177/1744259114543984

Vanpachtenbeke, M., Langmans, J., Roels, S., & Van Acker, J. (2015). Modelling cavity ventilation behind brick veneer cladding: How reliable are the common assumptions? *Energy Procedia*, *78*, 1467–1477. https://doi.org/10.1016/j.egypro.2015.11.172

Vereecken, E., & Roels, S. (2012). Review of mould prediction models and their influence on mould risk evaluation. *Building and Environment*, *51*, 296–310. https://doi.org/10.1016/j.buildenv.2011.11.003

Vereecken, E., Van Gelder, L., Janssen, H., Roels, S., Gelder, L. Van, Janssen, H., & Roels, S. (2015). Interior insulation for wall retrofitting - A probabilistic analysis of energy savings and hygrothermal risks. *Energy and Buildings*, *89*, 231–244. https://doi.org/10.1016/j.enbuild.2014.12.031

Viitanen, H., Krus, M., Ojanen, T., Eitner, V., & Zirkelbach, D. (2015). Mold risk classification based on comparative evaluation of two established growth models. *Energy Procedia*, *78*, 1425–1430. https://doi.org/10.1016/j.egypro.2015.11.165

Viitanen, H., & Ritschkoff, A. (1991). Mold growth in pine and spruce sapwood in relation to air humidity and temperature. *Uppsala : Swedish University of Agriculture Sciences, Department*

of Forrest Products.

Viitanen, H., Vinha, J., Salminen, K., Ojanen, T., Peuhkuri, R., Paajanen, L., & Lähdesmäki, K. (2010). Moisture and bio-deterioration risk of building materials and structures. *Journal of Building Physics*, *33*(3), 201–224. https://doi.org/10.1177/1744259109343511

Walker, I. S., & Wilson, D. J. (1993). Evaluating models for superposition of wind and stack effect in air infiltration. *Building and Environment*, *28*(2), 201–210. https://doi.org/10.1016/0360-1323(93)90053-6

Wang, L. (2018). *Stochastic Modelling of Hygrothermal Performance of Highly Insulated Wood Framed Envelopes*.

Wang, L., & Ge, H. (2017). Effect of air leakage on the hygrothermal performance of highly insulated wood frame walls: Comparison of air leakage modelling methods. *Building and Environment*, *123*, 363–377. https://doi.org/10.1016/j.buildenv.2017.07.012

Wang, L., & Ge, H. (2018). Stochastic modelling of hygrothermal performance of highly insulated wood framed walls. *Building and Environment*, *146*(July), 12–28. https://doi.org/10.1016/j.buildenv.2018.09.032

Wang, R. (2018). *Attic Ventilation in Extremely Cold Climate - Field Measurements and Hygrothermal Simulation*. (November).

Wolf, D., & Tyler, F. (2013a). Characterization of Air Leakage in Residential Structures — Part 1: Joint Leakage. *Proceedings of the ASHRAE Buildings XII International Conference*, (2004), 1–11.

Wolf, D., & Tyler, F. (2013b). Characterization of Air Leakage in Residential Structures — Part 2: Whole House Leakage. *Proceedings of the ASHRAE Buildings XII International Conference*, 1–11.

WTA. (n.d.). Retrieved June 9, 2019, from https://www.wta-international.org/en/technical-comissions/building-physics/

Younes, C., Shdid, C. A., & Bitsuamlak, G. (2012). Air infiltration through building envelopes: A review. *Journal of Building Physics*, *35*(3), 267–302.

https://doi.org/10.1177/1744259111423085

Zirkelbach, D., Künzel, H. M., & Bludau, C. (2008). Results of measured and simulated hygrothermal loads acting on mineral fiber insulation suggest a revision of durability test. *Building Physics 2008 - 8th Nordic Symposium*, 441–448.

Zirkelbach, D., Künzel, H. M., Schafaczek, B., & Borsch-Laaks, R. (2009). Vapour convection becomes calculable - Unsteady model for consideration of convective moisture ingress at the simulation of lightweight constructions. *1130541 Reader / International Symposium on Building and Ductwork Air Tightness (Buildair) ; (4 :; 2009 :; Berlin)*.

Appendix I – Mould Index Results

The following tables present the maximum mould index obtained for the parametric study cases.

Table 26: Mould index for Chicago and Montreal

kcl	Orientation	RSI-value	City → ACHcav	Chicago Tcat1 Cpi -0.2	0	Tcat2 -0.2	0	Tcat3 -0.2	0	Tcat4 -0.2	0	Montreal Tcat1 -0.2	0	Tcat2 -0.2	0	Tcat3 -0.2	0	Tcat4 -0.2	0
ASHRAE Standard	Max. Wind Pressure	3	0	0.0	0.0	0.0	0.1	0.3	1.5	1.4	3.4	0.0	0.0	0.1	0.2	0.4	1.7	1.5	3.7
			10	0.0	0.0	0.0	0.1	0.3	1.3	1.2	2.9	0.0	0.0	0.1	0.2	0.3	1.4	1.2	3.3
			100	0.0	0.0	0.0	0.0	0.1	0.4	0.4	2.0	0.0	0.0	0.0	0.1	0.1	0.4	0.3	1.9
			300	0.0	0.0	0.0	0.0	0.1	0.7	0.5	2.3	0.0	0.0	0.0	0.1	0.1	0.4	0.3	2.0
		6	0	0.0	0.0	0.1	0.3	1.0	2.4	2.2	4.2	0.0	0.1	0.2	0.4	1.2	2.8	2.4	4.5
			10	0.0	0.0	0.1	0.2	0.6	2.0	1.8	4.0	0.0	0.1	0.1	0.3	0.9	2.3	2.0	4.3
			100	0.0	0.0	0.0	0.1	0.2	1.2	1.1	3.0	0.0	0.0	0.0	0.1	0.2	1.2	0.8	2.9
			300	0.0	0.0	0.0	0.1	0.2	1.3	1.2	3.2	0.0	0.0	0.0	0.1	0.2	1.2	0.8	3.1
		7.85	0	0.0	0.0	0.1	0.3	1.2	2.7	2.5	4.3	0.0	0.1	0.2	0.6	1.4	3.1	2.8	4.5
			10	0.0	0.0	0.1	0.2	0.8	2.2	2.0	4.1	0.0	0.1	0.2	0.3	1.1	2.6	2.3	4.4
			100	0.0	0.0	0.0	0.1	0.3	1.3	1.2	3.2	0.0	0.0	0.0	0.1	0.2	1.3	1.1	3.2
			300	0.0	0.0	0.0	0.1	0.3	1.4	1.3	3.4	0.0	0.0	0.0	0.1	0.2	1.3	1.1	3.3
		10.5	0	0.0	0.0	0.1	0.3	1.3	2.8	2.6	4.3	0.0	0.1	0.2	0.7	1.5	3.4	3.0	4.5
			10	0.0	0.0	0.1	0.2	1.0	2.4	2.2	4.1	0.0	0.1	0.2	0.3	1.2	2.9	2.5	4.5
			100	0.0	0.0	0.0	0.1	0.3	1.4	1.3	3.3	0.0	0.0	0.0	0.1	0.3	1.4	1.2	3.4
			300	0.0	0.0	0.0	0.1	0.3	1.5	1.4	3.4	0.0	0.0	0.0	0.1	0.2	1.4	1.2	3.5
	North	3	0	0.0	0.0	0.0	0.0	0.1	0.8	0.4	2.1	0.0	0.0	0.0	0.1	0.2	0.9	0.5	2.2
			10	0.0	0.0	0.0	0.0	0.1	0.6	0.4	2.0	0.0	0.0	0.0	0.1	0.2	0.7	0.4	2.1
			100	0.0	0.0	0.0	0.0	0.1	0.3	0.3	1.5	0.0	0.0	0.0	0.0	0.1	0.3	0.3	1.5
			300	0.0	0.0	0.0	0.0	0.1	0.4	0.3	1.6	0.0	0.0	0.0	0.0	0.1	0.3	0.2	1.4
		6	0	0.0	0.0	0.0	0.1	0.3	1.6	1.4	3.5	0.0	0.0	0.1	0.2	0.4	1.7	1.4	3.7
			10	0.0	0.0	0.0	0.1	0.3	1.5	1.3	3.3	0.0	0.0	0.1	0.2	0.3	1.6	1.3	3.4
			100	0.0	0.0	0.0	0.1	0.2	1.1	0.8	2.6	0.0	0.0	0.0	0.1	0.2	1.1	0.6	2.5
			300	0.0	0.0	0.0	0.1	0.2	1.0	0.7	2.6	0.0	0.0	0.0	0.1	0.2	0.8	0.4	2.3
		7.85	0	0.0	0.0	0.0	0.2	0.4	1.8	1.5	3.8	0.0	0.1	0.1	0.3	0.5	2.0	1.6	4.0
			10	0.0	0.0	0.0	0.2	0.3	1.6	1.4	3.6	0.0	0.1	0.1	0.2	0.4	1.8	1.5	3.7
			100	0.0	0.0	0.0	0.1	0.2	1.2	1.0	2.9	0.0	0.0	0.0	0.1	0.2	1.3	0.9	2.8
			300	0.0	0.0	0.0	0.1	0.2	1.2	0.9	2.9	0.0	0.0	0.0	0.1	0.2	1.1	0.6	2.6
		10.5	0	0.0	0.0	0.0	0.2	0.5	2.0	1.7	4.0	0.0	0.1	0.1	0.3	0.7	2.2	1.8	4.1
			10	0.0	0.0	0.0	0.2	0.4	1.8	1.5	3.8	0.0	0.1	0.1	0.3	0.5	2.0	1.6	3.9
			100	0.0	0.0	0.0	0.1	0.2	1.3	1.1	3.1	0.0	0.0	0.0	0.2	0.3	1.4	1.1	3.1
			300	0.0	0.0	0.0	0.1	0.2	1.3	1.0	3.1	0.0	0.0	0.0	0.1	0.2	1.2	0.7	2.8

For Chicago only cases with T_{cat} 4 and C_{pi} 0 have mould index higher than 3. Montreal has slightly higher mould Index with two cases for T_{cat} 3 and C_{pi} 0. In both cities higher mould Index are obtained for the maximum wind pressure orientation, but there is no big difference in the number of cases exceeding a value of 3 or in the maximum value of mould Index. Both orientations can be considered to have similar results.

Table 27: Mould index for Rochester and St. Johns

k_{cl}	Orientation	RSI-value	City → T_{cat} → C_{pi} → ACH_{cav}	Rochester 1 -0.2	1 0	2 -0.2	2 0	3 -0.2	3 0	4 -0.2	4 0	St. Johns 1 -0.2	1 0	2 -0.2	2 0	3 -0.2	3 0	4 -0.2	4 0
ASHRAE Standard	Max. Wind Pressure	3	0	0.2	0.3	1.6	3.4	4.6	4.7	4.7	4.9	0.1	0.2	1.3	3.0	4.6	4.7	4.7	4.9
		3	10	0.2	0.3	1.6	3.2	4.6	4.7	4.7	4.9	0.1	0.2	1.2	2.7	4.5	4.7	4.7	4.9
		3	100	0.1	0.2	1.3	2.6	4.6	4.7	4.7	4.9	0.0	0.1	0.5	2.0	4.1	4.7	4.7	4.8
		3	300	0.1	0.2	1.4	2.9	4.6	4.7	4.7	4.9	0.0	0.1	0.5	2.0	4.3	4.7	4.7	4.9
		6	0	0.3	1.0	2.7	4.4	4.6	4.6	4.7	4.9	0.2	0.7	2.3	4.3	4.6	4.7	4.7	5.0
		6	10	0.3	0.8	2.5	4.3	4.6	4.6	4.7	4.9	0.2	0.4	2.1	4.1	4.6	4.7	4.7	4.9
		6	100	0.2	0.4	1.9	3.8	4.6	4.7	4.7	4.9	0.1	0.2	1.3	3.3	4.6	4.7	4.7	4.9
		6	300	0.2	0.4	2.0	3.9	4.6	4.7	4.7	4.9	0.1	0.2	1.3	3.2	4.6	4.7	4.7	4.9
		7.85	0	0.4	1.1	3.0	4.4	4.5	4.6	4.6	4.9	0.2	1.0	2.6	4.4	4.6	4.7	4.7	5.0
		7.85	10	0.3	1.0	2.8	4.4	4.6	4.6	4.6	4.9	0.2	0.6	2.4	4.3	4.6	4.7	4.7	5.0
		7.85	100	0.2	0.5	2.1	4.0	4.6	4.7	4.7	4.9	0.1	0.2	1.5	3.6	4.6	4.7	4.7	4.9
		7.85	300	0.2	0.5	2.2	4.1	4.6	4.7	4.7	4.9	0.1	0.2	1.4	3.5	4.6	4.7	4.7	4.9
		10.5	0	0.5	1.2	3.3	4.4	4.5	4.6	4.6	4.9	0.2	1.1	2.9	4.4	4.6	4.7	4.7	5.0
		10.5	10	0.3	1.1	3.0	4.4	4.5	4.6	4.6	4.9	0.2	0.9	2.6	4.4	4.6	4.7	4.7	5.0
		10.5	100	0.2	0.7	2.3	4.2	4.6	4.6	4.6	4.9	0.1	0.2	1.7	3.8	4.6	4.7	4.7	4.9
		10.5	300	0.2	0.6	2.3	4.2	4.6	4.7	4.7	4.9	0.1	0.2	1.5	3.8	4.6	4.7	4.7	5.0
	North	3	0	0.0	0.0	0.0	0.3	0.2	1.9	1.0	4.1	0.0	0.1	1.1	2.6	4.4	4.7	4.7	4.9
		3	10	0.0	0.0	0.0	0.2	0.2	1.8	0.9	4.0	0.0	0.1	1.0	2.4	4.4	4.7	4.7	4.9
		3	100	0.0	0.0	0.0	0.2	0.2	1.5	0.6	3.5	0.0	0.1	0.4	1.9	4.0	4.7	4.7	4.8
		3	300	0.0	0.0	0.0	0.2	0.2	1.6	0.6	3.7	0.0	0.1	0.4	1.9	4.1	4.7	4.7	4.9
		6	0	-0.1	0.1	0.0	0.7	0.6	3.4	1.7	4.5	0.2	0.5	2.0	4.1	4.6	4.7	4.7	5.0
		6	10	0.0	0.1	0.0	0.6	0.5	3.2	1.6	4.5	0.1	0.4	1.9	3.9	4.6	4.7	4.7	4.9
		6	100	0.0	0.1	0.0	0.3	0.3	2.6	1.3	4.5	0.1	0.2	1.4	3.3	4.6	4.7	4.7	4.9
		6	300	0.0	0.1	0.0	0.3	0.3	2.6	1.3	4.5	0.1	0.2	1.3	3.2	4.6	4.7	4.7	4.9
		7.85	0	-0.1	0.1	0.0	0.9	0.9	3.8	2.1	4.5	0.2	0.9	2.4	4.3	4.6	4.7	4.7	5.0
		7.85	10	-0.1	0.1	0.0	0.8	0.8	3.6	1.9	4.5	0.2	0.6	2.2	4.2	4.6	4.7	4.7	5.0
		7.85	100	0.0	0.1	0.0	0.4	0.4	2.9	1.5	4.5	0.1	0.3	1.5	3.6	4.6	4.7	4.7	4.9
		7.85	300	0.0	0.1	0.0	0.3	0.3	2.9	1.4	4.5	0.1	0.2	1.4	3.5	4.6	4.7	4.7	4.9
		10.5	0	-0.1	0.1	0.1	1.0	1.0	4.0	2.3	4.5	0.2	1.0	2.7	4.4	4.6	4.7	4.7	5.0
		10.5	10	-0.1	0.1	0.1	0.9	0.9	3.8	2.2	4.5	0.2	0.9	2.4	4.4	4.6	4.7	4.7	5.0
		10.5	100	0.0	0.1	0.0	0.5	0.5	3.2	1.6	4.5	0.1	0.3	1.7	3.9	4.6	4.7	4.7	4.9
		10.5	300	0.0	0.1	0.0	0.5	0.4	3.1	1.6	4.5	0.1	0.2	1.6	3.7	4.6	4.7	4.7	5.0

The maximum mould Index reached was 5.0 for St. Johns, this value is limited by the sensitivity class (sensitive) selected for the simulations in section 4.5.1. It can be observed that both orientations have practically the same results. In case of Rochester it can be see that different orientations might have a significantly different mould Index. The number of cases exceeding a mould Index of 3 is 81 for the maximum wind orientation, while for the North orientation only 24 cases exceeded the threshold value

Table 28: Mould index for Vancouver

k_{cl}	Orientation	RSI-value	City / T_{cat} / C_{pi} / ACH_{cav}	Vancouver 1 (-0.2)	1 (0)	2 (-0.2)	2 (0)	3 (-0.2)	3 (0)	4 (-0.2)	4 (0)
ASHRAE Standard	Max. Wind Pressure	3	0	0.0	0.0	0.0	0.0	0.0	0.0	0.0	0.2
			10	0.0	0.0	0.0	0.0	0.0	0.0	0.0	0.1
			100	0.0	0.0	0.0	0.0	0.0	0.0	0.0	0.1
			300	0.0	0.0	0.0	0.0	0.0	0.0	0.0	0.1
		6	0	0.0	0.0	0.0	0.0	0.1	0.3	0.2	0.9
			10	0.0	0.0	0.0	0.0	0.1	0.2	0.2	0.8
			100	0.0	0.0	0.0	0.0	0.0	0.2	0.1	0.4
			300	0.0	0.0	0.0	0.0	0.0	0.2	0.1	0.4
		7.85	0	0.0	0.0	0.0	0.1	0.1	0.4	0.3	1.2
			10	0.0	0.0	0.0	0.1	0.1	0.3	0.2	1.1
			100	0.0	0.0	0.0	0.0	0.0	0.2	0.2	0.7
			300	0.0	0.0	0.0	0.0	0.0	0.2	0.2	0.7
		10.5	0	0.0	0.0	0.0	0.1	0.2	0.6	0.3	1.3
			10	0.0	0.0	0.0	0.1	0.2	0.4	0.3	1.2
			100	0.0	0.0	0.0	0.0	0.1	0.3	0.2	0.9
			300	0.0	0.0	0.0	0.0	0.1	0.3	0.2	1.0
	North	3	0	0.0	0.0	0.0	0.0	0.0	0.0	0.0	0.1
			10	0.0	0.0	0.0	0.0	0.0	0.0	0.0	0.1
			100	0.0	0.0	0.0	0.0	0.0	0.0	0.0	0.0
			300	0.0	0.0	0.0	0.0	0.0	0.0	0.0	0.1
		6	0	0.0	0.0	0.0	0.0	0.0	0.2	0.1	0.5
			10	0.0	0.0	0.0	0.0	0.0	0.2	0.1	0.4
			100	0.0	0.0	0.0	0.0	0.0	0.1	0.1	0.3
			300	0.0	0.0	0.0	0.0	0.0	0.1	0.1	0.3
		7.85	0	0.0	0.0	0.0	0.0	0.1	0.2	0.2	0.8
			10	0.0	0.0	0.0	0.0	0.1	0.2	0.2	0.7
			100	0.0	0.0	0.0	0.0	0.0	0.2	0.1	0.4
			300	0.0	0.0	0.0	0.0	0.0	0.2	0.1	0.5
		10.5	0	0.0	0.0	0.0	0.1	0.1	0.3	0.3	1.1
			10	0.0	0.0	0.0	0.0	0.1	0.3	0.2	1.0
			100	0.0	0.0	0.0	0.0	0.0	0.2	0.2	0.7
			300	0.0	0.0	0.0	0.0	0.0	0.2	0.2	0.7

Vancouver does not present any case with mould index higher than 1.3, this due to the lower wind-induced exfiltration in comparison with other cities studied.

Appendix II – Terrain Category and Moisture Leakage

Relative humidity and moisture content vary directly with each other, a higher relative humidity will produce a higher moisture content and vice versa. Because of this direct relationship, all the findings regarding relative humidity in the previous sections are also valid for moisture content.
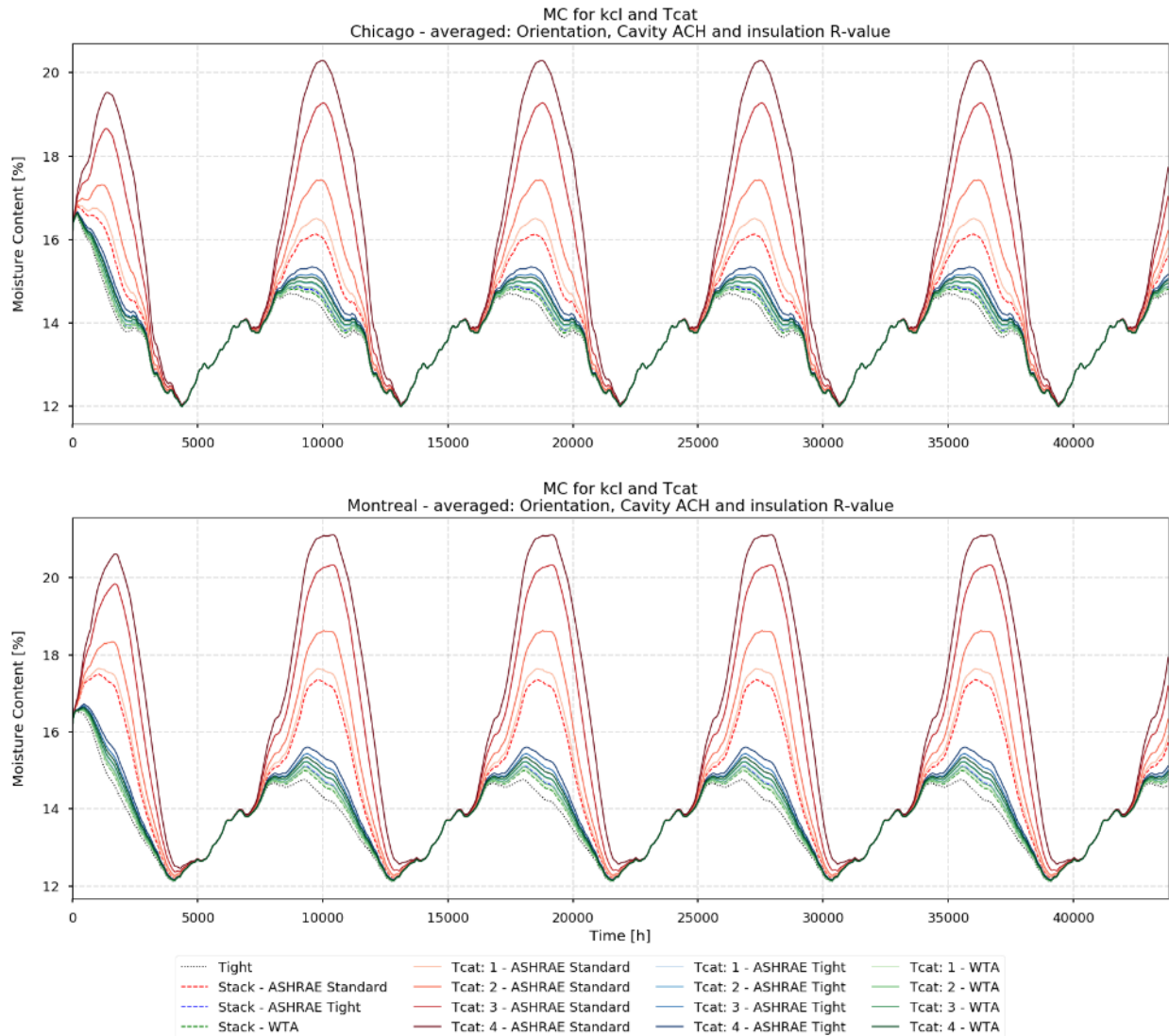
Figure 53: Moisture content for Chicago (top) and Montreal (bottom) depending on k_{cl} and Terrain category

Consequently to the results shown for Montreal and Chicago in section 5.1, where it can be seen that only considering a $T_{cat} = 4$ and ASHRAE Standard k_{cl} produced risk of mould development, the moisture content barely surpasses the 20% threshold referenced in section 3.2.2 when the aforementioned parameters are considered.
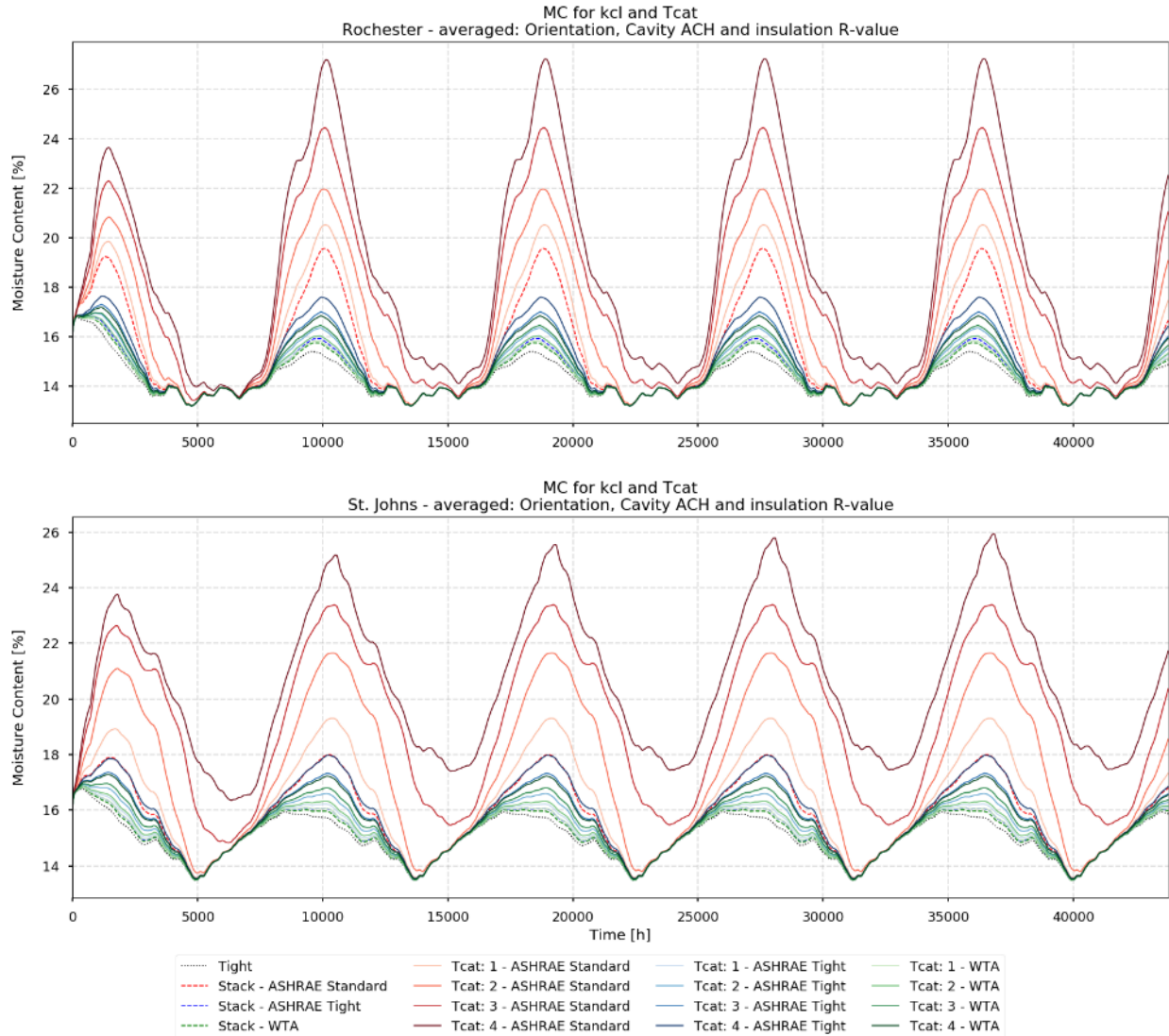
Figure 54: Moisture content for Rochester (top) and St. Johns (bottom) depending on k_{cl} and Terrain category

For St. Johns and Rochester the moisture content continually exceeds the 20% threshold, hence the higher number of cases that develop mould in these cities. By observing the peaks of moisture content in St. Johns for $T_{cat} = 4$ it can be noted a slight annual increment in the maximum moisture content, showing that the moisture deposition is not able to dry out completely, this also explains the much longer periods with higher moisture content in comparison to other cities.
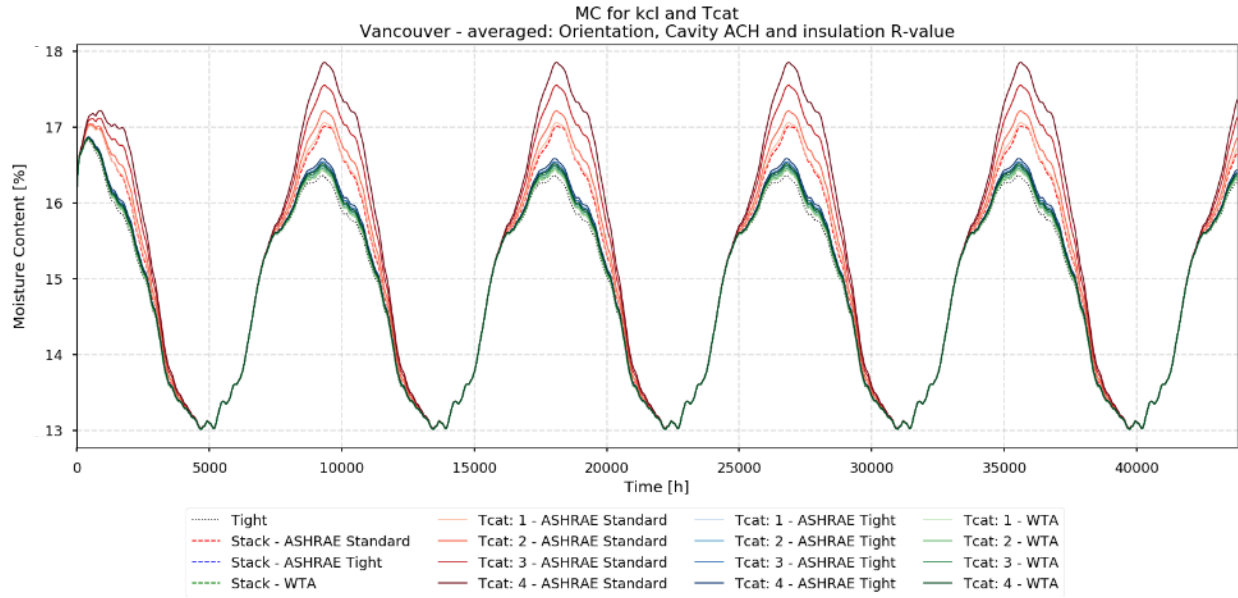
Figure 55: Moisture content for Vancouver depending on k$_{cl}$ and Terrain category

For Vancouver, the moisture content is always below 18%, explaining the results of the simulations were no case developed a mould Index higher than 3.

Appendix III – Terrain Category and Internal Pressure

The following results are consequent with results shown in section 5.2.2. In this case using moisture content to visualize the effect might be slightly clearer than using relative humidity. The graphs shown in section 5.2.2 reach a relative humidity closer to 100%, hence the curves tend to be collapsed, making it difficult to perceive differences in the peaks of relative humidity. When using moisture content the curves are more separated because the OSB sheathing has not reached the saturation moisture content, which is around 30%.
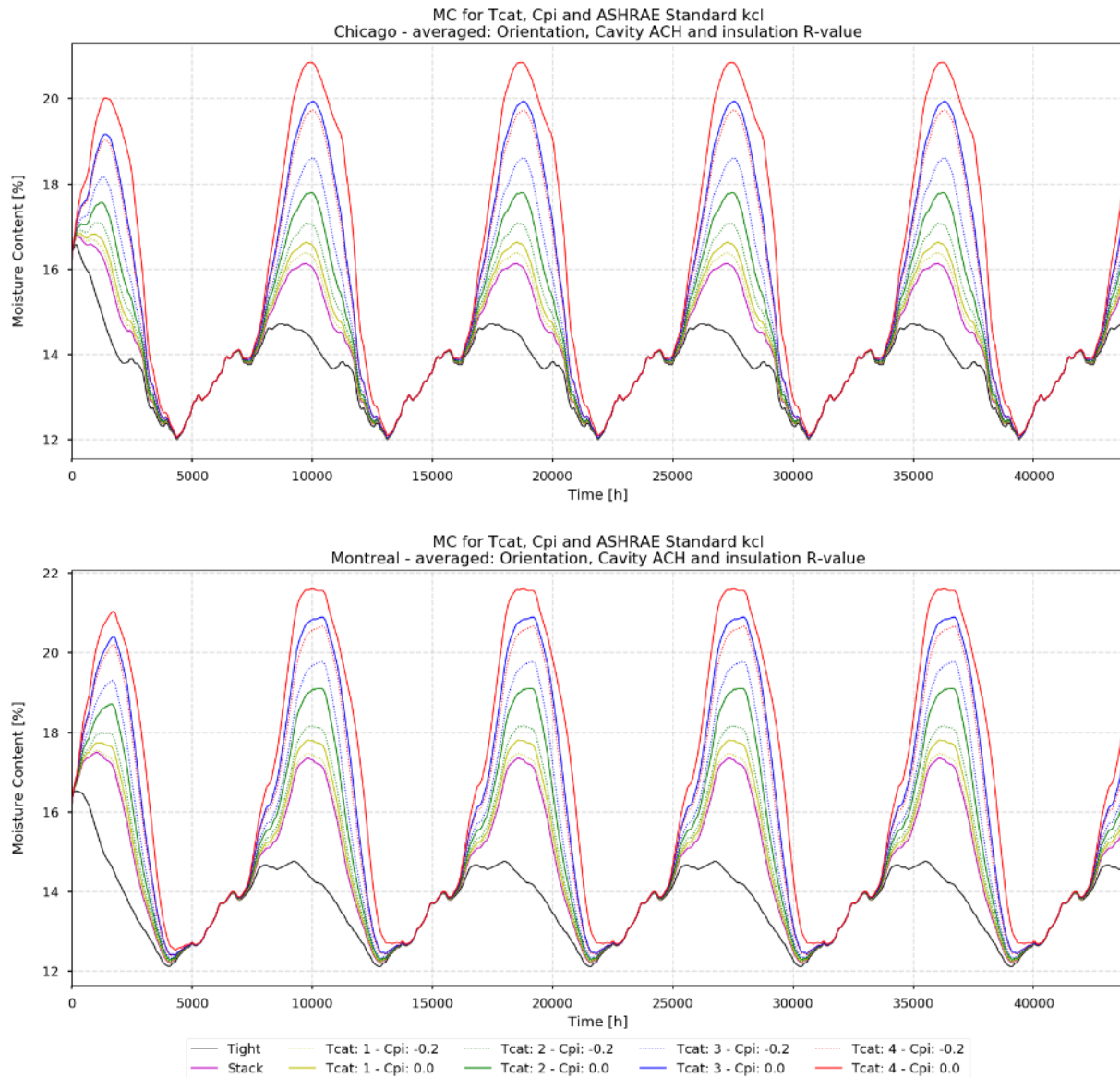
Figure 56: Moisture content for Chicago (top) and Montreal (bottom) depending on C_{pi}

For Chicago the moisture content threshold of 20% is only surpassed when considering $T_{cat} = 4$ and $C_{pi} = 0$. For Montreal $T_{cat} = 3$ and 4 with a $C_{pi} = 0$ results in a moisture content higher than 20%, this is consistent with the results shown in Table 26 were it can be observed that 2 cases developed a mould Index higher than 3 when $T_{cat} = 3$ and $C_{pi} = 0$ where considered.
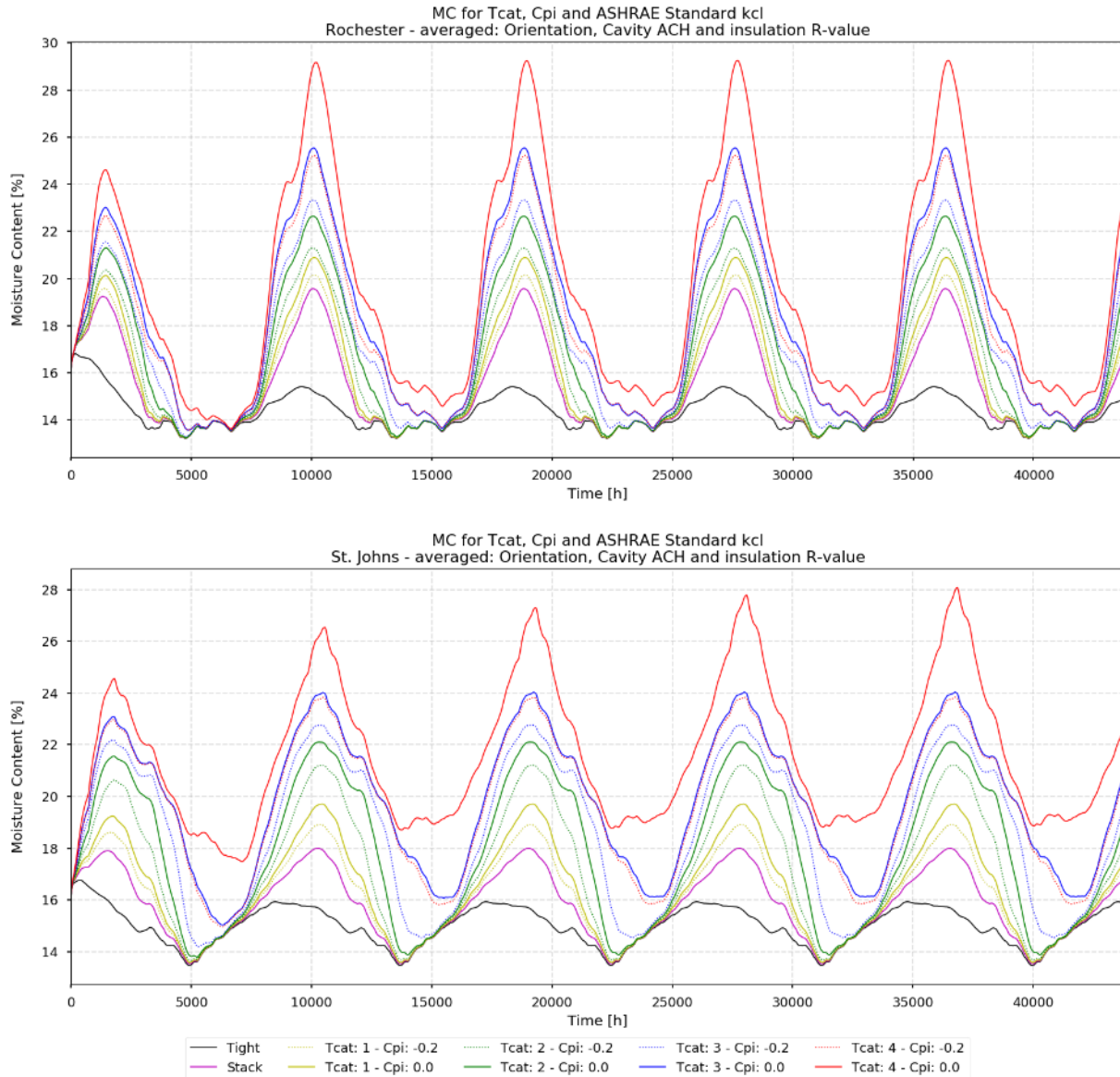
Figure 57: Moisture content for Rochester (top) and St. Johns (bottom) depending on C_{pi}

In the case of St. John it is possible to observe a slight constant increment in the moisture content that it is not observable in the relative humidity graphs. The increment is only observable in the case of $C_{pi} = 0$ and $T_{cat} = 4$.

MC for Tcat, Cpi and ASHRAE Standard kcl
Vancouver - averaged: Orientation, Cavity ACH and insulation R-value

| Tight | Tcat: 1 - Cpi: -0.2 | Tcat: 2 - Cpi: -0.2 | Tcat: 3 - Cpi: -0.2 | Tcat: 4 - Cpi: -0.2 |
| Stack | Tcat: 1 - Cpi: 0.0 | Tcat: 2 - Cpi: 0.0 | Tcat: 3 - Cpi: 0.0 | Tcat: 4 - Cpi: 0.0 |
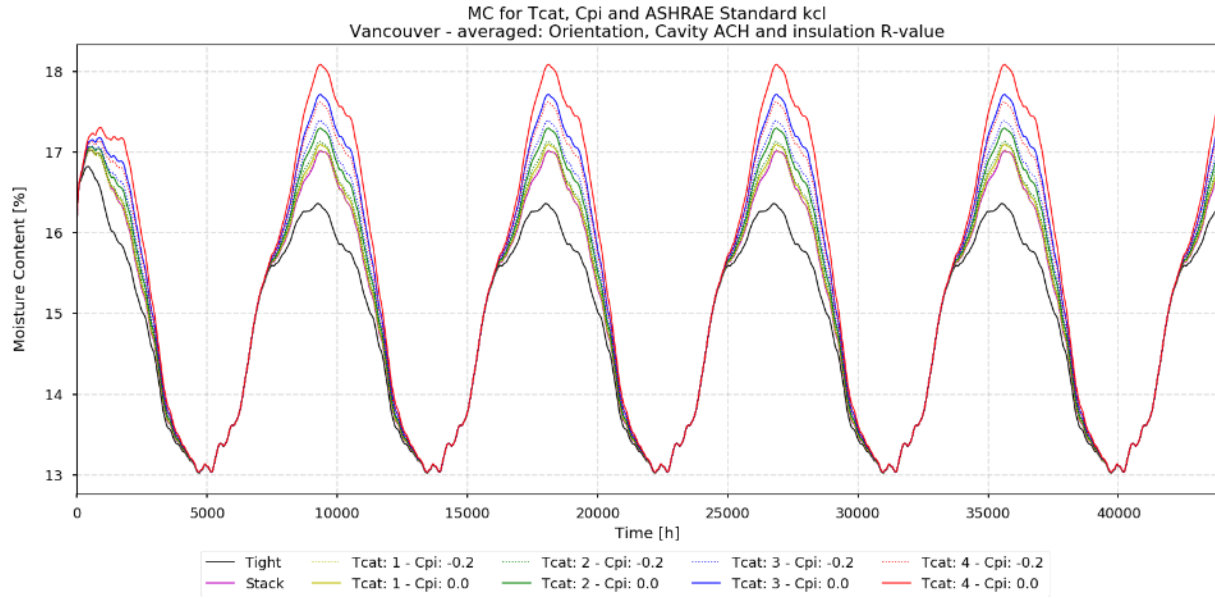
Figure 58: Moisture content for Vancouver depending on C_{pi}

Moisture content in Vancouver is lower than 18%, hence no mould index is expected.

Appendix IV – Moisture Leakage and Orientation

In section 5.3.1, it is highlighted the importance to assess different orientations from the North when considering wind for exfiltration calculation. The additional moisture deposition induced by the wind, or the reduction of stack exfiltration due to winds normal to the North façade can produce a different orientation with higher moisture content. Such effect is demonstrated for Rochester city.
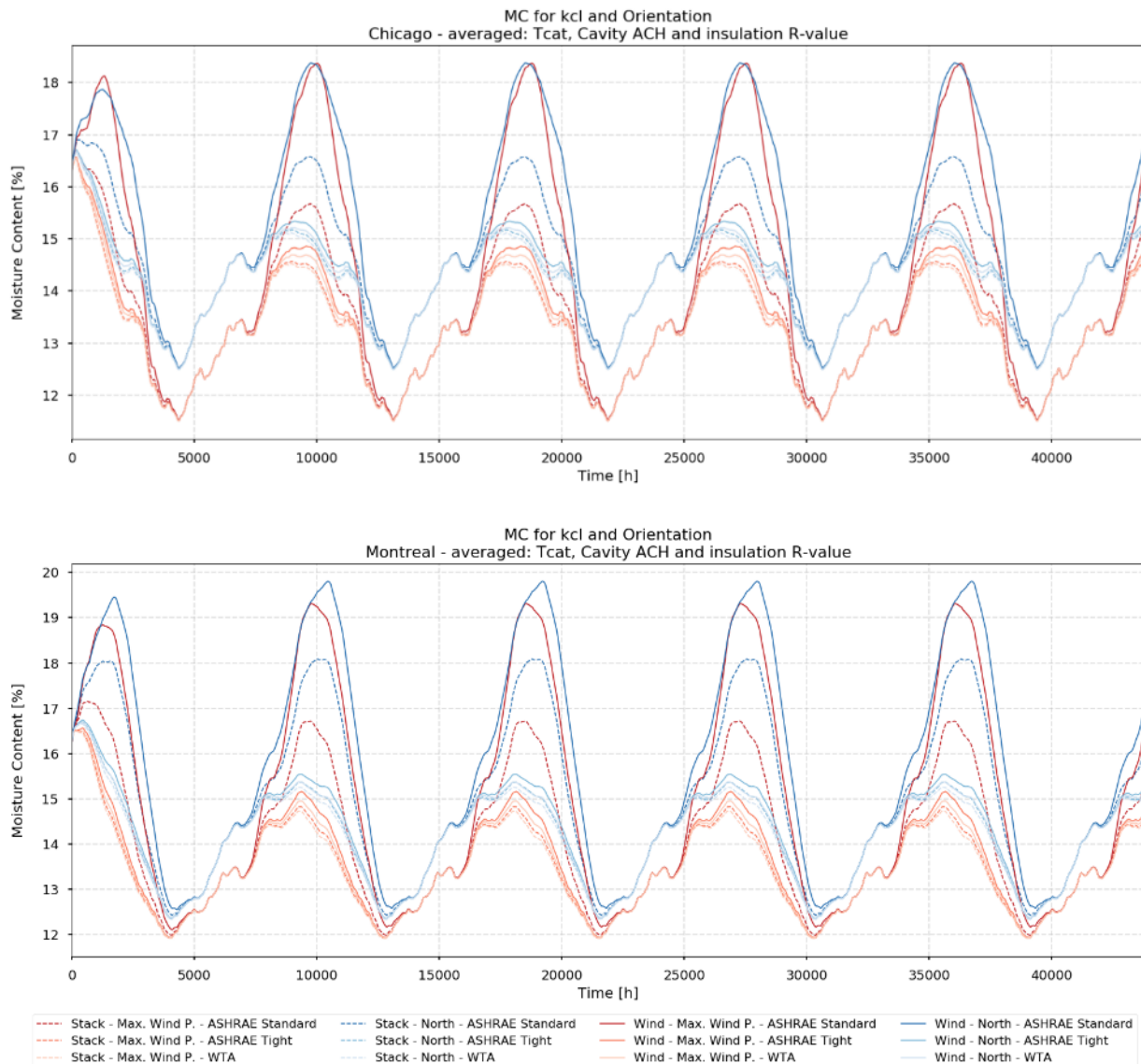
Figure 59: Moisture content for Chicago (top) and Montreal (bottom) depending on wall orientation

Both Chicago and Montreal present similar results in terms of the relative position of the curves from one orientation with respect of the other. It can be observed that independently from the

consideration of wind pressures the North orientation has a higher moisture content than the maximum wind pressure.
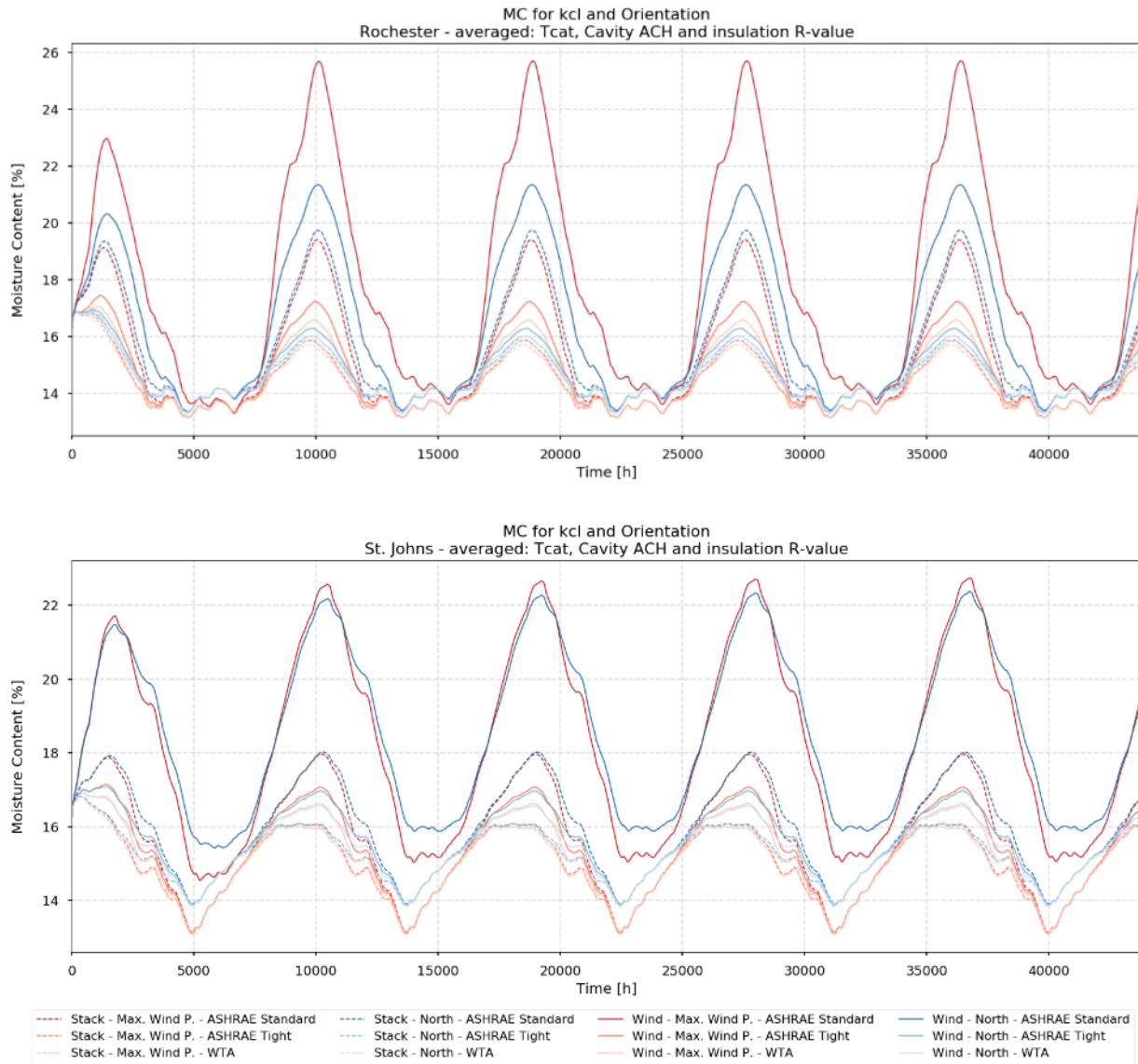
Figure 60: Moisture content for Rochester (top) St. Johns (bottom) depending on wall orientation

In Rochester it is possible to observe that when wind is included in the simulations, the maximum wind pressure orientation presents a higher moisture content. Peaks higher than 20% are present in both cities but only for ASHRAE Standard k_{cl}. St Johns presents very similar results for both orientations.
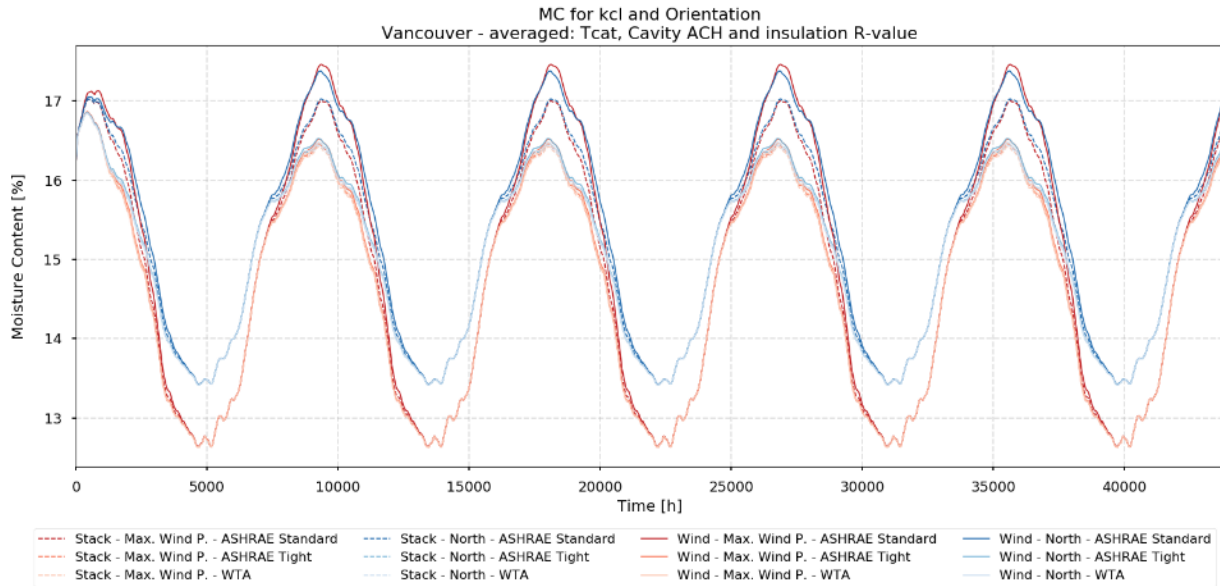
Figure 61: Moisture content for Vancouver (bottom) depending on wall orientation

For Vancouver there is practically no difference between both orientations. Moreover the difference between the simulations with only stack effect and the simulations including wind have less than 1% difference in moisture content.

Appendix V – Terrain Category and *RSI*-value

Section 5.3.2 showed the *RH* for different *RSI*-values, the differences for each *RSI*-value where clear for lower *RH*, but the curves tend to be collapsed at higher *RH*, using moisture content permits a better resolution when the relative humidity is closer to 100% as the curves are more clearly separated. In general it can be appreciated that the curves are grouped by T_{cat} and that the variations for the different *RSI* are less than 1% in moisture content.
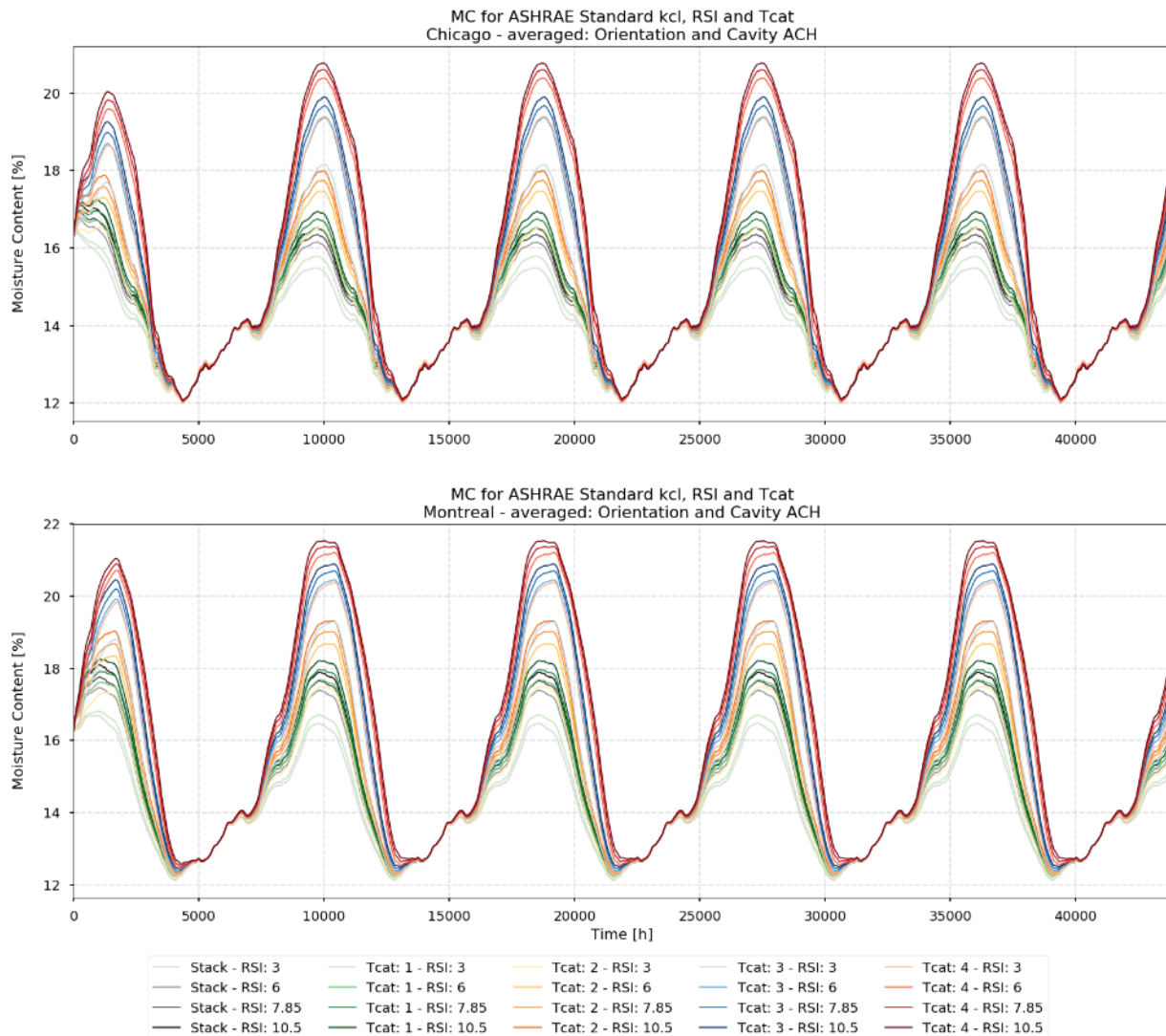
Figure 62: Moisture content for Chicago (top) and Montreal (bottom) depending on RSI and terrain category

For Montreal and Chicago it can be seen that during the dryer period there is no appreciable effect of the insulation, all curves are together independently of the T_{cat} and the *RSI*-value. As the moisture content increases, the different *RSI*-values start to separate from each other, with higher

RSI-value demonstrating a faster increase in the moisture content. The difference in *MC* between *RSI* 3 and *RSI* 10.5 is approximately 1%.
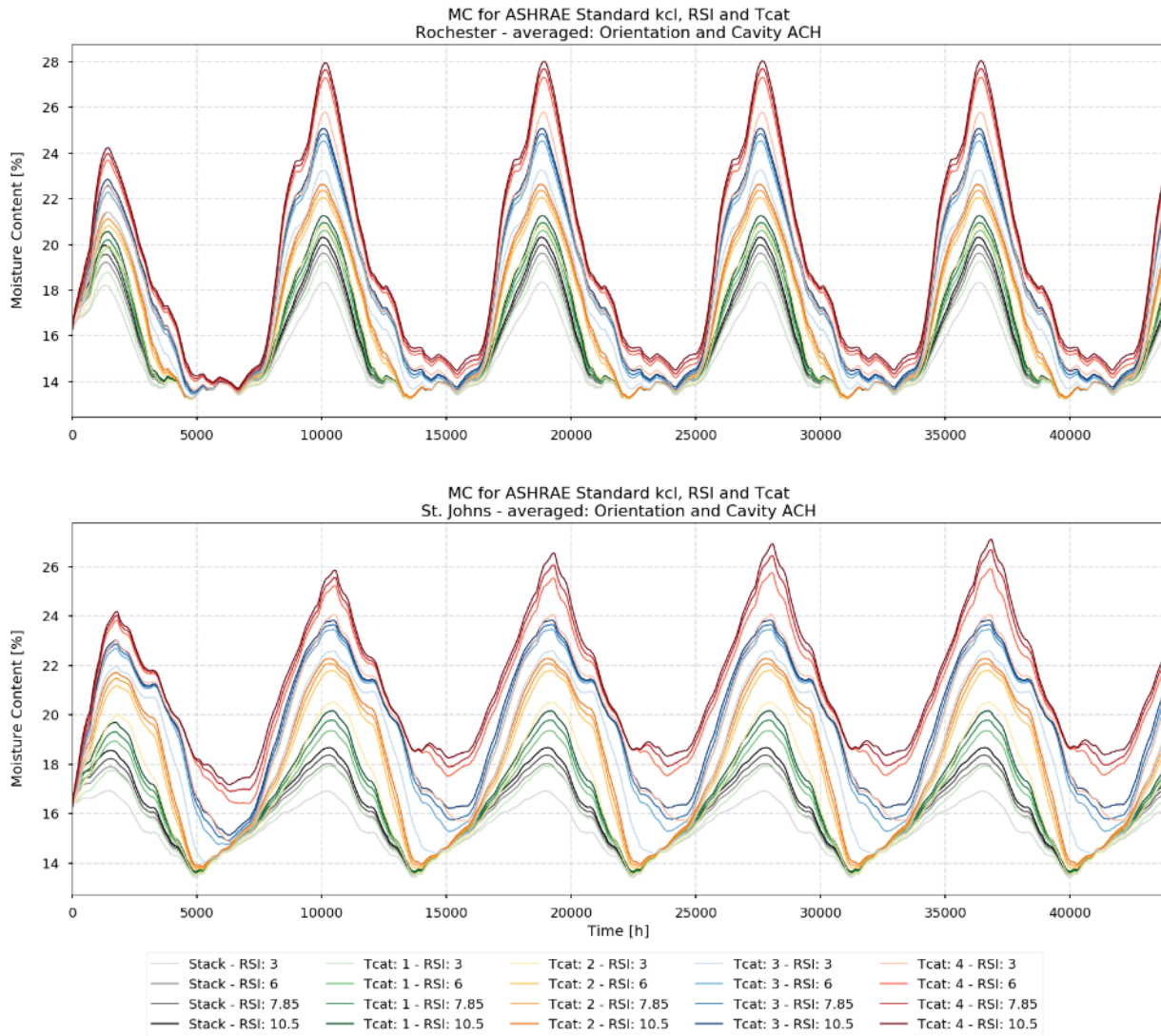
Figure 63: Moisture content for Rochester (top) and St Johns (bottom) depending on RSI and terrain category

In Rochester and St. Johns for T_{cat} 3 and 4 the moisture content does not reach minimum values compared to T_{cat} 1 and 2 and the curves stay apart during the dryer period. The difference in *MC* between *RSI* 3 and *RSI* 10.5 is approximately 2%, and the difference slightly increase in time for T_{cat} 4.
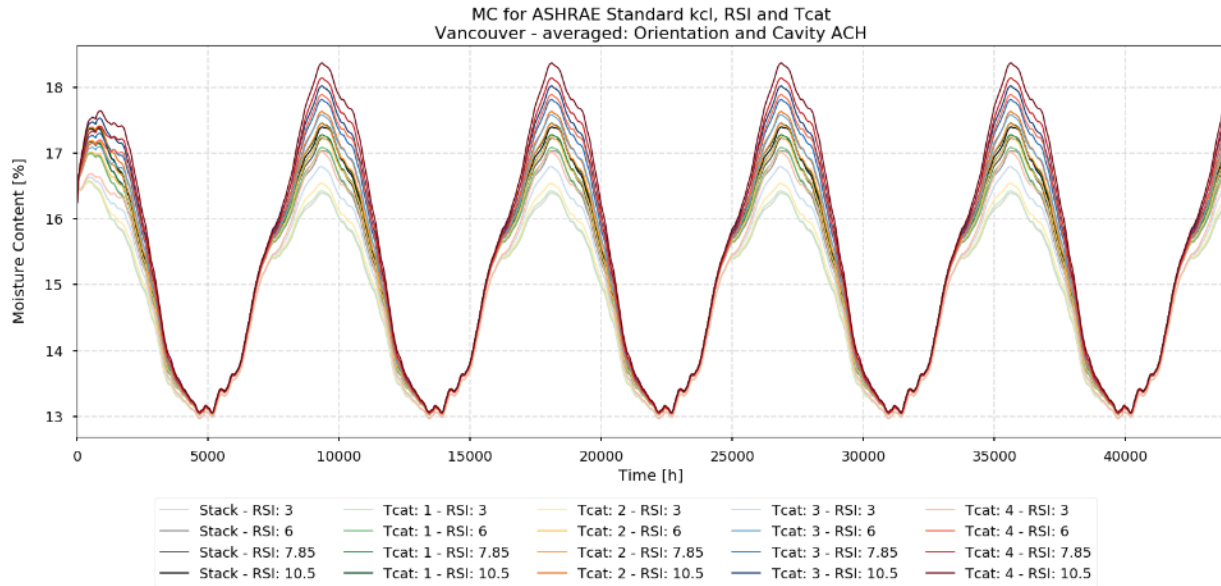
Figure 64: Moisture content for Vancouver depending on RSI and terrain category

For Vancouver the difference in *MC* is appreciable only during the wetter period, but there is no clear grouping by T_{cat} due to the lower wind pressures and, hence, lower exfiltration and moisture deposition.

Appendix VI – Terrain Category and Cavity Air Change Rate

Section 5.3.3 showed that the RH curves were grouped by T_{cat}, but a distinction between different ACH_{cav} was difficult to observe, especially at higher RH were the curves collapse with each other. The higher differentiation of the MC at higher RH allows to visualize the effect of the ventilation cavity rate during peak wet periods.
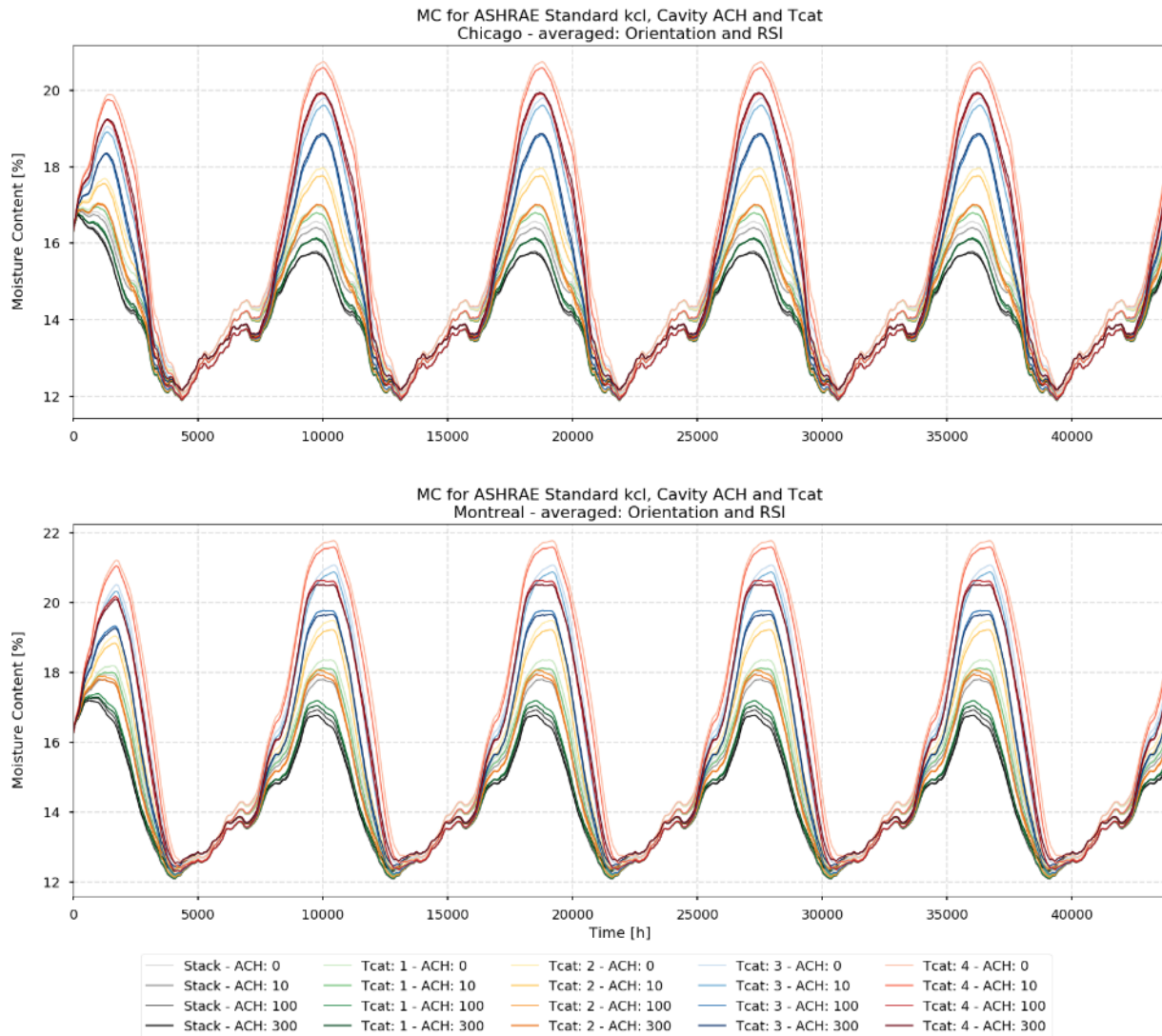
Figure 65: Moisture content for Chicago (top) and Montreal (bottom) depending on Cavity ACH rate

For Chicago and Montreal the effect of the ventilation rate can be seen especially at the peak MC were the two ranges of ACH (0-10 and 100-300) differ for about 1% in MC. During the dryer period there is no observable difference for the different ACH rates simulated.

116
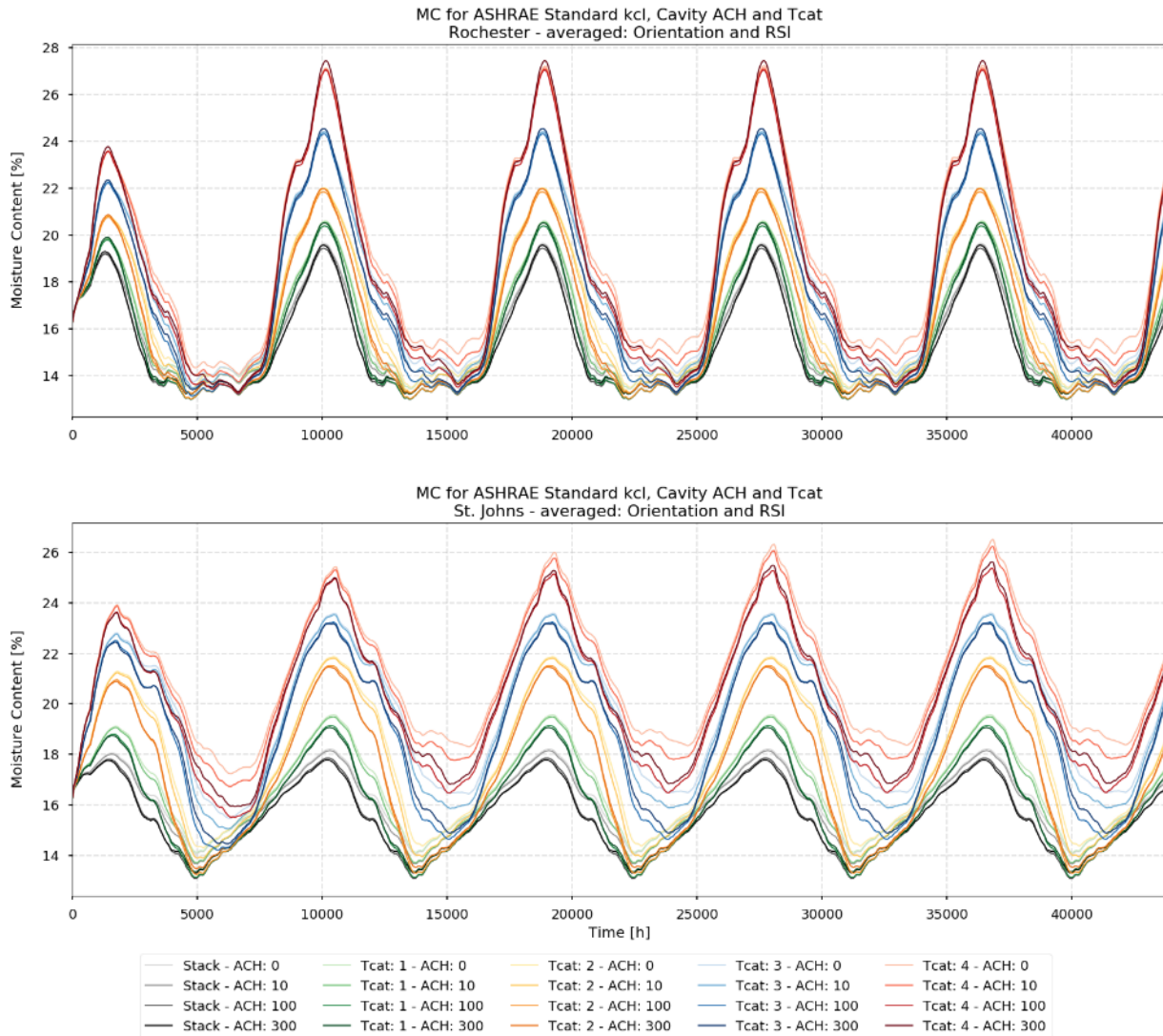
Figure 66: Moisture content for Rochester (top) and St Johns (bottom) depending on Cavity ACH rate

For Rochester the difference between the ACH rates is observable during the dryer period but the differences are lower than 0.5%. There is practically no difference in the maximum *MC* obtained for each T_{cat}. In St. Johns the difference is more noticeable than for Rochester with T_{cat} 3 or 4, although minor, the maximum MC for ACH_{cav} 100-300 is about 0.5% lower than for ACH_{cav} 0-10. During the dryer period the difference between each cavity ventilation rate is around 0.5% between consecutive rates, i.e., 0.5% between ACH_{cav} 0 and 10, 0.5% between ACH_{cav} 10 and 100 and so on. For T_{cat} 1 or 2 the differences in *MC* between ACH_{cav} are minor.
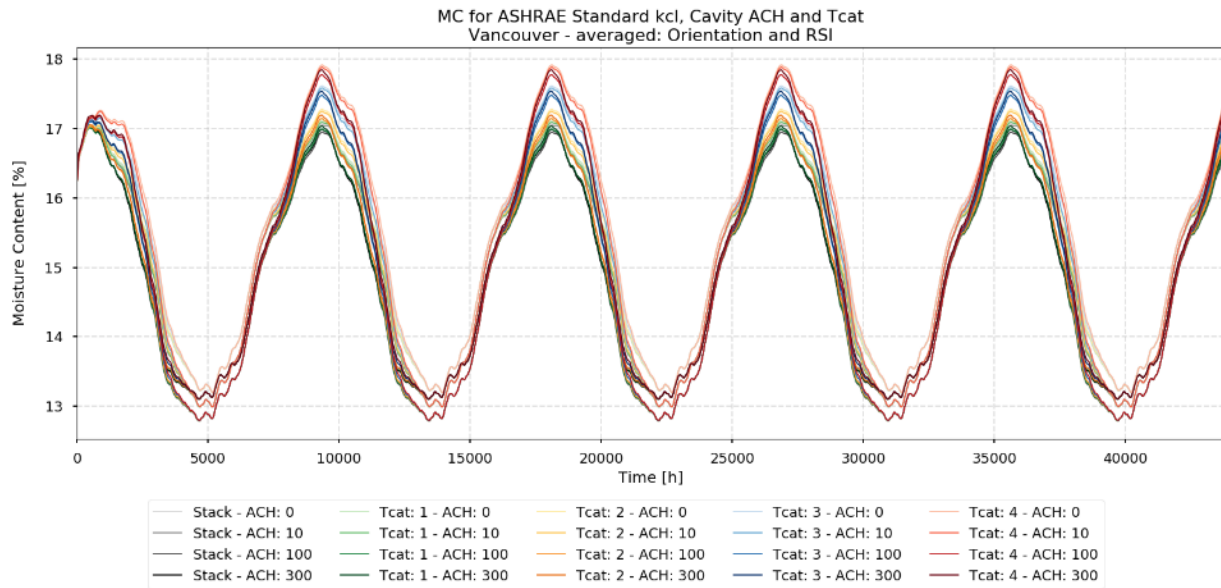
Figure 67: Moisture content for Vancouver depending on Cavity ACH rate

In Vancouver the difference in *MC* between different ACH_{cav} rates is less than 0.5%.